AN ABSTRACT OF THE DISSERTATION OF

Hilary F. Stockdon for the degree of Doctor of Philosophy in Oceanography presented on April 5, 2006.

Title: Predicting the Longshore-Variable Coastal Response to Hurricanes

Abstract approved: _____
Robert A. Holman

The longshore variability of the coastal response to hurricanes may be examined within the framework of a storm-impact scaling model that compares spatially-variable beach morphology and fluid forcing. The relative elevations of dune height and storm-induced water levels are used to define three impact regimes (swash, collision, and overwash), within which the magnitudes and processes of sediment transport are expected to be unique. Maximum total water-levels are modeled as the sum of astronomical tide, storm surge, and wave runup. The 2% exceedence level for runup, the sum of wave setup and swash, is calculated using a parameterization found to be accurate to 38 cm (rms error) based on comparisons to 491 data runs from ten field experiments. Techniques have been developed to extract accurate (15-cm rms) and detailed measures of large-scale coastal morphology and change from high-resolution topographic laser altimetry (lidar) surveys, allowing for quantification of relevant dune heights as well as the magnitudes and patterns of shoreline, dune, beach slope, and beach volume change in response to hurricanes.

Based on the relative elevations of modeled hurricane-induced water levels and lidar-derived measures of pre-storm (1997) dune morphology, the potential impact regimes for Hurricanes Bonnie (1998) and Floyd (1999) were defined at 20-m increments along a 70-km stretch of coast in Onslow Bay, North Carolina. Comparisons to the observed impact regime, quantified from calculations of dune erosion and overwash deposition, indicate that the predictive accuracy of the model was 55.4%, an improvement over the 33.3% accuracy associated with random chance. Regime-specific model sensitivity was highest

within the overwash regime (86.9%), decreasing to 55.8% and 1.5% in the collision and swash regimes, respectively. Shoreline and beach volume change in response to the storms were spatially-variable: the standard deviation of change was the same order of magnitude as the mean. Magnitudes of coastal change scaled with the observed impact regime. Beach volume change within the overwash and collision regimes was over two times greater than that within the swash regime. Little recovery was observed in overwashed locations where sand was transported inland and removed from the nearshore system. Here, the volume of sand removed from the beach was balanced by that in the overwash deposits.

Predicting the Longshore-Variable Coastal Response to Hurricanes

by

Hilary F. Stockdon

A DISSERTATION

submitted to

Oregon State University

in partial fulfillment of
the requirements for the
degree of

Doctor of Philosophy

Presented April 5, 2006
Commencement June 2006

Doctor of Philosophy dissertation of Hilary F. Stockdon presented on April 5, 2006.

APPROVED:

Major Professor, representing Oceanography

Dean of the College of Oceanic and Atmospheric Sciences

Dean of the Graduate School

I understand that my dissertation will become part of the permanent collection of Oregon State University libraries. My signature below authorizes release of my dissertation to any reader upon request.

Hilary F. Stockdon, Author

ACKNOWLEDGMENTS

I would like to express my sincere appreciation to my advisors, Dr. Rob Holman and Dr. Abby Sallenger, for their strong guidance and unwavering support. My unique experience at COAS and USGS gave me two people to count on for insight and advice. Rob usually recommended that I get to the essence of the problem and focus on the specifics (first principles). Abby generally suggested that I take a step back and look at the bigger picture (what ifs). At first, their advice seemed to send me in different directions. I later realized that this perfect combination provided me with a strong foundation for doing science and a wonderful way to look at the world. Ask big questions, find specific answers, and always be gutsy.

I am grateful to Dr. Peter Howd for his invaluable insights on beaches and waves. He was always available to discuss any aspect of this work – big or small. I appreciate Dr. Tuba Ozkan-Haller, an exceptional scientist and role model, for asking the hard questions about waves, runup, and setup and for kindly helping me to find the answers. I thank Dr. Paul Komar for his unique perspectives that often got me thinking about things in a new way. I also would like to acknowledge Dr. David Hamby and Dr. Jack Higginbotham who kindly served as my Graduate Council Representatives.

This research would not have been possible without the support of the U.S. Geological Survey, Coastal and Marine Geology Program and many of its dedicated and talented researchers (past and present): Karen Morgan, David Thompson, Kathy Weber, Peter Ruggiero, Kristy Guy, Laura Fauver, Jeff List, John Haines, Lisa Robbins, Nicole Elko, and Meg Palmsten. I would like give special thanks to Peter and Nicole for talking shop with me, showing a genuine interest in my work, and encouraging me to finish.

I am grateful to the USGS, NASA, and NOAA for a wealth of lidar data (at times, more than I wanted), the U.S. Army Corps of Engineers Field Research Facility for collecting one of the best long-term data sets of nearshore waves, and to the Coastal Imaging Lab at Oregon State University for sharing with me the most comprehensive

collection of runup data. I also owe a great deal to the amazing people at CIL whom I have worked with over my 12 years as a part of their family, from the early days with Todd, Diane, and Nathaniel to the last days with Chris as we pushed each other to the finish line. And of course, many thanks to John Stanley for his help over the years and for always making me feel at home whenever I returned to the lab.

Finally, I extend heartfelt gratitude to my parents Peter and Kathy for believing in me and everything I have chosen to do, to my brothers Ben and Max for keeping me in touch with the real world during this long haul, and to Dave and Ava for providing me with both motivation and distraction (and always knowing exactly which one I needed most). I thank you all for reminding me that there is so much in this world to experience, so much more than science.

This work was funded by the U. S. Geological Survey, Coastal and Marine Geology Program as a part of the National Assessment of Coastal Change Hazards.

CONTRIBUTION OF AUTHORS

Chapter 2 is reprinted from the *Journal of Coastal Research* (H.F. Stockdon, A.H. Sallenger Jr., J.H. List, and R.A. Holman, 2002. Estimation of shoreline position and change using airborne topographic lidar data, *Journal of Coastal Research,* 18(3), 502-513) with permission from the Coastal Education and Research Foundation. Abby Sallenger was the motivation behind this study and provided a wealth of lidar data for developing and testing the techniques. Jeff List provided ground survey data with which to compare the lidar-derived shorelines. Rob Holman assisted in defining the errors associated with the technique.

Chapter 3 is reprinted from *Coastal Engineering* (H.F. Stockdon, R.A. Holman, P.A. Howd, and A.H. Sallenger, Jr., 2006. Empirical parameterization of setup, swash, and runup, *Coastal Engineering*, 53(7), 573-588) with permission from Elsevier. Rob Holman was the author of earlier research defining an empirical parameterization for extreme runup. His extensive collection of runup data provided an additional nine experiments that were used to develop the new parameterizations. He also provided guidance on the scope of the research and many critical reviews of the manuscript. Peter Howd and Abby Sallenger gave insight into the statistical analyses of the various empirical models.

Chapter 4 will be submitted to *Marine Geology* (H.F. Stockdon, A.H. Sallenger Jr., R.A. Holman and P.A. Howd. A simple model for the large-scale, spatially-variable response to hurricanes). Abby Sallenger first introduced the storm-impact scaling model that is examined in this paper. Rob Holman helped to clarify the goals of the paper and to define objective measures of the observed storm-impact regime. Peter Howd offered valuable insights on longshore-variable coastal change. All provided thoughtful reviews of the paper.

TABLE OF CONTENTS

TABLE OF CONTENTS (Continued)

Page

LIST OF FIGURES

LIST OF FIGURES (Continued)

Figure Page

LIST OF TABLES

Dedicated to Charles W. Stockdon

PREDICTING THE LONGSHORE-VARIABLE COASTAL RESPONSE TO HURRICANES

1.0 GENERAL INTRODUCTION

Exploding development along the nation's shorelines combined with a recent increase in hurricane activity has placed U.S. Gulf and Atlantic coastal communities at a growing risk to hurricane-related damage. Much of the recent development along the coasts is concentrated on barrier islands, dynamic environments where sand is constantly shifting in response to wind and waves. During hurricanes the magnitudes of changes on these islands can become extremely large, threatening local communities, buildings, and infrastructure. An understanding of the large-scale, spatially-variable beach response to hurricanes is vital for developing a predictive assessment of our coasts' vulnerability. This type of information is required by coastal planners and emergency managers for locating future development sites, protecting vulnerable infrastructure, planning storm evacuation routes, and taking preventative measures to avoid continued loss of life and of property.

1.1 Recent Hurricane Activity

Hurricanes are powerful and dangerous storms characterized by strong winds and heavy rain. They begin as small low pressure disturbances in the tropics, where warm water and humid air provide the necessary fuel for their creation. As warm air rises, it begins to cool, allowing water vapor to condense. Condensation releases latent heat, or energy, that warms the surrounding atmosphere and causes more air to rise and expand. Ultimately, the cycle of condensation and latent-heat release creates an area of low pressure. As this process continues, the low pressure cell intensifies creating a steep pressure gradient. In the Northern Hemisphere, the resulting pressure gradient generates cyclonic winds that blow in towards and around the low pressure center, creating a counter-clockwise center of circulation. When the maximum sustained wind speed reaches 119 km/hr (74 mph), the storm is classified as a Category 1 hurricane, according

to the Saffir-Simpson scale. A major hurricane, defined as a Category 3 storm or greater, has wind speeds in excess of 178 km/hr (111 mph). The landfall of one of these major storms generates not only heavy winds, but also large waves and storm surge. Storm surge, the elevated water level at the coast due to the wind field and low atmospheric pressure associated with the hurricane, will likely exceed 3 m during a Category 3 storm. The combination of storm surge and waves create a highly destructive force that erode beaches and sand dunes and, ultimately, threaten the structures they serve to protect.

Major hurricane activity in the North Atlantic Basin has been shown to follow a somewhat regular, multi-decadal cycle [*Goldenberg*, 2001]. Interannual variability in both the number and intensity of hurricanes is constrained by large-scale atmospheric factors [*Webster et al.*, 2005]. For example, during El Niño years, there are fewer Atlantic and Gulf hurricanes due to increased wind shear associated with abnormally warm waters. From 1970 – 1994, only ten major hurricanes (Category 3-5) made landfall in the United States, a relatively low number compared to 19 landfalls in the prior 25 years [*Center*, 2006]. As evidenced by the record-breaking 2005 hurricane season, where there were more named storms (27) in the Atlantic in a single year since official record-keeping began in 1944, tropical cyclonic activity is currently in an active phase [*Goldenberg*, 2001]. In the eleven-year period from 1995-2005, ten major hurricanes have made landfall in the United States [*National Climate Data Center*, 2006]. It is likely that this present high level of hurricane activity will last for a total of 25-40 years [*Goldenberg*, 2001]. In order to better prepare coastal communities for future hurricane landfalls, it is critical to assess the vulnerability of our coastline to extreme coastal change during these storms. This begins with a better understanding of the nature and magnitude of the large-scale response of barrier island morphology to hurricanes

1.2 Spatially-Variable Storm Response

Observations of the large-scale response of beaches to storms have shown that significant spatial variability is superimposed upon a general mean response [*Stockdon et al.*, 2003]. Within the storm-impact zone, some areas may experience severe dune erosion

and overwash, while adjacent areas remain virtually unaffected. For example, coastal change within Onslow Bay, North Carolina was significantly longshore-variable following the landfall of Hurricane Bonnie in 1998 (Figure 1.1). Mean shoreline change, defined as the horizontal movement of the mean high water contour was -8.36 m along a 70-km stretch of beach between Carolina Beach and New River Inlets; yet, the standard deviation about this mean was of the same order of magnitude, 9.02 m. The spatial-variability of shoreline change persisted after the landfall of Hurricane Floyd, which occurred one year later. Large variations in the magnitude of shoreline and beach erosion were observed both along a single island and between islands. On Masonboro Island, shoreline and beach erosion appeared to be cumulative and longshore-variability of the signal increased after each storm. Alternatively, on Topsail Island the magnitude and spatial variability of shoreline change were similar following each storm [*Stockdon et al.*, 2003]. In order to accurately predict the large-scale coastal response to hurricanes, an understanding of the processes responsible for these observed patterns is required.

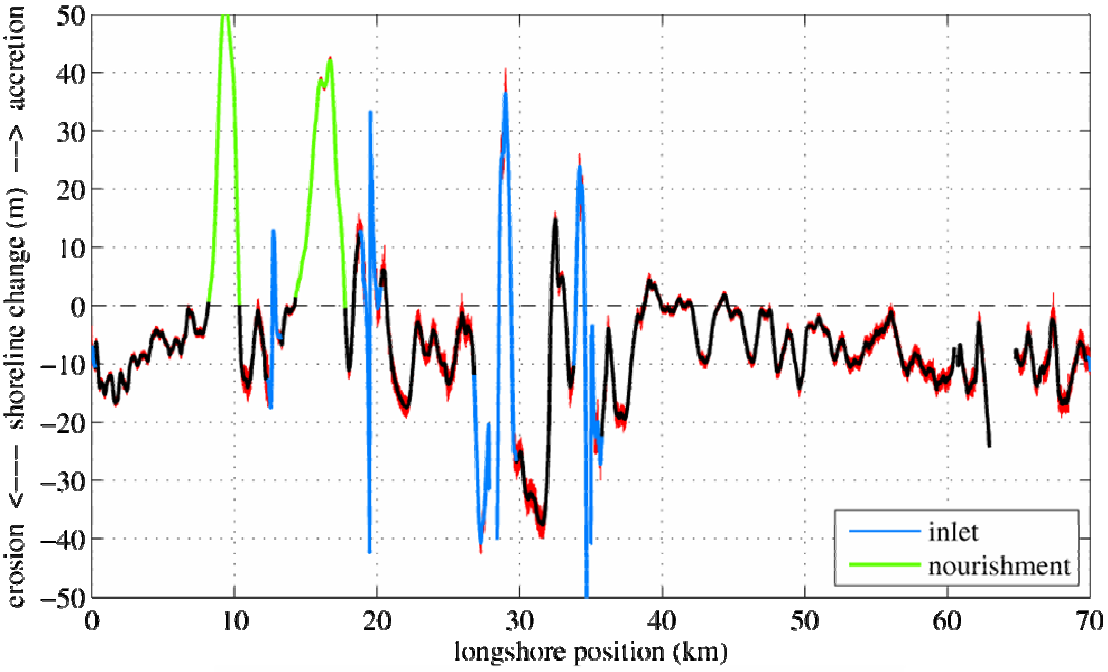

Figure 1.1. Shoreline change calculated after Hurricane Bonnie for a 70-km stretch of coast in Onslow Bay, North Carolina between Carolina Beach and New River Inlets. Negative values indicate erosion and positive values indicate accretion. The largest signal was observed near inlets or at renourished beaches. The mean shoreline change outside of these areas was -8.36 m (standard deviation = 9.02 m).

1.3 Predicting Coastal Vulnerability to Hurricanes

The main goals of this research are to implement and quantitatively test a model for scaling hurricane-induced coastal change and to investigate the observed patterns of shoreline and beach volume change. More specifically, this study explores the extent to which the observed longshore variability of coastal change can be attributed to the relationship between longshore changes in coastal morphology and extreme water levels that accompany the storm. We begin with the hypothesis that areas with low-lying dunes are more prone to overwash than beaches backed by a continuous, high dune. Additionally, longshore variations in wave height (and the resulting wave runup) exist due to refraction of waves over local bathymetry causing wave energy to focus and de-focus. These two ideas are combined through a simple scaling model that uses the relative elevations of sand dunes (or berms) and extreme water levels (defined as the sum of storm surge, wave runup, and astronomical tides) to delineate four unique storm-impact regimes on barrier islands [*Sallenger*, 2000]. The *swash* regime, the lowest impact level, occurs when the surge and runup are confined to the beach face and the dominant sediment transport gradients are directed offshore. When water levels reach the base of the dune, the system falls within the *collision* regime, marked by the beginning of significant erosion of the dune face. The *overwash* regime is defined when maximum runup levels exceed the crest of the dune or berm, often causing the landward transport of sand. The final and most extreme regime, *inundation*, occurs when total water levels continuously exceed the maximum elevation of the beach and dunes, completely submerging the island and allowing for cross-island flows.

In the following chapters, we investigate the accuracy with which the model can be used to predict the impact of an approaching hurricane and the extent to which these four storm-impact regimes may be used to scale the magnitudes of hurricane-induced coastal change. The model has been applied to three beaches in Onslow Bay, North Carolina in order to hindcast the vulnerability of the area to extreme coastal change during Hurricanes Bonnie and Floyd, which made successive landfalls near Cape Fear, North Carolina, in the late summers of 1998 and 1999, respectively. These hindcasts were compared to objective determinations of the observed hurricane impact regime in order to

evaluate the predictive accuracy of the model. Additionally, magnitudes of shoreline and beach volume change were quantified within each regime to examine whether processes unique to each regime are responsible for a longshore-variable response.

Critical to this work is the collection of detailed, large-scale (O(10 km)) measurements of coastal morphology and change. The advent of airborne laser mapping systems has made possible the rapid collection of high-resolution topographic datasets over large areas. NASA's Airborne Topographic Mapper (ATM), initially developed to detect changes in the thickness of the Greenland ice sheet [*Krabill et al.*, 1995], has more recently been applied to mapping beach morphology for the assessment of storm impacts [*Krabill et al.*, 2000; *Sallenger et al.*, 1999a]. Comparisons of lidar surveys collected before and after hurricane landfall provide an unprecedented, three-dimensional view of coastal change in response to the storm. The first goal of this work was to extract specific measures of coastal change from the full lidar data set that will be used to quantify the longshore-variable response to each hurricane (Chapter 2). We present a technique for calculating the horizontal position and movement of the shoreline, which has been used historically as a proxy for large-scale morphology and a direct measure of accretion and erosion. Lidar data are also used to quantify storm-induced coastal change and to objectively classify the observed storm-impact regime. We use the lidar data to extract additional beach morphology parameters, such as beach slopes and dune elevations, that provide the basis for hindcasting the potential storm-impact regime.

To use the storm scaling model in a predictive mode, estimates of runup (including swash and setup) during hurricane conditions are needed. The behavior of runup from monochromatic waves on a planar beach is well defined. However, natural beaches introduce complications of random waves and complex beach morphology. With knowledge of complete boundary conditions and wave spectra, it is possible to numerically model swash and runup [*Raubenheimer and Guza*, 1996; *Raubenheimer et al.*, 1995]. However, this approach is not practical for the large-scale prediction of hurricane-induced wave runup because details of the model input and boundary conditions are not known. Therefore, we investigate the degree to which an empirical

parameterization is useful for calculating extreme runup based on local beach slope and offshore wave conditions (Chapter 3). The most-often used parameterization for extreme runup [*Holman*, 1986] shows a dependence on foreshore beach slope, wave height and wave period. This equation was developed using data from a single experiment and is not necessarily applicable over a wide range of conditions. Therefore, we expand the work of Holman (1986) to water-level data collected during ten field experiments, representing different beach morphologies and wave climates. Unique to this work is the separate parameterization of wave setup and swash, the two physically different processes that comprise runup. The final equation, presented in Chapter 3, can be used to parameterize the 2% exceedence value of runup on a wide range of natural beaches.

Combining modeled estimates of storm-induced runup and setup elevations (Chapter 3) and measurements of coastal morphology and change (Chapter 2), we examine the large-scale, longshore-variable impacts of Hurricanes Bonnie and Floyd within the framework of the storm-impact scaling model (Chapter 4). First, we calculate the expected impact regime along a 70-km stretch of coast using topographic surveys of pre-storm beach morphology and a hindcast estimate of total water levels for each storm. Topographic surveys collected immediately after hurricane landfall allow objective determination of the observed hurricane-impact regime and a quantitative analysis of the predictive capabilities of the scaling model. Additionally, the longshore-variable response of the coast to these storms is examined by calculating hurricane-induced shoreline and beach volume change. The magnitudes of change within different impact regimes are used to determine to what extent the scaling model, and the processes delineated within the model, contribute to the longshore-variable coastal response.

2.0 ESTIMATION OF SHORELINE POSITION AND CHANGE USING AIRBORNE TOPOGRPAHIC LIDAR DATA

2.1 Abstract

A method has been developed for extracting shoreline position, defined as the horizontal location of a vertical shoreline datum, from cross-shore profiles of airborne scanning laser data. This technique allows rapid estimation of objective, GPS-based shoreline positions over hundreds of kilometers of coast, essential for the assessment of large-scale coastal behavior. Shoreline position is found by fitting a function to laser shots located in a vertical range around the datum and then evaluating the function at the specified datum. Error bars on horizontal position are directly calculated as the 95% confidence interval on the mean value based on the Student's *t* distribution of the errors of the regression. The technique was tested using lidar data collected with NASA's Airborne Topographic Mapper (ATM) in September 1997 on the Outer Banks of North Carolina. Lidar-derived shoreline position was compared to shoreline position as estimated by a ground-based GPS vehicle survey system. The two methods agreed closely with a root mean square difference of 2.9 m. The mean 95% confidence interval for shoreline position was ± 1.4 m. The technique has been applied to a study of shoreline change on Assateague Island, Maryland/Virginia, where three ATM data sets were used to assess the statistics of large-scale shoreline change caused by a major 'northeaster' winter storm. The accuracy of both the lidar system and the technique described provides measures of shoreline position and change that are ideal for studying storm-scale variability over large spatial scales.

2.2 Introduction

A recent focus in nearshore research has been large-scale coastal behavior [LSCB, *Thornton et al.*, 2000], changes in nearshore bathymetry and beach topography with spatial scales of order kilometers and temporal scales of order years. It is at these scales

that decisions are made in coastal zone management and at these scales that improvement to our scientific understanding is needed.

In order to accurately quantify the variability of large-scale coastal changes and to obtain a clearer understanding of the processes driving these changes, detailed measurement of large-scale morphology over regional scales is required. While change occurs over the entire active profile, the horizontal location and movement of the shoreline are two of the most commonly chosen variables of large-scale beach morphology and serve as direct indicators of erosion and accretion. Topographic maps (USGS Quadrangles and NOS Topographic Sheets), rectified aerial photographs, and traditional beach profiles have been the most common source for long-term, large-scale measures of shoreline position [*Dolan et al.*, 1980]. These historical shoreline locations are often compared to present shoreline locations to calculate rates of long-term shoreline change. Because of their long record length, maps and aerial photographs are invaluable in quantifying long-term shoreline change.

2.2.1 Traditional Shoreline Proxies

Quantification of shoreline location, the interface between the land and the water, usually involves a number of assumptions. Therefore, all estimates will have error associated with both the technique for measuring shoreline position and the assumptions made regarding the definition of the shoreline. Traditional methods using aerial photographs for shoreline measurement often involved non-stereo photography that has no vertical information. In this case, relationships must be assumed between some identifiable horizontal feature and its assumed vertical elevation.

For coastal change applications, the location of the high water line (HWL), defined as the landward extent of the last high tide [*Anders and Byrnes*, 1991; *Crowell et al.*, 1991; *Dolan et al.*, 1980; *Stafford*, 1971], is commonly used to mark the position of the shoreline. Often the HWL may be difficult to identify or may appear as a gradational zone of change. Here, other physical features, such as the wet/dry line [*Crowell et al.*,

1991], vegetation line, drift line, or dune line [*Morton*, 1991] are used as a proxy for shoreline location. This leaves the determination of the location of this feature up to the judgment of the operator [*Anders and Byrnes*, 1991], and it may often be confused with the latest swash excursion, a debris line, an erosional scarp, or changes in sediment type or color [*Crowell et al.*, 1991]. Since the relationship of these proxies and an actual tidal datum may vary depending on wave height, beach slope, storm surge, and sediment size [*Dolan et al.*, 1980], errors can potentially be large and cannot easily be quantified.

2.2.2 Techniques for Identifying Shorelines

The earliest historical shorelines for the coast of the United States are available from maps dating back to the late 1800's [*Anders and Byrnes*, 1991]. Topographic maps are most useful for examining long-term trends in shoreline change since the maps are produced infrequently, limiting the amount of detail that can be obtained concerning the short-term physical processes. Errors in shoreline location derived from maps may be attributed to surveyor error in identifying the shoreline feature, distortion of source maps (folding, tearing, shrinkage), and changes in the reference datum [*Anders and Byrnes*, 1991].

Since the 1920's, aerial photographs have been used to document shoreline position and change [*Anders and Byrnes*, 1991]. Aerial photographs are first transformed to map coordinates using ground control points and then a proxy for shoreline is digitized [*Crowell et al.*, 1991]. Aerial photographs were generally collected more frequently than maps were made, and therefore, may be used to develop a more detailed understanding of short-term shoreline variability. For unrectified aerial photographs, accuracy within or between images is limited by scale differences (caused by aircraft altitude changes), by camera geometry, by ground relief [*Crowell et al.*, 1991; *Dolan et al.*, 1980; *Hapke and Richmond*, 2000], and by the precision of the digitizing equipment and of the operator in following the trace of the HWL [*Anders and Byrnes*, 1991]. Since the errors in measuring a shoreline from aerial photographs are not independent, cumulative errors can be large. Crowell *et al.* [1991] estimate the total (operational) combined error for

1:10,000 scale, non-tidal coordinated, aerial photography to be ~ 7.6 m, not including errors associated with inaccurate interpretation of the location of the HWL.

Many of the errors associated with aerial photographs can be eliminated or reduced before features are identified within the image by using recent techniques involving softcopy photogrammetry where digital stereo images are used to georeference the image and remove distortion [*Hapke and Richmond*, 2000]. Elevation contours are generated on the photograph through the creation of a digital terrain model and shoreline position, or a specified contour, can be measured from the stereo pair [*Overton and Fisher*, 1996]. The accuracy of the extracted features depends on the known camera parameters, flight elevation, accuracy of ground control points, and the resolution of the image [*Hapke and Richmond*, 2000]. While the use of accurate digital images eliminates much of the error associated with aerial photographs, the process of identifying a shoreline and then extracting it from an image is very labor intensive and makes the analysis of large areas more difficult.

Shorelines have also been measured from ground-based surveys of cross-shore profiles of beach elevations. Since these surveys are relatively inexpensive to perform, closely spaced profiles can be collected frequently and used for detailed studies of short-term variations in shoreline position over a limited region [*Morton*, 1991]. While ground-based profiling techniques may yield an accurate measure of shoreline location, the measurements are spatially limited due to the intensive labor requirement of profiling. More recently, shoreline position has been measured using vehicle-mounted, ground-based GPS (global positioning system) surveys. All-terrain vehicles equipped with GPS antennae can quickly survey shore-parallel and shore-normal profiles [*Morton et al.*, 1993], a single transect along the length of the beach (100 km or more in length) [*List et al.*, 2000], or a complete, detailed mapping of beach topography (4 km or more in length) [*Plant et al.*, 1996; *Ruggiero et al.*, 1999; *Ruggiero and Voigt*, 2000]. Horizontal accuracy of shoreline positions measured using these techniques depends on, among other things, GPS accuracy, proximity of survey lines to the exact location of the shoreline, and beach slope. For example, using the vehicle-based mapping systems on a

beach with a 1:50 slope, the horizontal error in position is approximately 2.5 to 5.0 m [*Ruggiero et al.*, 1999].

While the spatial coverage of the vehicle-based GPS ground surveys can be very extensive, it is still somewhat limited compared to the capabilities of an airborne system. Recent developments in GPS and scanning airborne laser capabilities have made available extensive data sets of fully three-dimensional beach topography. These highly accurate and spatially dense surveys allow the possibility of making an objective and detailed determination of regional-scale shoreline position. Using laser data to quantify shoreline position and change over regional scales will contribute to an improved understanding of large-scale coastal behavior on both long-term and short-term (storm) scales.

Our objective is to develop a technique for measuring shoreline position from laser altimetry data. First, we describe the details of the lidar ATM system and the lidar shoreline extraction technique. We then discuss the results of the ground truth test in the Outer Banks of North Carolina in September 1997. Additionally, the advantages and limitations of lidar data as a measure of large-scale shoreline position are illustrated through examination of three data sets of shoreline position collected at Assateague Island, Maryland/Virginia. Finally, we examine the statistics and longshore variability of the response of the island to the northeaster storm season of 1997-1998 using lidar-derived shorelines and beach slopes.

2.3 Methods

2.3.1 Airborne Topographic Mapper

NASA's Airborne Topographic Mapper (ATM) is a scanning laser altimeter originally developed to study climate change by mapping changes in the thickness of the Greenland ice sheet [*Krabill et al.*, 1995]. Since the late 1990's the ATM has been mounted in a Twin Otter aircraft and used for mapping coastal change and assessing storm impacts on subaerial beaches [*Krabill et al.*, 2000; *Sallenger et al.*, 1999b]. The

ATM surveys elevation with a blue-green laser reflected towards the beach using a rotating mirror that produces an elliptical scan pattern. The ATM only records the first reflection of the laser so returns are also obtained from the surface of the water.

GPS determines aircraft position and an inertial navigation system (INS) measures the aircraft's pitch, roll, and heading [*Krabill et al.*, 1995]. The process of deriving elevation measurements from the ATM system is explained in Sallenger *et al.* [2003]. Elevation data can be obtained at a rate of 50 – 70 km/hr (based on an aircraft speed of 110 – 150 knots and multi-pass coverage). In a five-hour flight mission, the ATM can completely cover 250 – 350 km of coast with four overlapping passes, yielding a typical combined swath width of 600 – 700 m. Partially overlapping passes are flown to fully cover the region of interest, to eliminate gaps in the data, and to increase data density. The footprint, and subsequent horizontal resolution, of the laser is approximately one meter in diameter and an individual laser shot is collected every 2 m^2. The ATM beach surveys provide a dense data set of subaerial beach topography with both large spatial coverage and high spatial resolution.

Extensive tests of the vertical accuracy of the ATM instrument were conducted during the SandyDuck Nearshore Processes Experiment (SandyDuck) at the U.S. Army Corps of Engineers Field Research Facility (FRF) in Duck, NC from September to October 1997. Several GPS ground-based surveys of the beach were compared to ATM surveys of the same area. The root-mean-square (rms) vertical error attributed to the ATM was 15 cm [*Sallenger et al.*, 2003]. This represents a total error estimate that includes the many potential sources of error and bias for the lidar system. Based on this error estimate and a typical beach slope of 0.1, we can expect to obtain horizontal shoreline accuracy of ±1.5 m, an order of magnitude better than typical accuracies associated with shorelines from non-stereo aerial photographs. Therefore, the lidar data may offer an alternative to the traditional techniques for measuring shorelines by easily providing objective estimates that are spatially extensive, synoptic, and of sufficient accuracy to resolve a wide range of beach variability (horizontal changes in shoreline position > 3 m).

2.3.2 Shoreline Extraction from Lidar Profiles

The technique for extracting shoreline position, x_s, from ATM data is straightforward. For any particular longshore location, y', a cross-shore profile is extracted from the irregularly spaced full data set. Data from a 2 m wide band around the profile location (y' ±1 m) are included in the individual profile. The cross-shore profiles are extracted at any constant longshore spacing, dy, (dy = 20 m and 10 m for this work) chosen to resolve a particular scale of longshore variability. These profiles also allow determination of other important beach parameters such as beach slope and the location and elevation of the berm, dune base, and dune crest.

After the profiles have been created, any elevation datum, z_s, or elevation-based definition of shoreline, can be extracted. Lidar data contaminated by waves and runup are first removed from each profile by removing all of the data points that lie seaward of the intersection of the water (identified by the noisy laser returns, see Figure 2.1a) and beach. Along each lidar profile, the data are limited to a vertical range (typically ± 0.5m) around the specified elevation datum (Figure 2.1a). The range around the datum may be site specific and should be selected to minimize errors due to laser data in the foreshore area that still may be somewhat contaminated by returns from wave runup. A linear regression is then fit through these data with beach elevation, z_b, as the independent variable (Figure 2.1b). Finally, the function is evaluated at z_s to identify the horizontal position of the shoreline, x_s (Figure 2.1b, asterisk). The slope of the foreshore region, β, is also directly measured on each profile as the slope of the regression through the data around z_s. This procedure is repeated in the longshore for each profile to create a map of shoreline location.

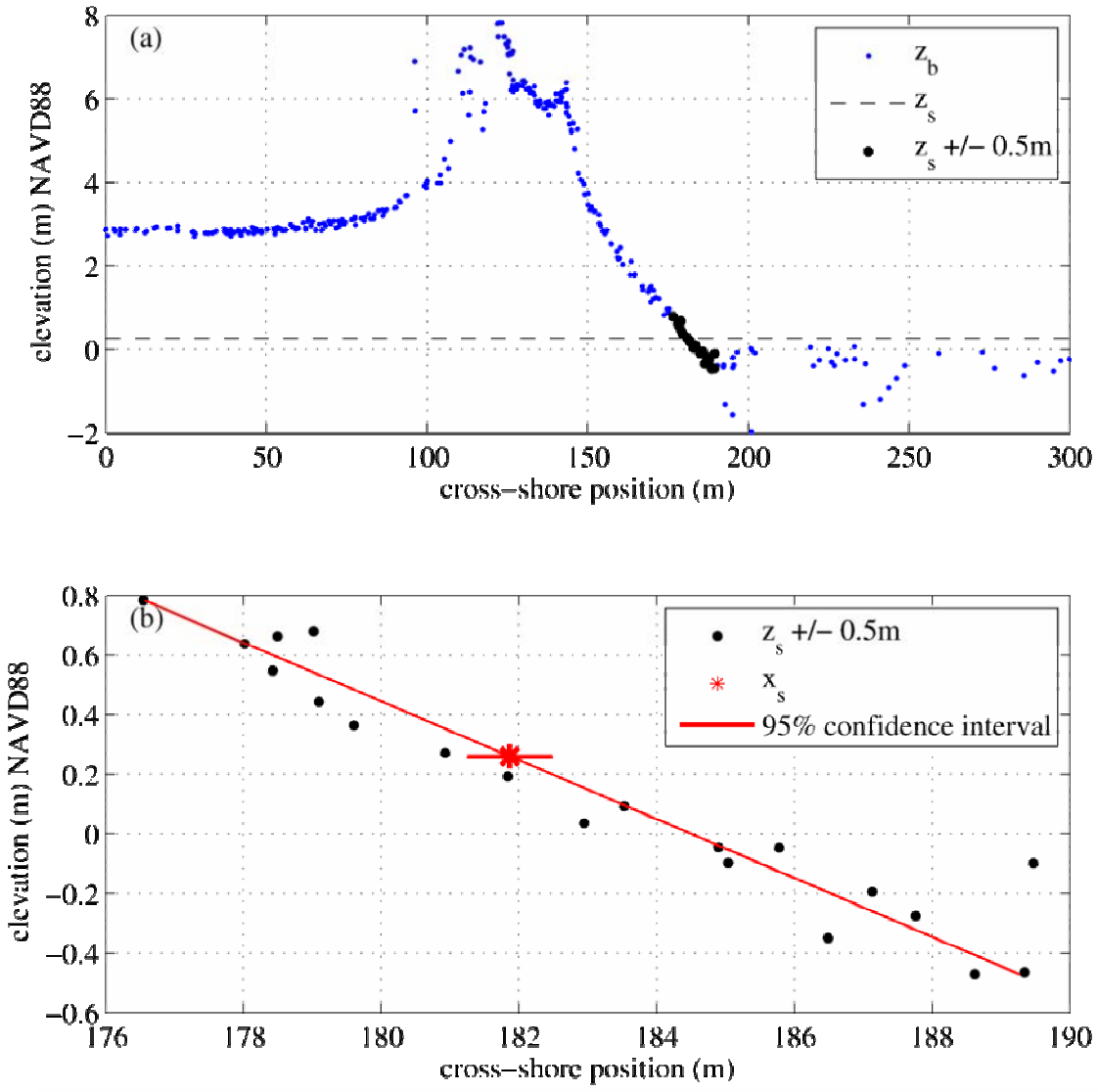

Figure 2.1. Lidar profile from September 26, 1997 at Kitty Hawk, North Carolina for (a) the entire cross-shore region and (b) an expanded view of the foreshore region. (a) Laser returns off of the water's surface are seen as the noisy signal seaward of x = 350 m. Bold symbols indicate data points (z_b) within ± 0.5 m of the MHW datum (z_s). (b) The asterisk marks the cross-shore position of the shoreline, x_s, on the foreshore. The horizontal error bar (±0.42 m) represents the 95% confidence interval about the estimate.

Typically, there are as many as 15-20 laser shots on a profile within the range of the shoreline datum, resulting in a statistically robust regression and estimate of shoreline position. Horizontal error bars, δ_x, on x_s (Figure 2.1b) represent the 95% confidence interval on the mean value based on a Student's t distribution of the errors with N-2

degrees of freedom (where N is the number of points in each regression). The error bars represent the scatter present in the data and account for the random error (noise) of the system. There may also be biases, unaccounted for in these error bars, which may include, but are not limited to: bias in the range walk correction of the instrument, bias in the INS data, instrument mounting bias, or a low-frequency drift of the GPS systems (see below, as well as Sallenger *et al.* [2003] for details).

2.4 Results

2.4.1 Ground Truth Testing

The shoreline extraction technique was tested using laser altimetry data collected on the Outer Banks of North Carolina in September 1997 as a part of the SandyDuck experiment. The data used in the following example were obtained along a 55 km stretch of coast between Corolla and Oregon Inlet (Figure 2.2, lower left) on September 26, 1997. Relatively straight, sandy, barrier island beaches characterize this coastline. Beach slopes, as measured from the lidar data, ranged from 0.05 to 0.11, with a mean value of 0.08. The wave conditions on this day, measured by a waverider buoy in 18 m of water at the FRF in Duck, NC, were relatively calm with a deep-water wave height, H_0, of 0.57 m and a peak wave period of 7.6 s.

As a part of the SandyDuck experiment, GPS-based ground surveys were conducted, providing an opportunity to ground truth shorelines measured from the lidar data. Using a GPS and inclinometer-equipped all-terrain vehicle (ATV), List *et al.* [2000] measured the elevation and beach slope along one longshore transect from Corolla to Oregon Inlet. From these two measurements, the location of the NOAA defined mean high water (MHW, z_s = 0.26 m NAVD88) line was extrapolated from the ATV elevation based on the measured beach slope. Error bars on horizontal shoreline locations are derived from the elevation of the driven track and an estimated variability of the measured beach slope. Details of this technique, termed the SWASH (Surveying Wide Area Shorelines) system, and the calculation of shoreline location and associated error bars can be found in List *et al.* [2000].

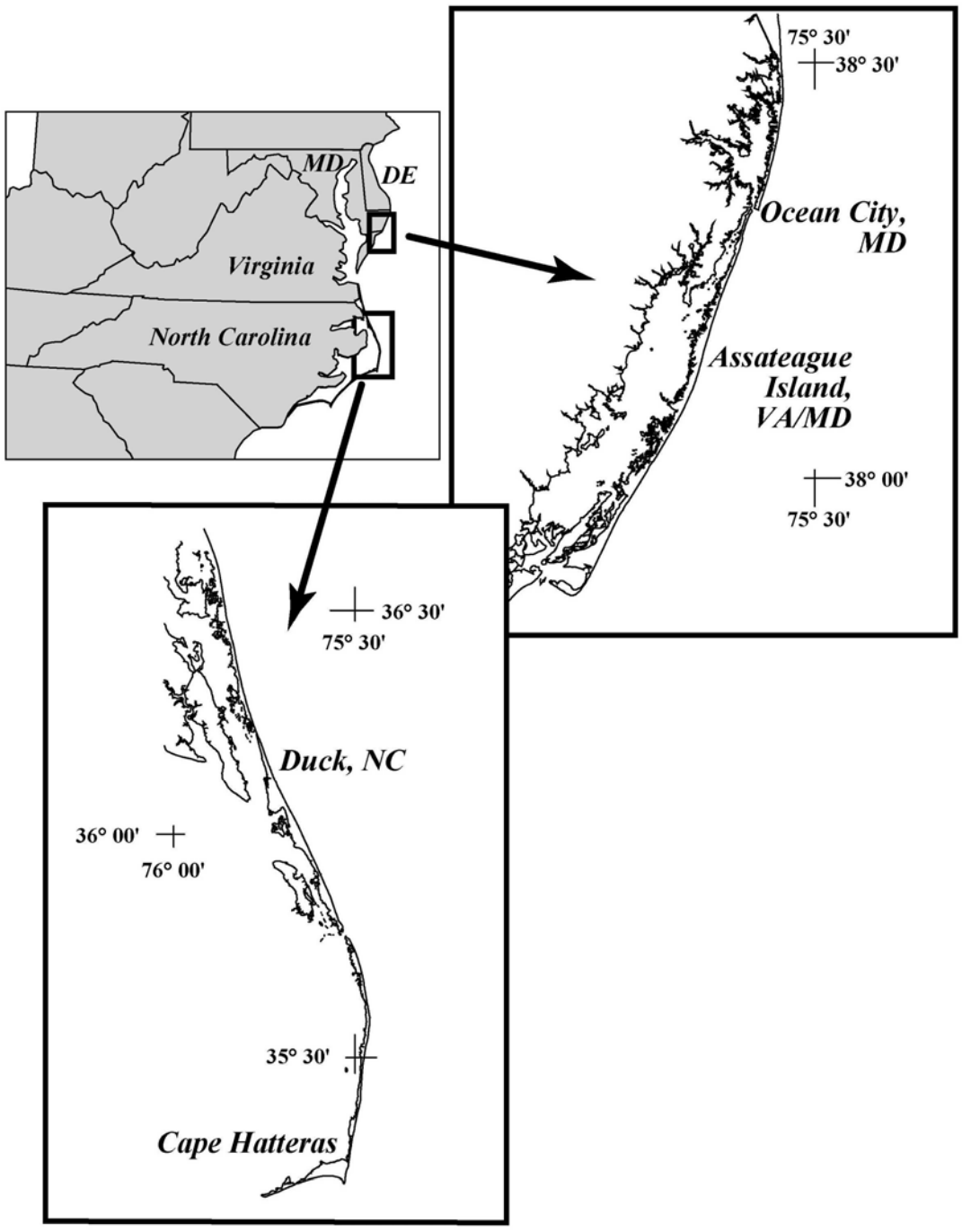

Figure 2.2. Location map of Duck, North Carolina (lower left) and Assateague Island, Virginia/Maryland (upper right).

The horizontal position of the lidar (ATM) shoreline, $x_{s\_atm}(y)$, was compared to the SWASH shoreline, $x_{s\_swash}(y)$ to test the accuracy of the technique. The shoreline position derived from lidar profiles compares well to the SWASH shoreline with an rms

difference, $(\Delta x_s)_{rms}$, of 2.9 m (Figure 2.3). Based on the rectangular coordinate system used, positive values of Δx_s indicate that the lidar shoreline is generally seaward of the SWASH shoreline; the mean offset, $\overline{\Delta x_s}$, between the two shorelines was 2.12 m.

The longshore distribution of shoreline position differences between the two systems, Δx_s, and their combined error bars are shown in Figure 2.4a. In the northern part of the study region, the differences between the two techniques are not statistically significant because the 95% confidence interval for the differences lies around zero. In the southern part of the study region, where the lidar shoreline tends to fall seaward of the SWASH shoreline, there are more significant differences between the two systems. This may be partially due to lidar data points included in the polynomial fit that are actually returns from the wave runup rather than the actual beach surface. While most of the returns from the water's surface are removed from the profile prior to shoreline extraction, a few contaminated returns sometimes remain within the range of z_s and may serve to flatten out the regression, pulling $x_{s\_atm}(y')$ seaward.

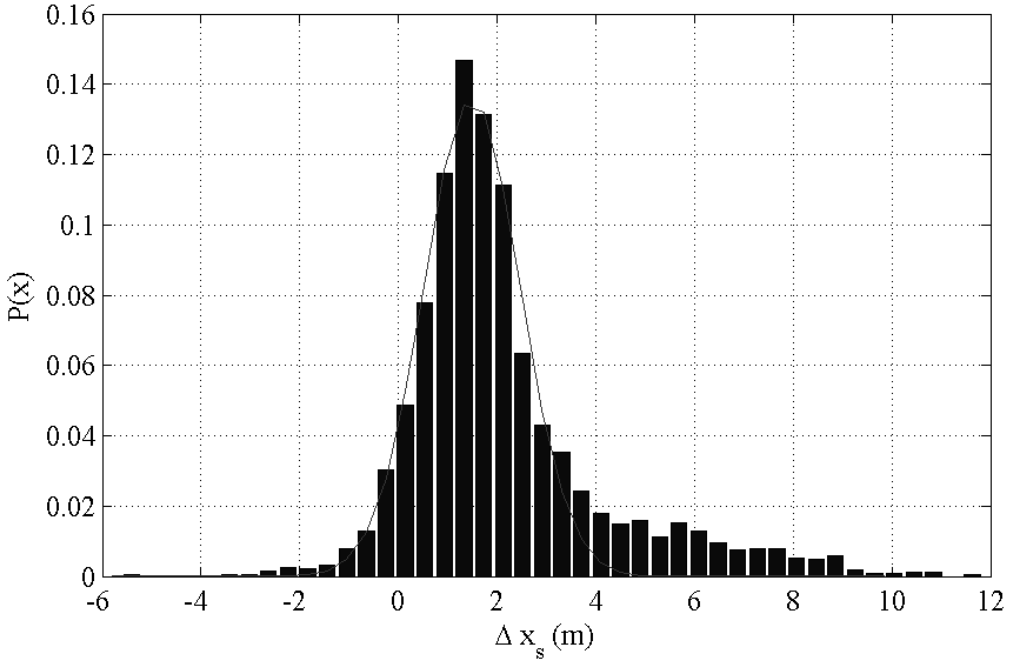

Figure 2.3. Probability density function of differences between ATM and SWASH estimated shoreline positions, Δx_s. The rms difference, $(\Delta x_s)_{rms}$, is 2.90 m and the mean difference, $\overline{\Delta x_s}$, is 2.12 m.

Another reason for the seaward bias may be due to extrapolation errors within the SWASH data caused by the larger distance between the MHW contour and the track driven the ATV on this particular day. Estimating the location of the MHW line by extrapolating along a steep slope that may tend to flatten lower in the profile will cause the location of the shoreline to fall more landward than it truly is. The beach slopes used in the SWASH system for the extrapolations were compared to foreshore slopes measured directly around the shoreline vertical datum using the lidar data. In locations where the slope used by SWASH was steeper than that measured around z_s by the ATM, the largest discrepancies between the two systems occur with SWASH estimates falling more landward of the ATM shoreline.

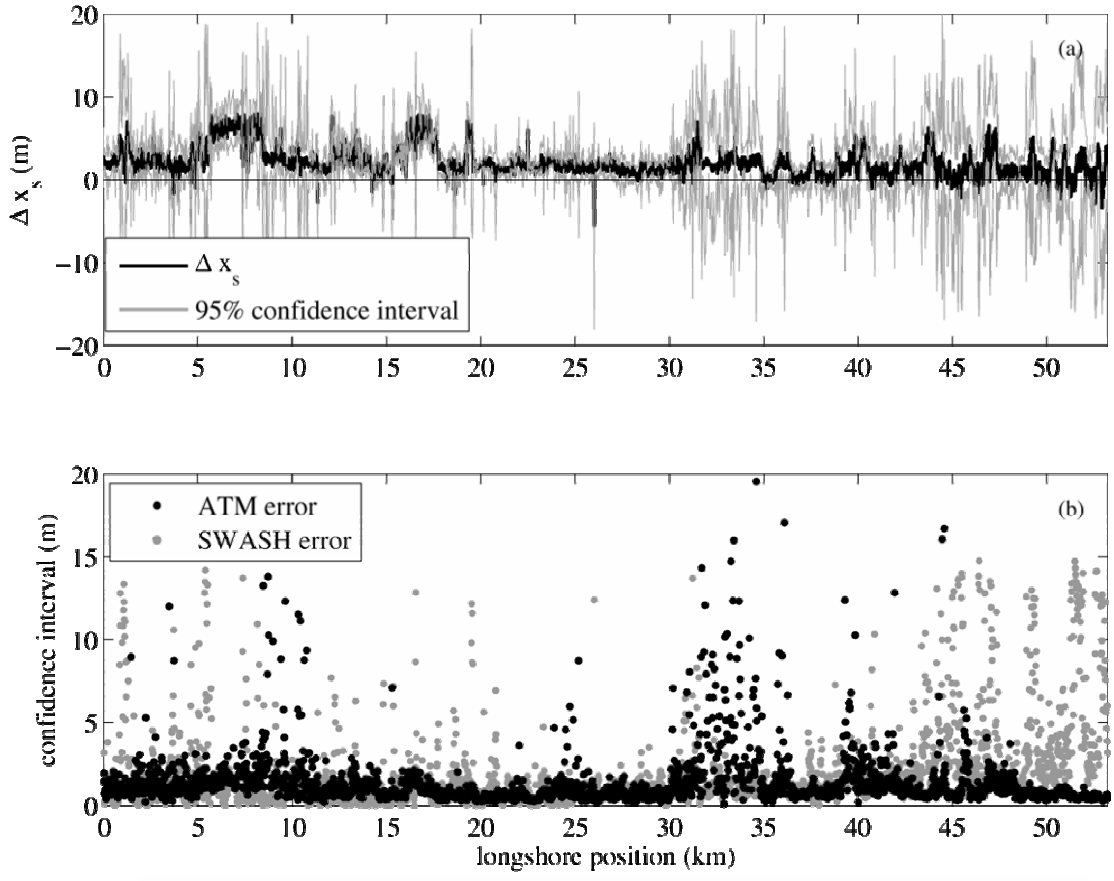

Figure 2.4. Longshore distribution of (a) differences between ATM and SWASH estimated shoreline positions, Δx_s, and (b) ATM and SWASH error bars for September 26, 1997 in Duck, NC. The mean horizontal error bar for x_{s_swash} was ± 1.7 m, and the mean horizontal error bar, $\overline{\delta_x}$, for x_{s_atm} was ± 1.4 m.

Figure 2.4b shows the longshore structure of the individual error bars for each system. The mean horizontal error bar, $\overline{\delta_x}$, for x_{s_atm} was ± 1.4 m. These error bars represent the random noise of the system and robustness of the data used in the regression. For the lidar-derived shorelines, the largest error bars occur on profiles where only three data points were used in the regression and the R^2 value of the regression was low. This occurred in areas of low data density where there were an insufficient number of lidar data points to clearly define the foreshore. The mean error bar for x_{s_swash}, based on assumptions of the typical variations in β, was ± 1.7 m [*List et al.*, 2000]. For the SWASH system, error bars are calculated directly from slope and distance from the datum; hence, the error bars are larger on flatter beaches and in locations where the vehicle drove farther away from the datum.

Extensive comparisons of individual, raw ATM and SWASH data points reveal a mean vertical difference, $\overline{\Delta z_b}$, between the two of 8.7 cm [*Sallenger et al.*, 2003]. This vertical difference is thought to be primarily due to a low frequency drift inherent in both the ATM and SWASH GPS systems. This low-frequency drift is specific to GPS systems, in general, and is not particularly well understood or documented. Based on a mean GPS drift of 8.7 cm and a mean beach slope of 0.08, the site-specific, horizontal error attributable to low frequency drift is on the order of ±1 m. (This horizontal GPS drift error is separate from the system noise error discussed above.) Since the GPS drift error has been realized just recently, the amount of drift at different sites generally will not be known. Several tests of stationary GPS systems (separate from the lidar GPS equipment) have been performed in different parts of the country and reveal a low frequency vertical drift of 6 to 8 cm over an hour period [*Sallenger et al.*, 2003]. Based on this estimate, we feel the ±1 m horizontal drift error is a conservative estimate and may be smaller in some locations. The total vertical accuracy of the ATM system (15 cm) is a bulk estimate representing all potential error sources, including this GPS drift [*Sallenger et al.*, 2003]. Details of the comparisons between the raw data points and of the GPS drift can be found in Sallenger *et al.* [2003] and Krabill *et al.[2002]*.

The vertical offset between the raw ATM and SWASH data contains a trend that decreases to the north. In the southern region of the study area Δz_b = 12 cm while in the northern region Δz_b = 2 cm. In order to examine the robustness of the technique and the ideal, expected error in the absence of GPS low frequency drift, the longshore trend in vertical differences due to the drift was removed from the lidar elevation data. The corrected $x_{s\_atm}(y)$ was then compared to $x_{s\_swash}(y)$ which, for our ground truth study, represents the 'real' shoreline position. The corrected lidar-derived shoreline position closely agrees with the SWASH-derived shoreline with an rms difference, $(\Delta x_s)_{rms}$, of 1.49; however it is still somewhat seaward of the SWASH shoreline; $\overline{\Delta x_s}$ = 0.44 m. Reasons for this seaward bias are explained above.

2.4.2 Application to Shoreline Change

The technique for extracting shoreline position from lidar profiles was applied to laser altimetry data collected on Assateague Island in 1997 and 1998. Assateague Island is an undeveloped stretch of barrier island along the eastern shore of Maryland and Virginia (Figure 2.2, upper right). The moderately straight coastline is marked by areas of relatively high dunes alternating with low-lying areas that are frequently overwashed during large storm events. Shoreline position was measured over 60 km of coast from three lidar data sets. The first was collected on September 15, 1997 (1600 – 1900 GMT) before the start of the winter storm season. The second overflight was on February 9, 1998 (1600 - 1900 GMT), after the passage of two major northeaster storms when maximum wave heights exceeded 7 m [*Sallenger et al.*, 1999a]. Two months later on April 3, 1998 (2200 – 2300 GMT), a third survey was conducted that documented the initial recovery stage for the island.

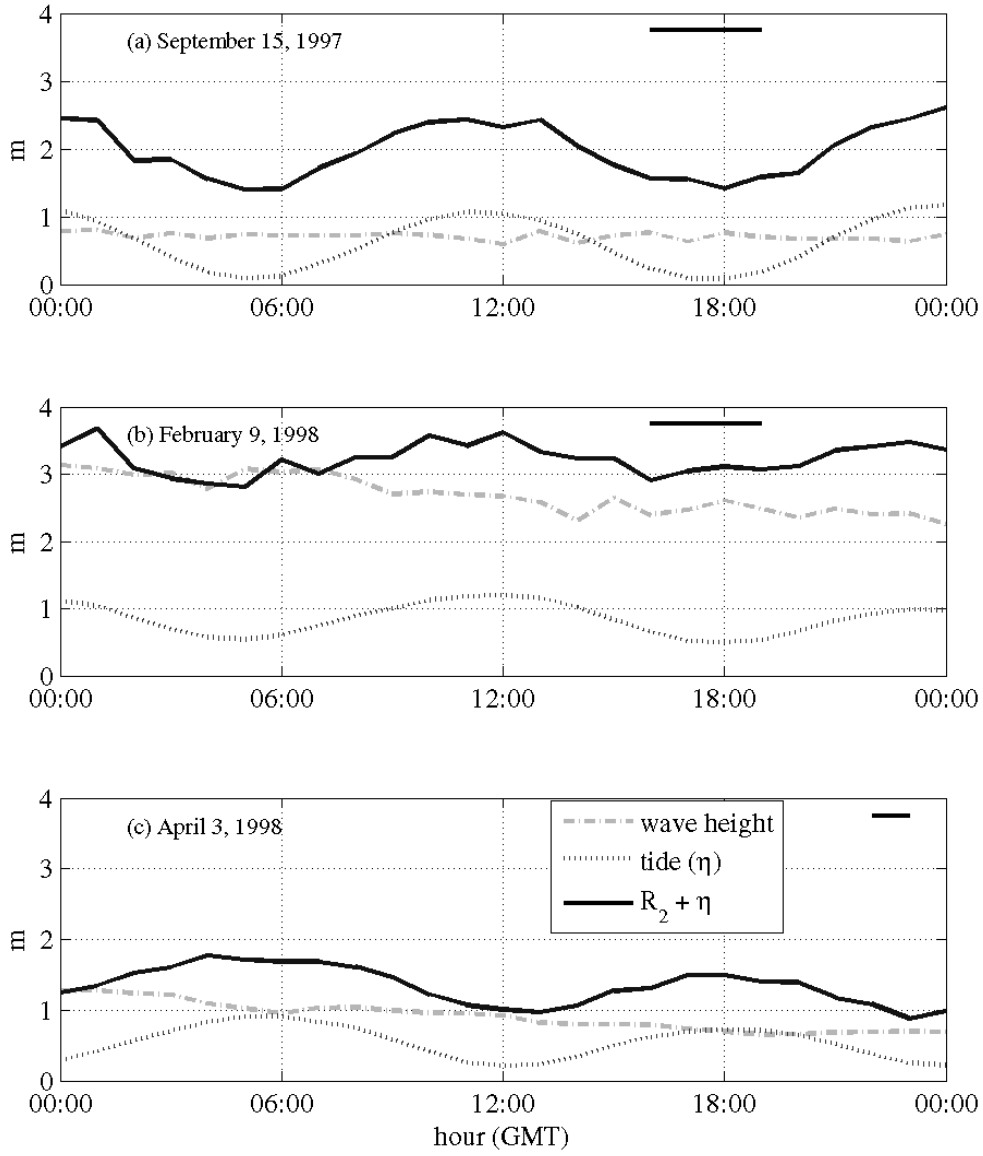

Figure 2.5. Wave height, tide level, and estimated total runup during the three Assateague lidar flights on (a) September 15, 1997, (b) February 9, 1998, and (c) April 3, 1998. Total runup elevation of February 9, 1998 was much higher than during the other two flights, making the extraction of the MHW contour (z = 0.31 m) very difficult on this day. The solid horizontal bar in each panel indicates the time during which the lidar data were collected.

The tide level and wave conditions during the February 9, 1998 ATM flight were much higher than conditions during the other two surveys (Figure 2.5). In order to

quantitatively assess whether the MHW contour was seriously contaminated by wave runup on the February 9, 1998 profiles, the total water level (the tide level, η, plus the runup due to waves) was calculated for each survey date. The elevation of the total water level represents a maximum, not mean, total water level due to the superposition of wave crests. The 2% exceedence values runup estimates, R_2, were based on an empirical formulation of Holman [1986],

$$\frac{R_2}{H_s} = 0.83\xi_0 + 0.2, \text{ where} \tag{2.1}$$

$$\xi_0 = \frac{\beta}{\sqrt{H_0 / L_0}}, \tag{2.2}$$

ξ_0 is the Iribarren number, and L_0 is the deep-water wavelength. Foreshore beach slope, β, was measured from each lidar profile. Data on wave height and period were obtained from NDBC station 44009 located outside of Delaware Bay. Tide data were obtained from NOAA tide gauge 8570283 located near Ocean City Inlet, Maryland. Wave heights and tide levels during the February 9, 1998 survey (H_0 = 3.0 – 2.5 m) were both greater than that during the other two surveys (H_0 ~ 0.7 m on September 15, 1997 and H_0 ~ 1.0m on April 3, 1998). The total water elevation on February 9, 1998 during the lidar flight was 3.04 m, well above the elevation of MHW, 0.31 m NAVD88 (Figure 2.5b). Since the MHW datum was obscured in the February 9, 1998 data by elevated tide levels and large wave runup, z_s extracted for the Assateague data set was 0.81 m (0.5 m above MHW), which still lies on the active foreshore of the beach.

Shorelines were calculated from all three data sets along the 60 km stretch of beach at profiles spaced 10 m in the longshore. (The 10 m spacing was selected for a different application of the data in which smaller scale shoreline features were studied.) Figure 2.6 illustrates two example profiles from September 1997 and February 1998. The large scatter seaward of x = 550 m is due to the reflection of the laser off of the water's surface. Since data passes are combined, the surface appears more like noise than actual waves. Along this profile, a well-defined berm was completely eroded and the shoreline recessed 32.4 ± 0.8 m. (Note: The 95% confidence intervals on measures of shoreline change

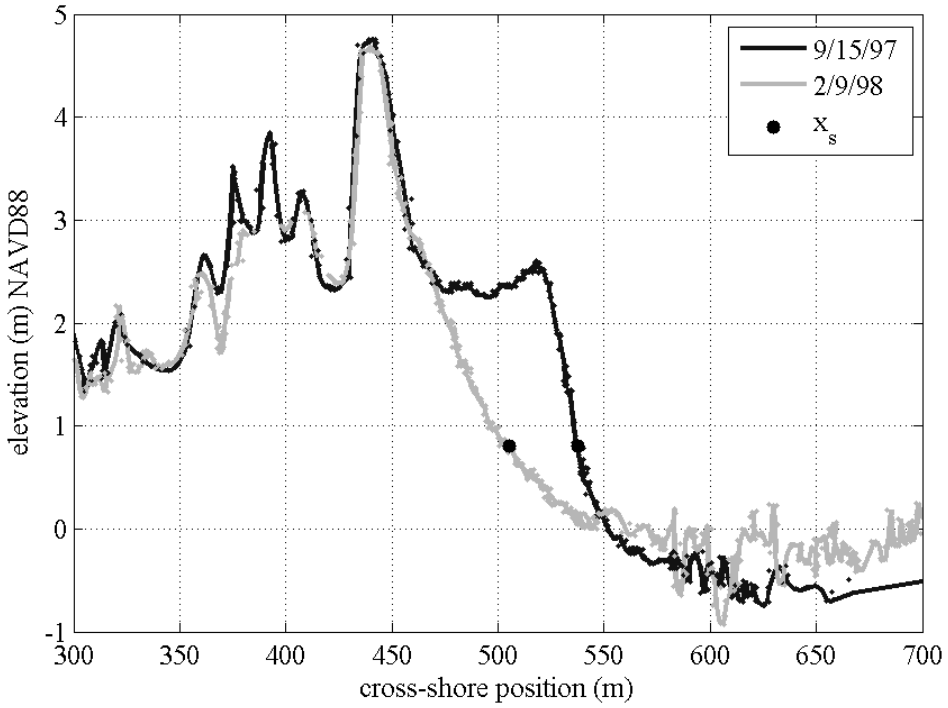

Figure 2.6. Example lidar profiles for Assateague Island from September 15, 1997 (black line) and February 9, 1998 (gray line). The large solid symbol indicates the location of the 0.81 m contour (MHW + 0.5m). The 95% confidence intervals on each estimate are ± 0.28 m and ± 0.75 m, respectively. Noisy data located offshore of x = 550 m are laser returns off of the water's surface. A prominent beach berm is shown to have eroded away during the winter's northeaster storms. The mean shoreline erosion along this profile was 32.4 ± 0.8 m.

represent statistical error bars associated with the regression. The instrument (lidar) bias is not included.)

Shoreline change was computed for all 5730 profiles between September 1997 and February 1998 (Figure 2.7, black line) to examine the spatial variability of the response of the beach to the extreme storm events on January 28, 1998 and February 5, 1998. Error bars, indicating the 95% confidence interval about each estimate of shoreline change, were calculated as the RMS of the combined variance of the two individual measures of shoreline position. The mean shoreline change indicates approximately 28.6 ± 0.02 m of erosion; however, there is substantial spatial variability in the data (standard deviation of shoreline change, $\sigma(\Delta x_s)$, = 16.2 m), ranging from nearly no net change to a maximum of ~150 m of erosion.

The shoreline position calculated from the April 1998 data set shows that the post-storm beach had started to recover to the pre-storm conditions (Figure 2.7, gray line). The mean shoreline change during this two-month recovery period was approximately 13.5 ± 0.02 m of accretion ($\sigma(\Delta x_s)$ = 11.0 m). Both storm and recovery curves of shoreline change show the same order of longshore variability and the same general pattern. This is shown by a negative correlation between the two shoreline change curves with an R^2 value of 0.27, which is significant for the 95% confidence interval (N = 5170, R^2_{sig} = 0.001). This spatial pattern of erosion and accretion was not documented until recently along the Outer Banks, North Carolina and Cape Cod, Massachusetts by List and Farris [1999]. The advent of the lidar system makes it possible to reveal this type of behavior over large areas and provides a mean to study the longshore variability of coastal change.

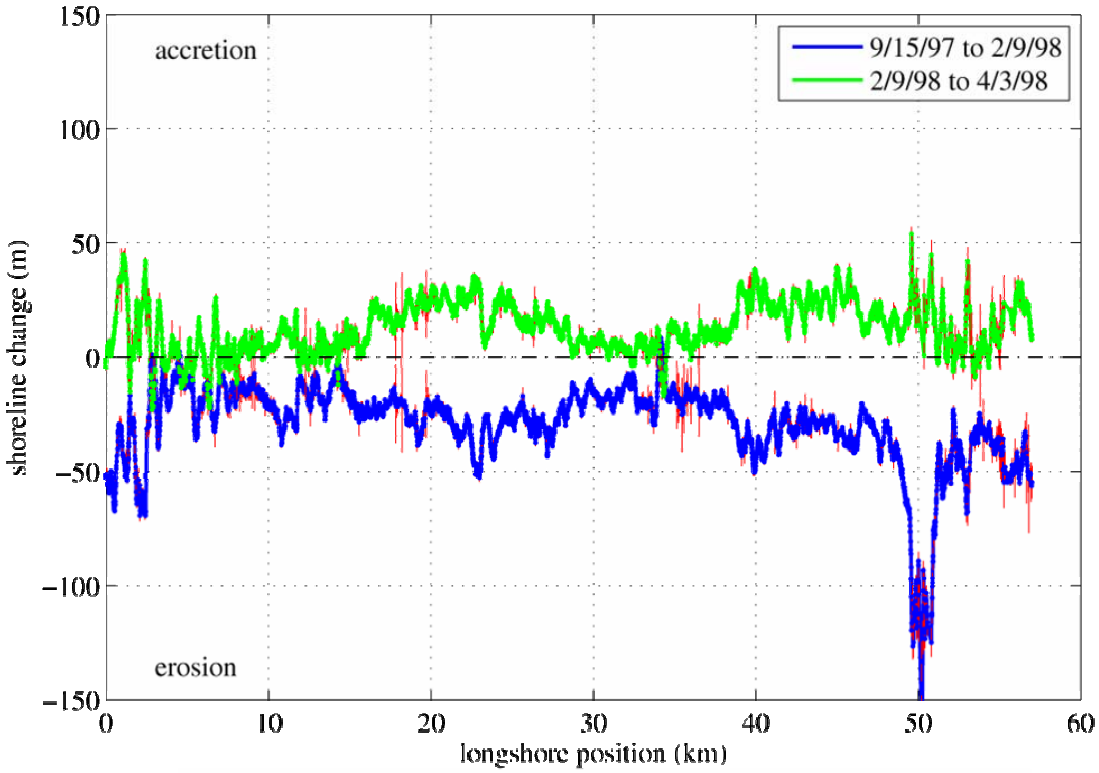

Figure 2.7. Shoreline change for Assateague measured from lidar-derived shorelines. Shoreline change between September 15, 1997 and February 9, 1998 (black line) shows mean erosion of 28.6 ± 0.02 m with a large amount of longshore variability. Shoreline change measured between February 9, 1998 and April 3, 1998 shows mean accretion of 13.5 ± 0.02 m with similar longshore variability. Vertical error bars indicate the 95% confidence interval about each estimate of shoreline change.

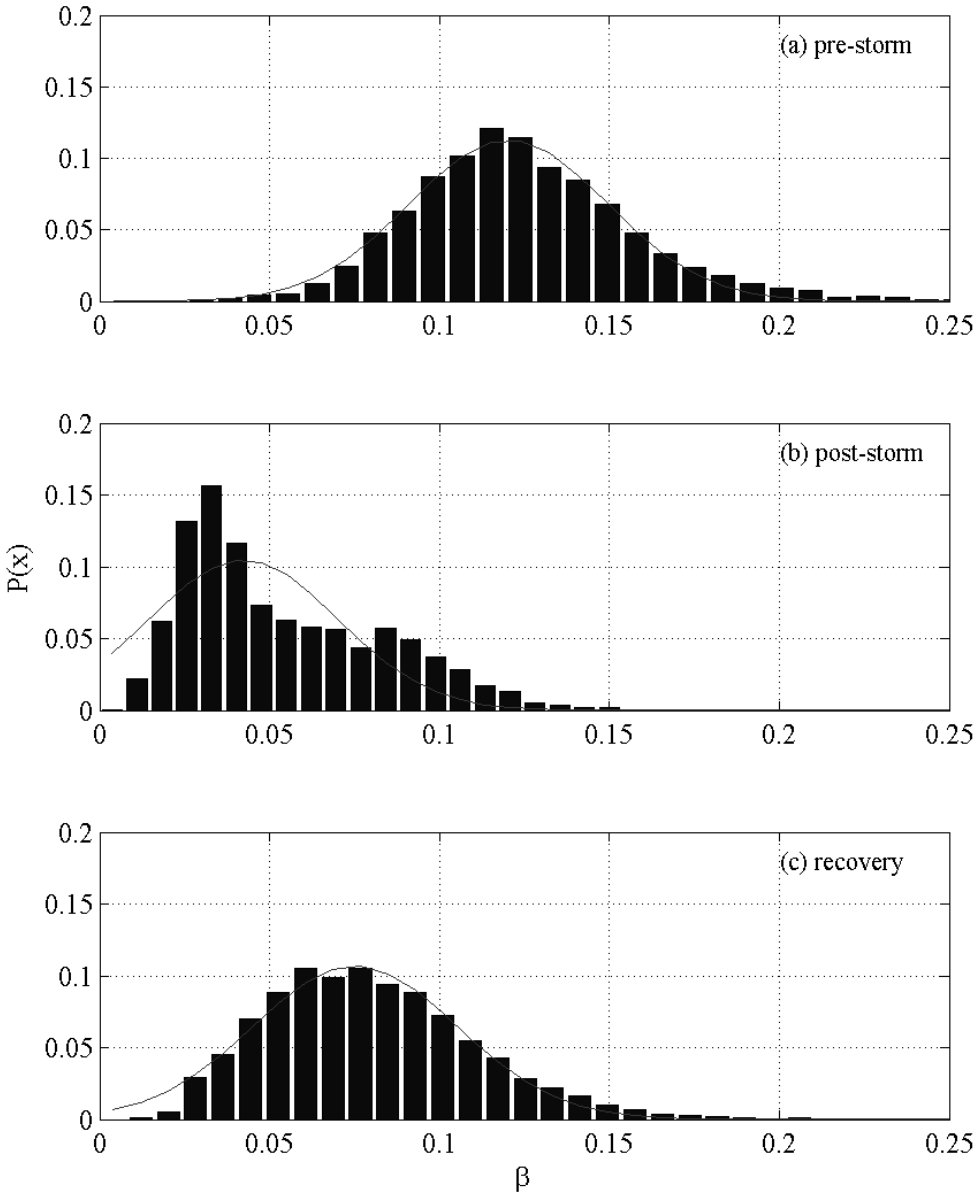

Figure 2.8. Probability density functions of Assateague beach slope measured using lidar data from (a) September 15, 1997, (b) February 9, 1998, and (c) April 3, 1998. The normally distributed pre-winter beach slopes (a) are shown to significantly flatten out after the winter storms (b). The beach recovery can be seen in the increasing beach steepness measured in April (c).

Another measure of beach morphology that can be easily obtained from the laser altimetry data is beach slope, β, calculated from the regression in the shoreline extraction technique. The spatially-dense data allow the measure the spatial variation of beach slope over large areas. Figure 2.8 presents three probability density functions of beach slope calculated along Assateague Island from lidar data. The pre-winter beach slopes (Figure 2.8a) are normally distributed with a mean value, $\overline{\beta}$, of 0.13 (standard deviation of β, σ(β), = 0.034). After the winter's northeaster storms, the slopes were reduced significantly, $\overline{\beta}$ = 0.054 (σ(β) = 0.029), as the beach responded to large wave events (Figure 2.8b). The April 1998 slope distribution reveals that the beach is slowly recovering as indicated by the steepening slopes, $\overline{\beta}$ = 0.08 (σ(β) = 0.032), and the increasingly Gaussian distribution (Figure 2.8c). While these observations are not unexpected, the collection of such an extensive set of slope and shoreline data at such high accuracy is unprecedented.

2.5 Discussion

There are many research and practical management applications for lidar-derived shoreline positions. As previously discussed, lidar shorelines can be used to study the large-scale impacts of storms on beaches. Accurate measures of large-scale, storm-induced beach change, with confidence intervals, can be determined using lidar surveys collected before and after storm events (i.e. Figure 2.7). Beach recovery can also be examined using lidar data collected some period after the passage of the storm. Profiles that are very closely spaced in the longshore will make full use of the dense three-dimensional lidar data and can be used to resolve smaller scale details of beach topography and morphologic change. Multiple lidar shorelines from one location can also be used to determine the natural variability of the shoreline position.

Studies of long-term, large-scale shoreline change are another possible use for the lidar shorelines. Accurate rates of shoreline change are of great interest today to coastal scientists, engineers, and planners. A set of profiles extracted from lidar data collected

during calm weather conditions can be used to quickly and accurately determine the location of the shoreline. The shoreline can be compared to historical shoreline positions as measured from photographs or maps to calculate rates of shoreline change.

When considering the different uses for lidar-derived shorelines, the proper selection of the vertical datum becomes important. One of the major advances of the technique discussed in this paper is that subjectivity is removed from shoreline determination since the exact location of any vertical datum for the shoreline (MHW, MHHW, etc.) can be easily and accurately found. The specific datum selected depends on the ultimate use of the lidar-derived shorelines. If the lidar shorelines will be compared to historical shorelines measured as wet/dry lines from aerial photographs or maps, then a vertical datum that may serve as a proxy for the digitized wet/dry line should be selected. However, such a vertical datum is not clearly defined making it difficult to quantify the precise elevation of wet/dry line (see previous discussion). If lidar shorelines are to be used in conjunction with contour-based shorelines measured from ortho-rectified photographs or ground surveys, then the same shoreline datum should also be used to define a lidar shoreline. With this technique any relevant datum can be extracted from the data and used to study coastal change.

In order to obtain the most accurate estimate of the horizontal location of the shoreline datum, it is important to have dense sampling of the foreshore region. The largest error bars on shoreline location occur along profiles with sparse data due to poor lidar returns. This problem could be improved by creating wider cross-shore profiles using a larger swath region, perhaps ± 2 m.

For this technique to produce accurate estimates, it is essential that the data be collected during low tide and times of low wave energy. High tides, large waves, storm surge, and run-up may obscure the location of the vertical datum, z_s, particularly if the datum is very low on the beach face (i.e. MHW). If z_s lies beneath the water surface or the effect of waves and run-up, it may be necessary to look at changes occurring at a datum higher on the beach face. However, if a specific shoreline datum, such as MHW,

is required, it may be possible to extrapolate to identify the cross-shore location of the shoreline, x_s, using methods similar to List *et al.* [2000]. Future work includes expanding this technique to allow for extrapolation to the location of the shoreline datum.

We recognize that reducing the lidar data set to profiles to find shorelines is not the only way to extract the shoreline position from the data. Other research groups [e.g.*Revell et al.*, 2002] locate the position of the shoreline by extracting a contour from previously gridded data. While shorelines from these traditional gridding techniques are commonly used and accepted, they do not readily allow for confidence intervals to be placed on the estimates of position. This will ultimately limit the applicability of the shoreline data and subsequent measures of shoreline change. Future work will examine alternate gridding techniques, such as the quadratic loess smoother, which produce error surfaces in addition to the gridded field [*Schlax and Chelton*, 1992]. The error surface can then be used to place confidence intervals on measures of shoreline and beach volume change derived from these grids.

2.6 Conclusion

An objective technique has been developed for the extraction of accurate and detailed shoreline position from ATM laser data. The data from one ATM flight can provide estimates of shoreline position spaced as closely as several meters in the longshore and over large expanses (hundreds of kilometers) of coastline. While the extensive record length of historic topographic maps and aerial photographs provides a rich data set for measuring long term shoreline change, the precision and accuracy of the lidar shorelines allow for more reliable measurement of shoreline change over shorter time periods. Lidar shorelines can be also used to establish more accurate shoreline positions for future monitoring of long-term shoreline trends.

Lidar profiles are extracted from the full three dimensional data set and a linear regression is fit to the data points within a specified range about the vertical shoreline elevation. The function is evaluated at the vertical datum to determine the cross-shore location of shoreline position. Foreshore beach slope is measured directly from the linear

fit. Error bars on shoreline position represent the 95% confidence interval on each estimate based on the Student's t distribution of the errors of the regression. The accuracy of the lidar-derived shoreline was tested by comparing it to a shoreline measured using ground-based GPS techniques. The ground-based SWASH method and air-based ATM method agree closely with an rms difference of 2.9 m (1.49 m excluding a GPS drift). The longshore-averaged horizontal error bar for shorelines extracted from lidar data was ± 1.4 m for the Outer Banks and ± 1.1 m for Assateague Island.

To illustrate the power of this technique, lidar-derived shorelines were used to assess large-scale coastal change after the winter's northeaster storms along Assateague Island. After the storms, the mean shoreline change along the 60 km stretch was -28.6 ± 0.02 m with a large degree of alongshore variability, $\sigma(\Delta x_s)$, = 16.2 m. Shorelines measured from a survey collected after a two-month recovery period reveal 13.5 ± 0.02 m of accretion ($\sigma(\Delta x_s)$ = 11.0 m). The longshore variability and distribution of beach slopes are also revealed in the lidar data. The technique showed that the mean beach slope decreased from 0.13 to 0.054 over the study area. The beach was shown to start recovering from the winter's storms as the distribution of beach slope became increasingly Gaussian and the mean value increased from 0.054 to 0.08. Using the lidar-derived shorelines, the longshore variability in the large-scale response of the coastline to storms can be accurately quantified which may lead to a more complete understanding of large-scale coastal processes.

2.7 Acknowledgments

The success of the lidar investigations is possible because of a cooperative effort between NASA (Solid Earth and Natural Hazards Program), NOAA and the USGS (Coastal and Marine Program) and the help of many talented researchers. We would like to thank W. Krabill, S. Manizade (NASA), R. Swift, and J. Sonntag (EG&G, Wallops Island) for collecting and post-processing the data. K. Hanson, J. Brock, K. Guy (USGS, St. Petersburg), P. Howd (USF, St. Petersburg), and K. Weber (USGS, Woods Hole) offered valuable insight into lidar data processing and manipulation. We would like to

thank A. Farris (USGS, Woods Hole) for helping us to compare GPS ground survey data to lidar data. We are especially grateful to A. Meredith (Coastal Services Center) and K. Morgan (USGS, St. Petersburg) for their instrumental contributions to lidar data processing and profile extraction. This work was funded by the U. S. Geological Survey, Coastal and Marine Geology Program as a part of the National Assessment of Coastal Change Hazards.

3.0 EMPIRICAL PARAMETERIZATION OF SETUP, SWASH, AND RUNUP

3.1 Abstract

Using shoreline water-level time series collected during 10 dynamically diverse field experiments, an empirical parameterization for extreme runup, defined by the 2% exceedence value, has been developed for use on natural beaches over a wide range of conditions. Runup, the height of discrete water-level maxima, depends on two dynamically different processes; time-averaged wave setup and total swash excursion, each of which is parameterized separately. Setup at the shoreline was best parameterized using a dimensional form of the more common Iribarren-based setup expression that includes foreshore beach slope, offshore wave height, and deep-water wavelength. Significant swash can be decomposed into the incident and infragravity frequency bands. Incident swash is also best parameterized using a dimensional form of the Iribarren-based expression. Infragravity swash is best modeled dimensionally using offshore wave height and wavelength and shows no statistically significant linear dependence on either foreshore or surf-zone slope. On infragravity-dominated dissipative beaches, the magnitudes of both setup and swash, modeling both incident and infragravity frequency components together, are dependent only on the offshore wave height and wavelength. Statistics of predicted runup averaged over all sites indicate a -17 cm bias and an rms error of 38 cm; the mean observed runup elevation for all experiments was 144 cm. On intermediate and reflective beaches with complex foreshore topography, the use of an alongshore-averaged beach slope in practical applications of the runup parameterization may result in a relative runup error equal to 51% of the fractional variability between the measured and the averaged slope.

3.2 Introduction

When ocean waves approach a coast, the majority of wave energy is dissipated across the surf zone by wave breaking. However, a portion of that energy is converted to potential energy in the form of runup on the foreshore of the beach [*Hunt*, 1959]. This

wave runup is important because it deliver much of the energy responsible for dune and beach erosion [*Ruggiero et al.*, 2001; *Sallenger*, 2000]. Thus, understanding the magnitude and longshore variability of extreme runup is critical to accurate prediction of the impacts on protective dunes and adjacent properties. The goal of this work is to devise a simple parameterization for maximum runup elevation, improving upon an earlier empirical formula for wave runup by Holman [1986]. These elevations, in turn, can be used as input into a storm-impact model [*Sallenger*, 2000].

In the discussion below, it will be apparent that wave height, H, deep-water wave length, L_0, wave period, T, and beach steepness, β, form a commonly-accepted environmental parameter set. Of these, deep-water wavelength and period are assumed to be interdependent, linked by the linear dispersion relationship,

$$L_0 = \frac{gT^2}{2\pi}. \tag{3.1}$$

The three independent parameters may provide a first-order description of a beach environment and are often expressed in terms of a non-dimensional surf similarity parameter, the Iribarren Number [*Battjes*, 1974],

$$\xi = \frac{\beta}{\left(H/L_0\right)^{1/2}}. \tag{3.2}$$

The Iribarren Number can be interpreted as a dynamic beach steepness, comparing the beach slope to the square root of deep-water wave steepness.

In early laboratory experiments of monochromatic waves on planar beaches, all quantities were well defined. However, application of this scaling to natural beaches introduces several complications. For random waves, both wave period and wave height become statistical measures, often described by the peak period, T_p, and the root mean square (rms) or significant wave height, H_{rms} or H_s, (defined as 2.8 and 4 times the standard deviation of the time series of sea-surface elevation, respectively). Additionally, wave-height measures can be expressed in deep water (H_0), at the break point (H_b), or locally. Definition of a single beach slope becomes difficult on natural beaches with typically concave profiles and is further complicated by the common presence of offshore

sandbars. Estimation of runup statistics under these complicated conditions may be handled by appropriate numerical models along with knowledge of boundary conditions [*Raubenheimer and Guza*, 1996; *Raubenheimer et al.*, 1995] such as the directional wave spectra and bottom bathymetry. However, such an approach is incompatible with most applications because the details of the offshore profile and incident spectra are not always available. Therefore, we will investigate the degree to which simple parameterizations provide useful predictions of extreme runup on natural beaches.

3.3 Background

Runup, $R(y, t_i)$, is defined here as the set of discrete water-level elevation maxima (Figure 3.1a) measured on the foreshore, with respect to the still water level (that which would occur in the absence of waves). The values of runup depend on the longshore location, y, time, t, and the discrete times of maxima, t_i. Runup results from two dynamically different processes: (1) maximum setup, $<\eta>(y)$, the time-averaged water-level elevation at the shoreline, and (2) swash, $S(y, t_i)$, the time-varying, vertical fluctuations about the temporal mean (Figure 3.1a).

Setup, the super-elevation of the mean water level, is driven by the cross-shore gradient in radiation stress that results from wave breaking [*Longuet-Higgins and Stewart*, 1963; *Longuet-Higgins and Stewart*, 1964]. The relationships between setup and environmental conditions, and resulting expressions for setup at the shoreline, have been the topic of many research studies. Bowen et al. [1968] derived a simplified expression for setup by assuming normally incident shallow-water waves whose heights within the surf zone were limited to a constant fraction of the local water depth, $\gamma = H/h$. The resulting expression is

$$\frac{<\eta>}{H_b} = 0.38\gamma, \tag{3.3}$$

where H_b is the breaking wave height. Measured setup values were found to be greater than that predicted by theory due to the asymptotic approach of setup to the beach surface [*Bowen et al.*, 1968]. Examining data from gently sloping beaches of southern

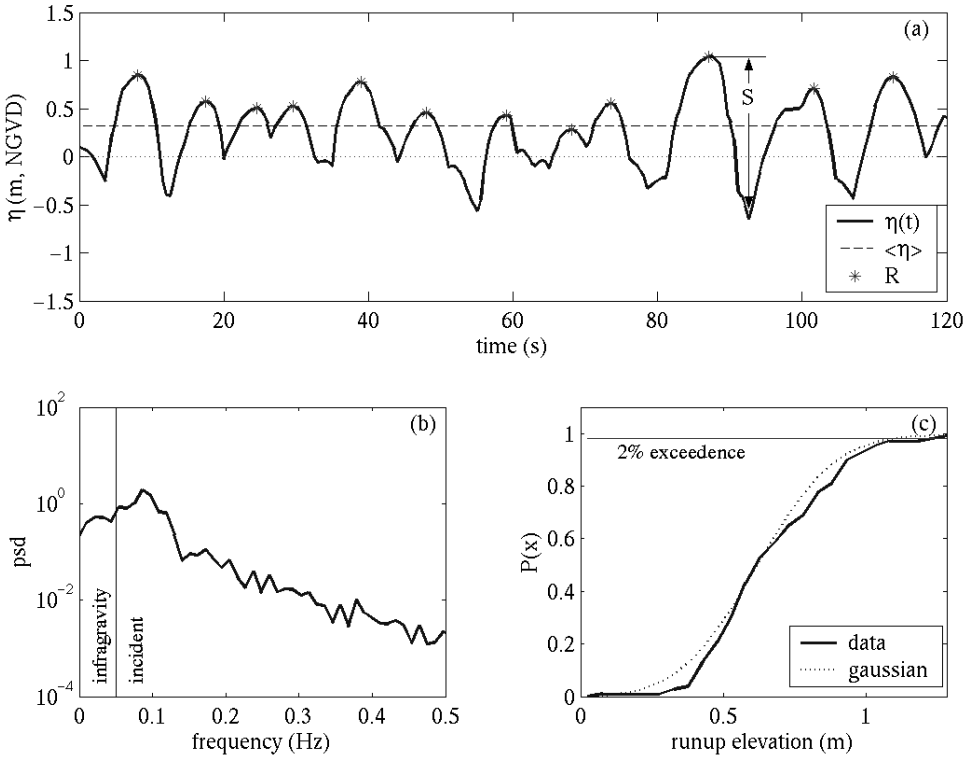

Figure 3.1. Water-level time series (a), extracted from timestack in Figure 3.2, indicating individual runup maxima, R, setup at the shoreline, $<\eta>$, and swash excursion, S. Significant swash statistics, S, were calculated from the spectra (b) of the water-level time series. The 2% exceedence value of runup, R_2, was calculated from the cumulative PDF of the discrete measures of R (c).

California, Guza and Thornton [1981] found $<\eta>$ to be proportional to the significant wave height (10-m depth), H_s, with a constant of proportionality equal to 0.17. In contrast, analysis of data from the steeper beach in Duck, NC [*Holman and Sallenger*, 1985] showed that a direct correlation between setup and wave height was highly scattered and that non-dimensional setup (normalized by offshore wave height) scaled better with the Iribarren number, ξ_0. The Guza and Thornton [1981] data were found to be consistent with the Holman and Sallenger [1985] relationship at low Iribarren numbers. While the Holman and Sallenger [1985] relationship between ξ_0 and $<\eta>$ significantly reduced the scatter in the data, there remained a tidal dependence. The relationship failed during the lowest tides when waves significantly dissipated over an offshore sandbar. Using observations of setup on beaches in Australia, Hanslow and

Nielsen [1993] found that the maximum setup on dissipative beaches showed no dependence on beach slope and, therefore, could not be scaled with ξ_0.

Swash, *S*, is generally defined as the time-varying location of the intersection between the ocean and the beach. According to Miche [1951], monochromatic waves are composed of two parts: a progressive component whose energy is dissipated during wave breaking and a standing, reflected component that has its maximum at the shoreline. Swash represents this standing component whose amplitude cannot exceed some critical value that is dependent on both β and T_0. Early studies on swash and runup were conducted in laboratories in order to determine the impacts of waves on structures. Based on Miche's ideas, Hunt [1959] stated that there is a critical wave steepness below which wave energy will be totally reflected by a beach with a planar slope. Under surging wave conditions there is little dissipation of wave energy across the beach slope, and the majority of the energy is reflected on the steep beach slope [*Hunt*, 1959]. For the more common situation of breaking waves, energy is dissipated across the surf zone. Using a critical value based on wave steepness and β [*Iribarren and Nogales*, 1949], which defines a threshold between breaking and non-breaking conditions, Hunt [1959] proposed an empirical formulation for vertical wave up-rush, *R*, that can be re-written in terms of ξ,

$$\frac{R}{H} = K\xi\,, \tag{3.4}$$

where Hunt assumes that $H \approx H_0$, and *K* is a constant.

Using field data collected from Duck, NC, Holman [1986] found a clear relationship between 2% exceedence value of runup, R_2, normalized by H_s (in 18-m depth) and ξ_0,

$$\frac{R_2}{H_s} = 0.83\xi_0 + 0.2\,, \tag{3.5}$$

which includes a linear dependence on the foreshore beach slope, β_f. For experiments on natural beaches, wave breaking over offshore sandbars can significantly attenuate offshore waves. Thus, coefficients from data gathered during a single experiment (such as in equation 3.5) may vary with sand-bar configuration and profile shape, introducing significant noise into empirical relationships. Baldock and Holmes [1999] found in

numerical simulations that incident band swash saturation was related to bore-driven swash, which also scales with wave period and beach slope.

The relationship between ξ_0 and the distribution of runup was examined on a wider range of Iribarren space by Nielsen & Hanslow [1991]. They found that the vertical scaling for runup distributions was proportional to ξ_0 for steep beaches, further supporting the original formulation of Hunt [1959], equation 3.4, and the empirical formulation of Holman [1986], equation 3.5. However, for beaches with $\beta < 0.1$, they suggest that the dimensional vertical scaling of runup distributions may be independent of beach slope and proportional to $(H_0L_0)^{1/2}$ [*Nielsen and Hanslow*, 1991]. The behavior of swash on a highly dissipative beach ($\xi_0 < 0.25$, $\beta < 0.02$) was studied by Ruessink et al. [1998] who found that the swash signal was dominated by energy in the infragravity band (frequencies, f, < 0.05 Hz) and scaled with H_0. Ruggiero et al. [2001] also studied runup under highly dissipative conditions and found that the elevation of R_2 scaled best with H_0 and with $\beta^{1/2}$, rather than β as implied by relationships between runup and ξ_0.

Several studies have examined the relative roles of infragravity and incident ($f > 0.05$ Hz) band swash (S_{IG} and S_{inc}, respectively) for particular field sites. Guza and Thornton [1982] showed that infragravity swash height increases linearly with offshore significant wave height, while energy in the incident band becomes saturated due to dissipation across the surf zone. This linear dependence of S_{IG} on H_0 has been confirmed by several other studies [*Holman and Bowen*, 1984; *Howd et al.*, 1991; *Raubenheimer and Guza*, 1996]; however, the constants of proportionality were found to vary between sites and with the wave and beach conditions present during each experiment. Howd et al. [1991] examined the relationship between infragravity motions at the shoreline and offshore wave height at a number of field sites and found their ratio to be dependent on ξ_0: larger constants of proportionality between infragravity motions and wave heights were observed on beaches with larger ξ_0 values. Ruessink et al. [1998] noted that the literature presents a wide range of constants of proportionality for the ratio S_{IG}/H_0, particularly between dissipative and reflective beaches, also suggesting that the ratio may depend on ξ_0.

Based on the previous studies described above, we propose the following general relationship for the elevation of extreme (2%) runup, R_2, for any data run:

$$R_2 = <\eta> + \frac{S}{2}, \text{ where} \tag{3.6}$$

$$S = \sqrt{(S_{inc})^2 + (S_{IG})^2}\ , \text{ and} \tag{3.7}$$

$$<\eta>, S_{inc}, S_{IG} = f(H_0, T_0, \beta_f)$$

where T_0 is the deep-water wave period. The specific goal of this work is to improve the predictive equation for runup on natural beaches by extending Holman's original analysis [1986] to data sets from 10 experiments representing a wide variety of beach and wave conditions and by separately parameterizing the individual runup processes: setup and swash.

In the next section we describe our methods including details of the runup and swash statistics, the environmental parameters measured at each site, and the specific field experiments. Next, we present the results of our analysis, showing the parameterization of setup, incident swash, and infragravity swash, and evaluate the performance of the empirical parameterizations. The consequences of a longshore variable-topography on the parameterizations are also examined. In the discussion section, the use of breaking wave height and surf zone slope in the model, as alternatives to H_0 and β_f, is evaluated. Finally, improved parameterizations for setup and swash under dissipative conditions are presented.

3.4 Methods

3.4.1 Runup Measurement Technique and Statistics

All runup data in this study were collected using optical techniques developed in the Coastal Imaging Lab at Oregon State University and previously tested extensively against in-situ runup instruments [*Holland et al.*, 1995; *Holman and Guza*, 1984]. Holman and Sallenger [1985] discussed the difficulties with digitizing faint downwash, particularly on

very low-sloping beaches. While variations in digitization can introduce noise in swash and setup statistics, Holman and Sallenger showed that they did so in a way that cancelled when runup peak elevations were found; slight lows in swash height were balanced by highs in set-up, and visa-versa. Other errors associated with video runup measurements are discussed in detail by Holman and Guza [1984] and Holland et al [1995]. The video pixel resolution, dependent on the field of view of the camera, the height of the camera, and the distance to the observed ground location [*Holland et al.*, 1997], was typically 5 – 15 cm in the vertical with corresponding horizontal resolutions of 20 – 80 cm.

Cross-shore transects of pixel intensity (example from Duck, NC, Figure 3.2a) were sampled at 1 or 2 Hz over 17- to 120- min record lengths, depending on the site. This created timestacks of pixel intensity on which runup and rundown can be seen as a white edge moving back and forth in the swash zone (Figure 3.2b). The leading edge of runup was digitized from cross-shore timestacks of pixel intensity and then, using published photogrammetric relationships [*Holland et al.*, 1997], was converted to time series of water level elevations measured relative to mean sea level. For each experiment, 17-min records were extracted from the longer time series to minimize the effects of changing tide levels on the location of wave breaking and on the area of the foreshore over which swash propagates. In order to calculate wave setup, measured tidal curves were removed from each time series. All statistics presented are representative of elevations measured relative to the still-water level.

Both continuous and discrete statistics were calculated from raw time series (Figure 3.1a). After subtraction of the setup, $<\eta>$, the 17-min time average, swash statistics were calculated from the spectra, *PSD(f)*, of the continuous water-level time series (Figure 3.1b). The significant swash height, *S*, was calculated as,

$$S = 4 * \sqrt{\sum PSD(f)df}\ , \tag{3.8}$$

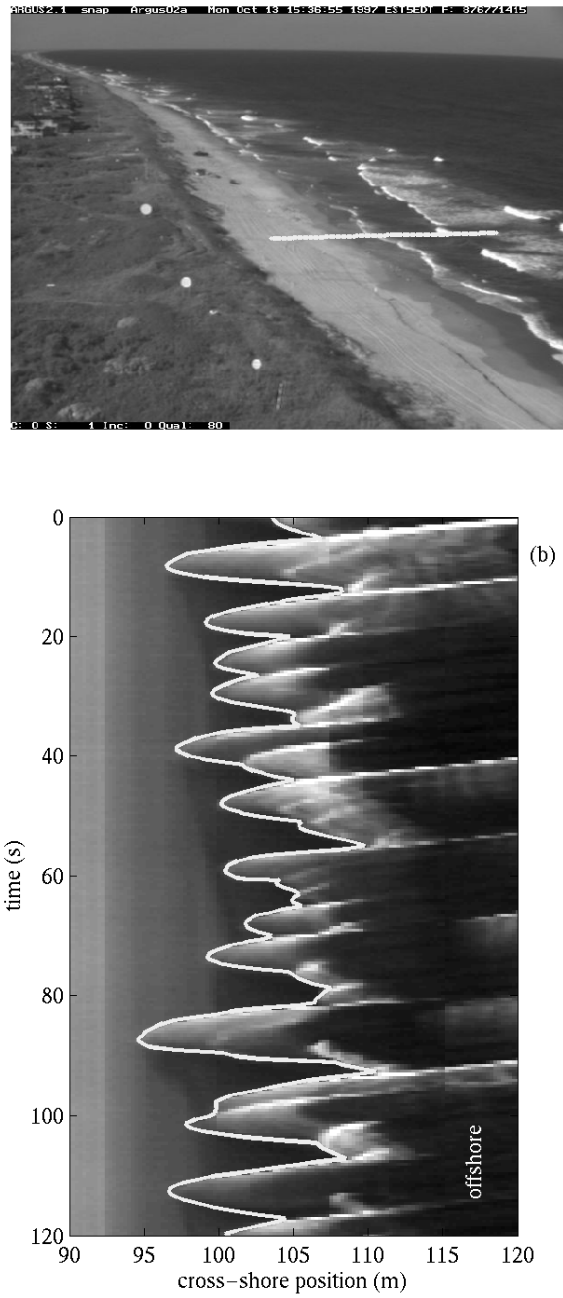

Figure 3.2. Camera view from Duck, NC (a) and runup timestack (b). The cross-shore transect in (a) indicates the location of a single runup array. In the 120-second timestack of pixel intensity (b), each horizontal slice is the spatial variability of intensity at a single time step. The leading edge of swash is digitized through time (heavy, white line) and then converted into a time series of water-level elevations.

similar to the calculation of significant wave height [*Guza and Thornton*, 1980]. The significant swash in the incident (distinction based on wave frequency, $f > 0.05$ Hz, and not on direction of propagation) and infragravity ($f < 0.05$ Hz) bands were calculated by summing only over frequencies within the specified limits.

Runup statistics, R, were defined as the elevation of individual water-level maxima above the still-water level (Figure 3.1a), merging contributions from setup and swash (equation 3.6). The 2% exceedence value for runup, R_2, was calculated from the cumulative probability density function of runup elevations (Figure 3.1c). This statistic, which represents the value of R that will be exceeded 2% of the time, is often used in engineering applications [*Holman*, 1986] and may be important for use in scaling the impacts of severe storms on beaches [*Ruggiero et al.*, 2001].

3.4.2 Environmental Parameters

To make comparisons between sites where wave heights were measured in water depths varying between 7 and 20 m, an effective deep-water significant wave height, H_0, was calculated. To estimate H_0 during each water-level time series, measurements of significant wave height from local buoys and instrument arrays, H_s, were reverse shoaled to deep water using linear wave theory assuming a shore-normal approach. While this procedure neglects local generation, friction, white-capping, refraction, and diffraction, it allows for inter-comparisons of deep-water equivalent wave heights between different field sites. Breaking wave height, H_b, was calculated by shoaling H_s over local bathymetry using Thornton and Guza's [1983] wave transformation model, with the limiting ratio $\gamma = H_{rms}/h$ equal to 0.42 [*Thornton and Guza*, 1982] and the bore dissipation coefficient, B, equal to 1.0. While B was not tuned due to lack of appropriate field observations at each site, model error has been shown to be less than 10% when B is within 25% of its optimal value [*Thornton and Guza*, 1983]. H_b was defined as the wave height occurring at the onset of wave breaking, identified as the seaward-most location where dissipation exceeded 20 W/m^2. Alternatively, the cross-shore location of breaking and H_b may be defined by the percent of waves breaking.

For each water-level time series, β_f was defined as the average slope over a region $\pm 2\sigma$ around $<\eta>$, where σ is the standard deviation of the continuous water level record, $\eta(t)$. Surf zone slope, β_{sz}, is also considered here and was defined for each timestack as the slope between the mean shoreline (the cross-shore position of $<\eta>$), x_{sl}, and the cross-shore location of wave breaking, x_b. On barred profiles, the magnitude of β_{sz} may change significantly over the course of a day as the break point shifts from the sandbar at low tide toward the shoreline at high tide. These cases will be of special interest when trying to isolate the relative importance of foreshore and surf-zone slope.

3.4.3 Field Experiments

Swash and runup data from 10 field experiments were compiled for this study: Duck, North Carolina, USA (1982, 1990, 1994, 1997); Scripps Beach, California, USA (1989); San Onofre, California, USA (1993); Terschelling, the Netherlands (1994, 1994); Gleneden, Oregon, USA (1994); and Agate Beach, Oregon, USA (1996). Table 3.1 provides details of experiment dates, mean wave and beach conditions (calculated over the durations of each experiment), as well as the number of runup measurements collected. The beach and wave conditions during these experiments represent a full range of ξ_0 with Terschelling and Agate Beach representing the dissipative end ($\xi_0 < 0.3$) and San Onofre representing the most reflective conditions (mean Iribarren number, $\overline{\xi_0}$, =2.2). Mean beach profiles, averaged over the duration of each experiment, illustrate the differences in beach slope and offshore bathymetry (Figure 3.3).

The bulk of the data (91%) was collected at the U.S. Army Corps of Engineers Field Research Facility (FRF) in Duck, NC, and represents intermediate to reflective conditions (as defined by Wright and Short [1983], $0.3 < \xi_0 < 4.0$). The typical profile at Duck is characterized by an offshore sandbar and a mean foreshore slope of 0.1. H_s and T_0 were recorded hourly with a Waverider buoy located in ~18 m of water. Tide level was measured every 6 min at a NOAA tide gauge mounted at the end of the FRF pier. Bathymetry was sampled roughly daily during the Duck experiments in 1990, 1994, and

Table 3.1.: Average environmental conditions for each experiment.

Site	*Date*	$\overline{H_s}(m)$	$\overline{T_0}(s)$	$\overline{\beta_f}$	$\overline{\xi_0} \pm \sigma$	N (N_{single})
Duck, NC (Duck82)	5-25 Oct 1982	1.7	12.0	0.11	1.4±0.5	149 (36)
Scripps Beach, CA	26-29 Jun 1989	0.7	10.0	0.04	0.6±0.1	42 (41)
Duck, NC (Delilah)	6-19 Oct 1990	1.5	8.9	0.10	0.9±0.4	1829 (138)
San Onofre, CA	16-20 Oct 1993	0.8	14.9	0.10	2.2±0.3	59 (59)
Gleneden, OR	26-28 Feb 1994	2.1	12.4	0.08	0.9±0.2	52 (42)
Terschelling, NL	2-22 Apr 1994	2.4	8.0	0.02	0.1±0.04	41 (6)
Terschelling, NL	1-21 Oct 1994	1.4	8.1	0.01	0.1±0.05	27 (8)
Duck, NC (Duck94)	3-21 Oct 1994	1.5	12.1	0.08	1.1±0.3	975 (52)
Agate Beach, OR	11-17 Feb 1996	2.5	13.2	0.02	0.2±0.05	126 (14)
Duck, NC (SandyDuck)	3-30 Oct 1997	1.3	9.5	0.10	1.2±0.7	491 (95)

$\xi_0 \pm \sigma$ - mean Iribarren number ± the standard deviation
N - number of individual estimates of runup statistics, includes multiple longshore lines
N_{single} - number of individual estimates of runup statistics used in bulk parameterization

1997 and every few days during the 1982 experiment using the Coastal Research Amphibious Buggy [*Birkemeier and Mason*, 1984]. Additional high-resolution foreshore topographic surveys were usually collected daily during all experiments. During Duck82 (1982), runup was digitized from 35-min time-lapse photography along selected longshore locations [*Holman*, 1986] following methods outlined in Holman and Guza [1984], resulting in 149 estimates of runup and swash statistics. The runup array during the Delilah experiment (1990) consisted of 26 longshore lines with a longshore spacing, *dy,* of 10 m, sampled at 2 Hz [*Holland and Holman*, 1993]. During the Duck94 experiment (1994), 120-min runup timestacks were collected at up to 48 equally spaced (*dy* = 5 m) cross-shore lines [*Holland and Holman*, 1996]. The runup array from SandyDuck (1997) consisted of five cross-shore transects from which approximately 500 17-min swash timestacks were collected.

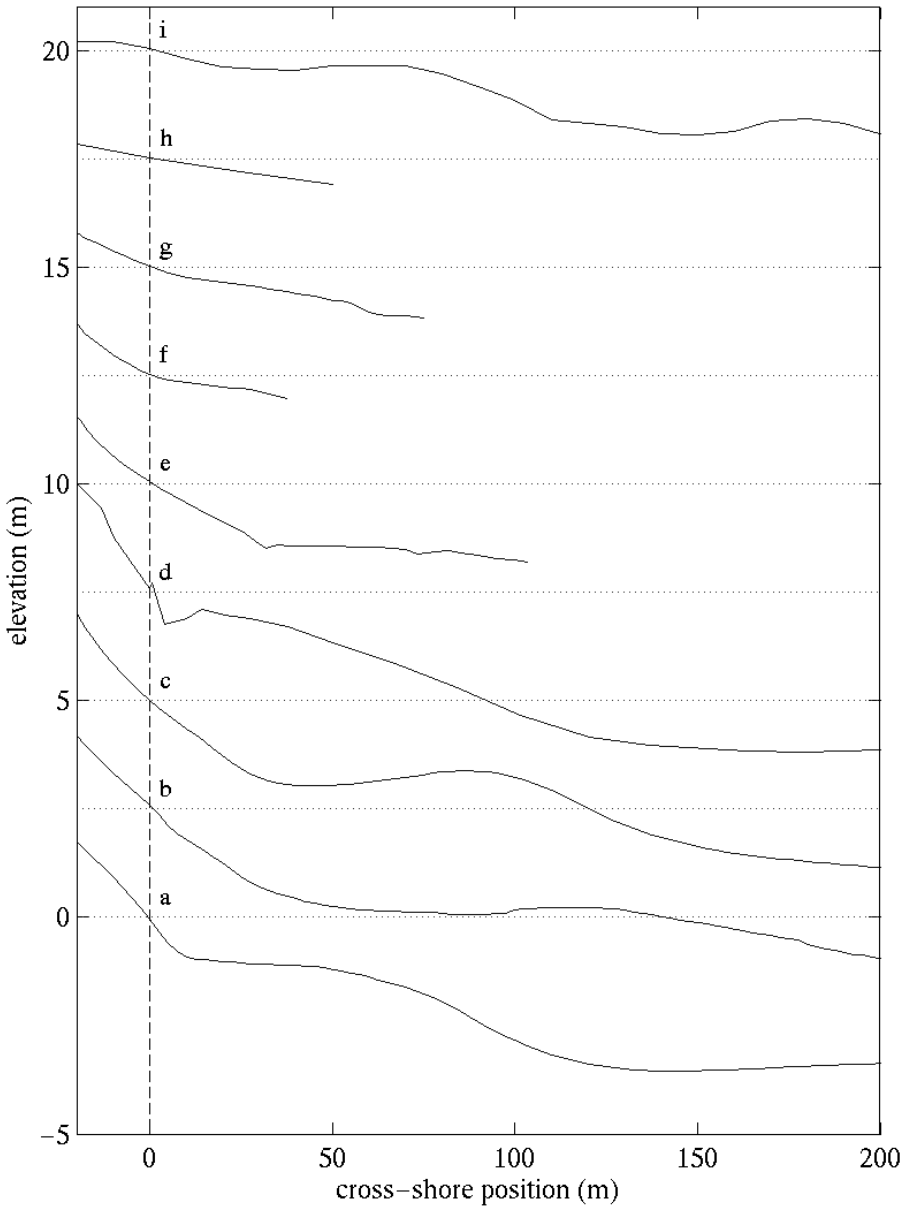

Figure 3.3. Time-averaged profile (topography and bathymetry) from each experiment illustrating differences in foreshore slope and offshore profiles: SandyDuck (a), Duck94 (b), Delilah (c), Duck82 (d), San Onofre (e), Gleneden (f), Scripps Beach (g), Agate Beach (h), and Terschelling (i). The profiles are offset 2.5 m in the vertical. Mean sea level is indicated by the horizontal dotted lines. The vertical dashed line marks the cross-shore location of MSL for each profile (x=0). The average profile was calculated over the time period of the experiment at a single cross-shore transect.

More limited data exist from three other intermediate/reflective conditions. The Uswash experiment was conducted June 26 - 29, 1989 at Scripps Beach, CA, a fine-grained sandy beach [*Holland et al.*, 1995]. Offshore bathymetry was not measured on a daily basis and was approximated offshore of the 1-m depth contour using an offshore slope of 0.01 [*Holland et al.*, 1995]. Wave height and period were measured every 6 hours in 7 m water depth, a few hundred meters offshore, as a part of the Coastal Data Information Program (CDIP) [*Seymour et al.*, 1985]. Six 8-Hz data runs were collected over the course of the experiment [*Holland et al.*, 1995]. A more reflective data set was collected during a October 1993 experiment in San Onofre, CA. The offshore slope was measured to be 0.013 from a cross-shore profile, surveyed early in the experiment (October 10, 1993) that extended approximately 100 m offshore. Wave data were obtained from a CDIP buoy located offshore of Oceanside, CA, in approximately 10 m of water, a few kilometers southeast of the field site. Tide measurements were obtained from a NOAA gauge located in La Jolla, CA. 120-minute timestacks of runup were collected at 2 Hz at a single cross-shore transect over a 5-day period. The final data set on an intermediate beach was obtained from an experiment at Gleneden, OR, in late February 1994. A linear offshore profile ($\beta = 0.025$) was extrapolated from a survey that extended from the beach across the surf zone. Incident wave conditions were measured at a CDIP buoy located approximately 190 km to the southwest in 11 m of water. Tides measured at Yaquina Bay, OR, located 35 km to the south, were corrected so that the values were representative of the tides at Gleneden. 120-minute video runup timestacks were collected at 2 Hz multiple times a day along a single cross-shore transect.

Data from two beaches dominated by dissipative conditions ($\xi_0 < 0.3$) are also included in the data set, providing a small (5.3% of the total data) but important extension into highly dissipative domains. Two data sets were collected from Terschelling, the Netherlands, in April and October 1994 by Ruessink et al. [1998]. Terschelling features multiple offshore sandbars with offshore slopes generally 0.005 or less, as measured from a single offshore bathymetry profile. Daily beach surveys were conducted and an alongshore-averaged foreshore slope was calculated for the analysis of runup statistics at

seven cross-shore transects [*Ruessink et al.*, 1998]. H_s, as measured by an offshore buoy located approximately 5 km offshore in 15 m water depth, ranged from 0.5 m to almost 4 m. 45-minute runup timestacks were collected at 2 Hz along nine cross-shore lines once a day. Because the only beach slope available for this site was an alongshore-averaged foreshore slope, the runup and swash statistics computed at each cross-shore line were alongshore averaged before being compared in bulk to the other sites. (Runup statistics were fairly longshore uniform during each data run. Over the duration of the experiment, the mean and standard deviation, $\mu \pm \sigma$, of longshore-variable swash and setup were 69±8 cm and 16±5 cm, respectively.) The second dissipative site is Agate Beach, OR, a multiple-barred, low-sloping beach where runup data were collected in February 1996 as a part of a larger experiment on the nearshore dynamics of high-energy beaches [*Ruggiero et al.*, 2001]. Foreshore slopes were measured daily using GPS topographic surveys. Offshore survey data were not available for this experiment; however, a typical offshore slope was measured from surveys collected in 1998 to be ~0.01. Wave height and period were obtained from a CDIP buoy located approximately 170 km to the southwest in 64 m water depth. Measured tides were taken from a NOAA gauge located at Yaquina Bay, OR, approximately 8 km from Agate Beach. 120-min runup timestacks were collected at 1 Hz at five cross-shore transects.

3.5 Results

For the initial analysis of bulk runup statistics, the complications of longshore variability were avoided by selecting a single cross-shore transect from each experiment. Limiting the data to one runup line per experiment also helped to minimize the bias towards intermediate conditions since the most extensive longshore coverage occurred during the Duck experiments. This resulted in 491 independent measures of runup and swash, distributed as follows: Duck82 (36), Uswash (41), Delilah (138), San Onofre (59), Terschelling (14), Gleneden (42), Duck94 (52), Agate Beach (14), and SandyDuck (95). The statistics of longshore variability from multiple-transect runs are examined later in the paper.

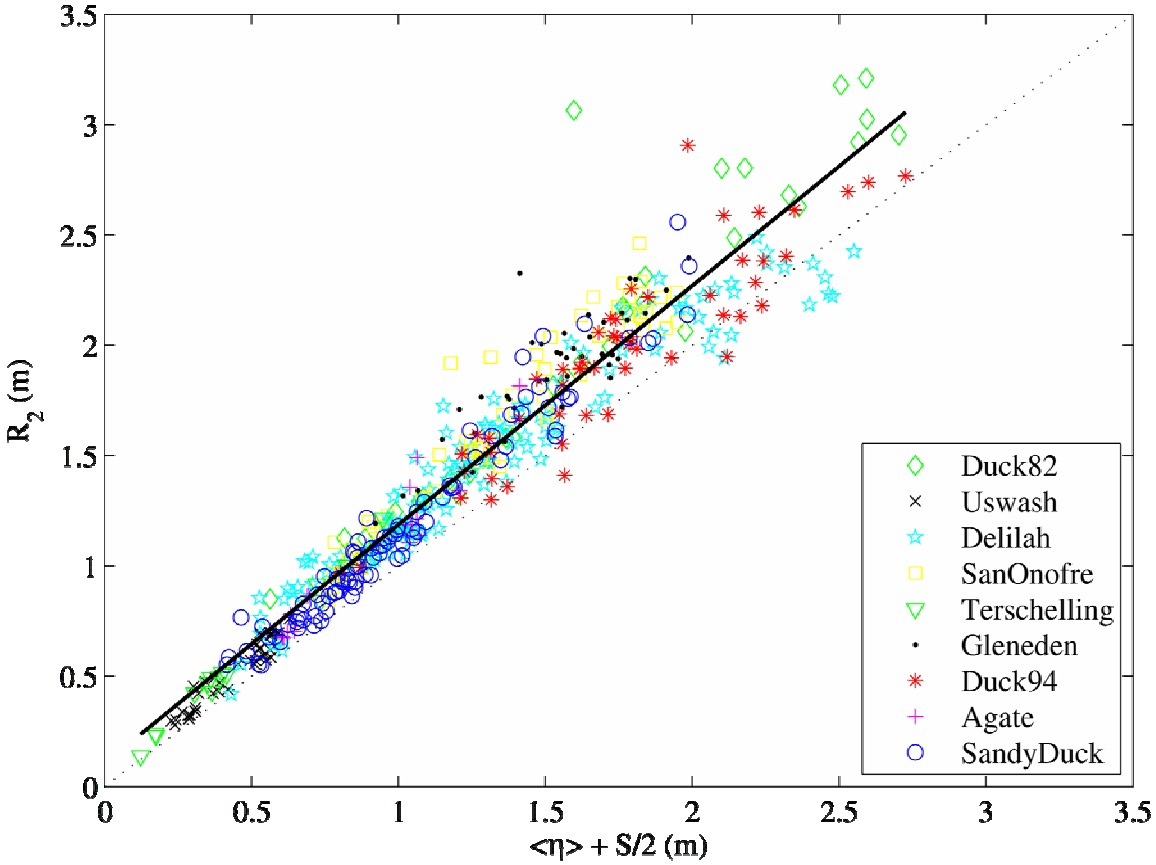

Figure 3.4. The sum of setup and half of the swash excursion plotted against the 2% runup peak elevation. The dashed line is a 1:1 line. The heavy solid line is the best fit to the data ($m = 1.1$, $b = 0.10$, $\rho^2 = 0.94$).

The assumption that the 2% exceedence level for runup approximately equals $\langle\eta\rangle + S/2$ (equation 3.6) was first tested. S is calculated as four times the square root of the swash variance (4σ) and, for a Gaussian process, would encompass 95.4% of the values. The remaining 4.6% defines the extreme high and low values and is split evenly between the tails of the distribution. Accordingly, the actual value of the extreme low value of runup (the 98% exceedence value) would be defined as the mean (setup) minus half of the spread (2σ, or $S/2$), and the extreme high value of runup (the 2% exceedence value) would be defined as the mean (setup) plus half of the spread. The squared-correlation between the measured values of $\langle\eta\rangle + S/2$ and R_2, is 0.94, which is significant at the 99% confidence level (Figure 3.4). The slope of the regression is 1.1, which reflects the slightly non-Gaussian nature of natural swash. To test whether the observed swash was Gaussian, the skewness and kurtosis of each swash distribution were calculated for all

experiments, except Duck82, and compared to values defining Gaussian distributions (skewness = 0, kurtosis = 3). The mean kurtosis for all data was 2.9 (σ = 0.80). The mean skewness for all swash distributions was 0.19 (σ = 0.38) indicating that natural swash is slightly skewed. To account for this skewness, the slope of the regression in Figure 3.4 is included in equation 3.6, resulting in a more complete definition of runup,

$$R_2 = 1.1 \cdot \left[< \eta > + \frac{S}{2} \right]. \qquad (3.9)$$

The empirical models described in the following sections will be presented in dimensional space and based on regressions forced through the origin. Synthetic tests based on samples with known statistical characteristics indicate a danger in carrying out the least-squares analysis in non-dimensional space, as has been common in the literature. In a regression between non-dimensional R_2 (normalized by H_0) and ξ_0, it is found that small errors in data from small wave cases will map to large errors in ξ_0 and can introduce large errors in regression statistics. Thus, in order to avoid undue influence of these errors and to better weigh storm events, the dimensional parameterization is preferable to its non-dimensional counterpart. Regressions through the origin are used, rather than allowing least squares intercepts, in order to avoid non-physical results in setup and swash models. For example, a significant intercept in a relationship between wave height normalized swash and ξ_0 would results in a value of swash when $H_0 = 0$. In most models presented here, the computed intercept was not significantly different than zero, supporting the selection of regression through the origin methodology. To evaluate each empirical model, the squared-correlation, ρ^2, referred to hereafter simply as correlation, and the 95% significance level, ρ^2_{sig}, are presented as a measure of the linear relationship between the two parameters. The goodness of fit of the empirical model is measured using an rms error, *rmse*.

3.5.1 Setup

No single constant of proportionality between $<\eta>$ and H_0 was found (ρ^2 = 0.30, *rmse* = 25.3 cm; Figure 3.5a). The setup parameterization was improved by inclusion of

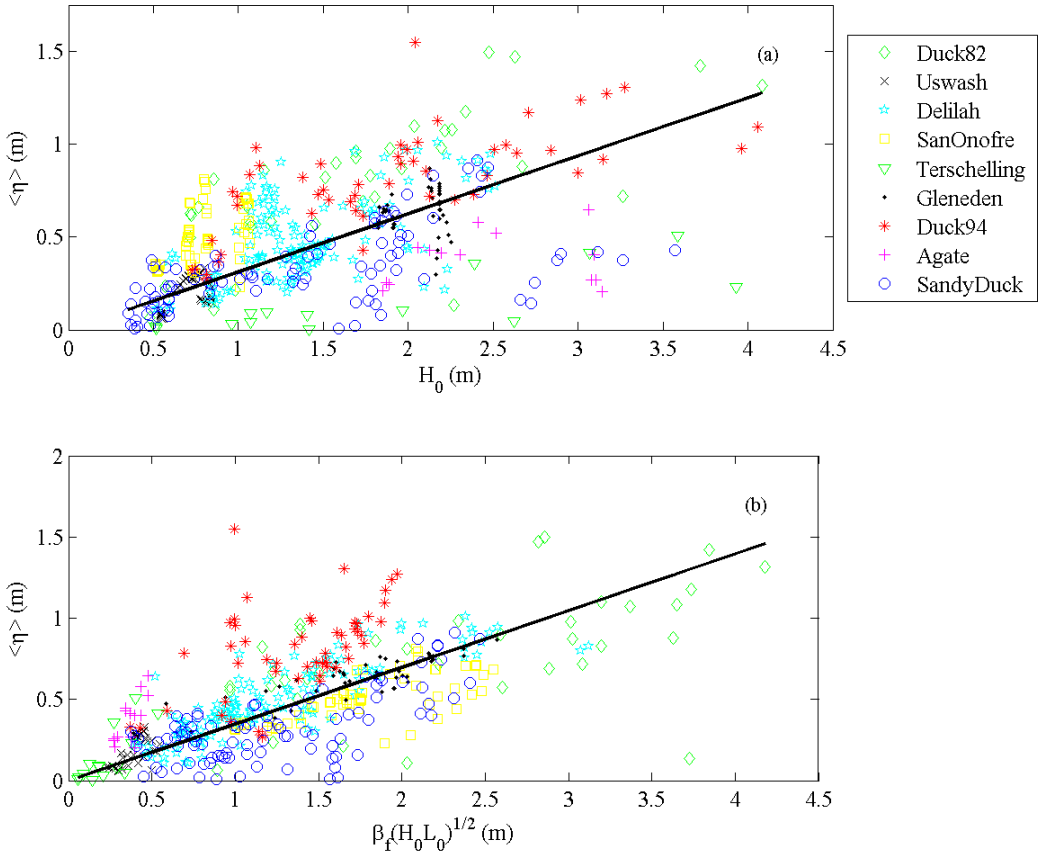

Figure 3.5. (a) Setup vs. wave height ($\rho^2 = 0.30$) and (b) setup vs. $\beta_f(H_0L_0)^{1/2}$ ($\rho^2 = 0.48$). The $\beta_f(H_0L_0)^{1/2}$ dimensional parameterization also has the lowest rms error, 21.3 cm.

L_0 (T_0) and β_f (Figure 3.5b), modeling setup using a dimensional, Iribarren-like form ($\xi_0 H_0$),

$$< \eta >= 0.35\beta_f (H_0 L_0)^{1/2}. \tag{3.10}$$

The squared-correlation of the dimensional model is $\rho^2 = 0.48$ ($\rho^2_{sig} = 0.01$) and *rmse* = 21.3 cm. A summary of the regression coefficients, squared-correlations, and rms error for all suggested parameterizations is presented in Table 3.2.

Setup data were divided into low-, mid-, and high-tide groupings with divisions defined as 1/3 (low to mid) and 2/3 (mid to high) of the tidal range observed at each site. As was observed in the Duck82 data by Holman and Sallenger [1985], the goodness of fit

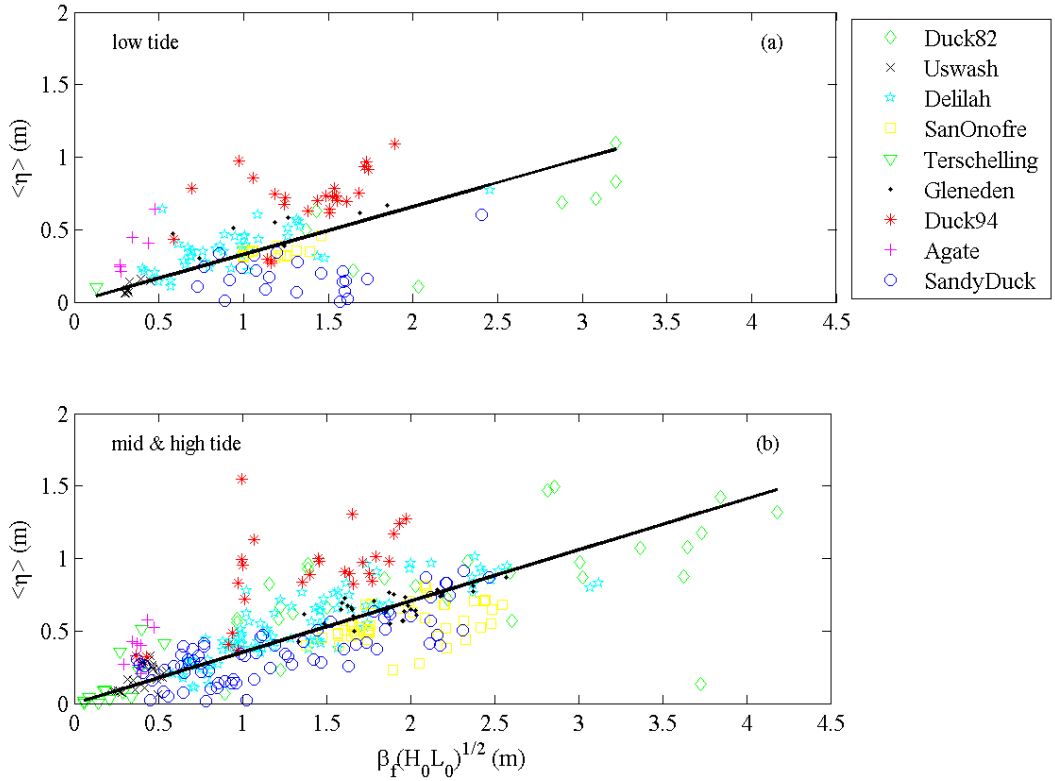

Figure 3.6. Setup vs. $\beta_f(H_0L_0)^{1/2}$ during (a) low tide and mid- and (b) high tide. The correlation of the model during low tide ($\rho^2 = 0.29$) is significantly lower than that for mid- and high-tide values ($\rho^2 = 0.52$).

Table 3.2. Regression parameters for components of runup model.

	Quantity modeled	*Model input*	*Slope, m*	*Intercept, b^+*	*ρ^2 (ρ^2_{sig})*	*rmse (cm)*
All sites	$<\eta>$	$\beta_f(H_0L_0)^{1/2}$	0.35 (±0.01)	0	0.48 (0.01)	21.3
	S_{inc}	$\beta_f(H_0L_0)^{1/2}$	0.75 (±0.03)	0	0.44 (0.01)	46.9
	S_{IG}	$(H_0L_0)^{1/2}$	0.06 (±0.002)	0	0.65 (0.01)	25.7
$\xi_0<0.3$	$<\eta>$	$(H_0L_0)^{1/2}$	0.016 (±0.003)	0	0.68 (0.22)	11.9
	S	$(H_0L_0)^{1/2}$	0.046 (±0.004)	0	0.78 (0.22)	15.7

[+] Regressions were forced through the origin to avoid non-physical intercepts.

of the parameterization for $<\eta>$ varied during different stages of the tide (Figure 3.6). When low-tide values of $<\eta>$ were examined separately from those occurring during mid- and high tide, the correlation between $<\eta>$ and $\beta_f (H_0 L_0)^{1/2}$ fell to $\rho^2 = 0.29$ (Figure 3.6a). For the mid- and high-tide values, the correlation remained high, $\rho^2 = 0.52$ (Figure 3.6b). It was suggested by Holman and Sallenger [1985] that offshore morphology and surf-zone slope play a larger role in $<\eta>$ at low tide, with breaking patterns over barred topographies producing more complex patterns in radiation stress gradients [*Raubenheimer et al.*, 2001]. However, the use of surf-zone slope in any form of a setup parameterization for the low-tide data did not improve the model performance over the β_f-dependent parameterization (equation 3.10) that was derived from the data set as a whole.

3.5.2 Incident and Infragravity Swash

On dynamically different beaches, energy in the incident and infragravity frequency bands will contribute varying amounts to the total swash [*Guza and Thornton*, 1982]. Swash heights within these two bands are forced by different processes and therefore require separate parameterizations. Incident swash is best parameterized by a dimensional version of an Iribarren-like relationship (Figure 3.7a),

$$S_{inc} = 0.75\beta_f (H_0 L_0)^{1/2}. \qquad (3.11)$$

The correlation for the model is $\rho^2 = 0.44$ ($\rho^2_{sig} = 0.01$) and *rmse* = 46.9 cm, lower than that for the non-dimensional version. When the same dimensional model is used to describe the infragravity band (Figure 3.7b), the correlation remains high, $\rho^2 = 0.56$ (*rmse* = 34.2 cm). However, when local foreshore slope is removed from the expression (Figure 3.7c), the correlation improves to $\rho^2 = 0.65$ ($\rho^2_{sig} = 0.01$) and the rms error decreases to 25.7 cm. The magnitude of infragravity swash is, therefore, linearly independent of β_f and best parameterized as

$$S_{IG} = 0.06\left(H_0 L_0\right)^{1/2}. \qquad (3.12)$$

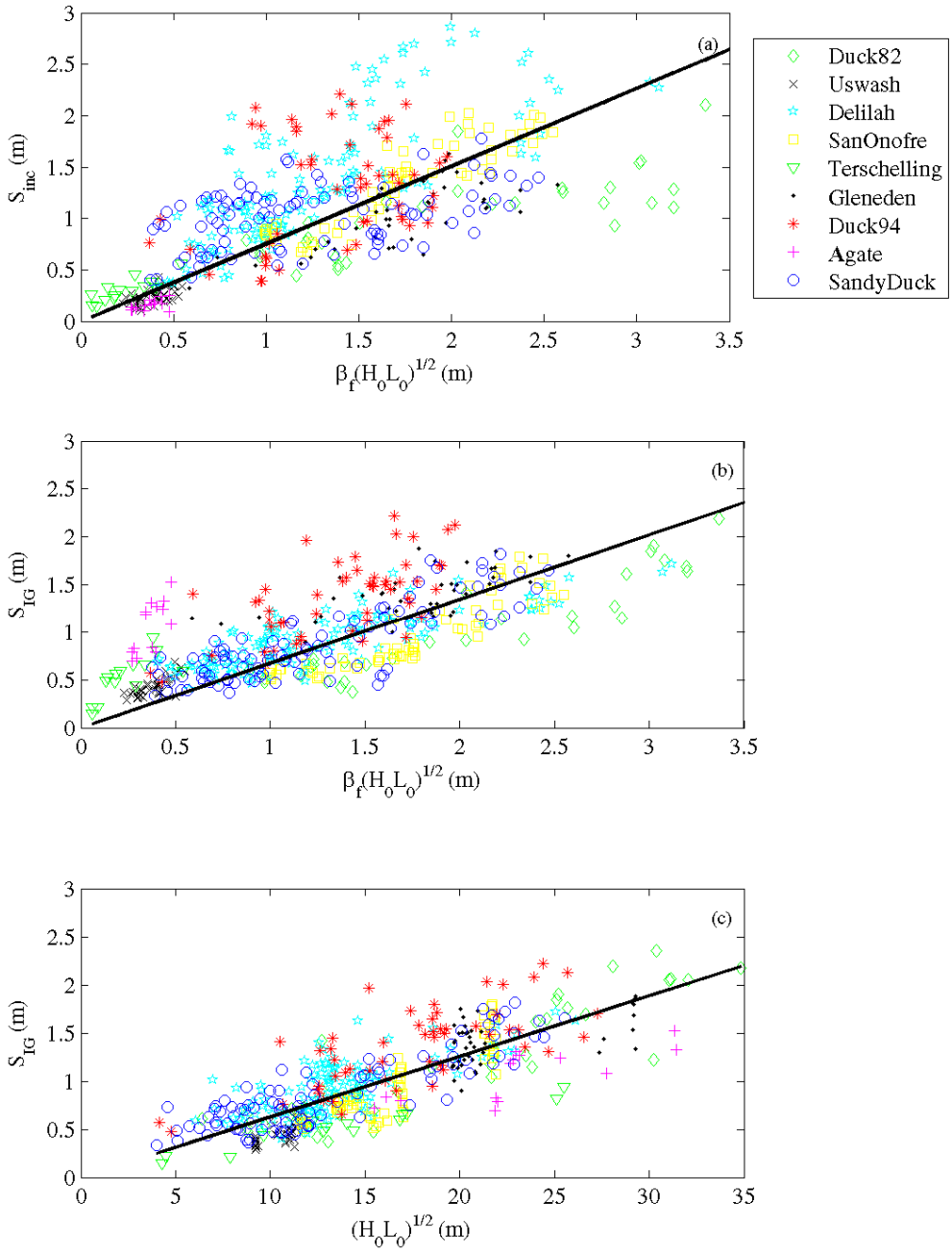

Figure 3.7. (a) Incident (ρ^2 = 0.44, rmse = 46.9 cm) and (b) infragravity swash (ρ^2 = 0.56, *rmse* = 34.2 cm) parameterized in a dimensional form of the traditional Iribarren-based equation. (c) The parameterization of infragravity swash improves when beach slope is removed from the model (ρ^2 = 0.65, *rmse* = 25.7 cm).

The absence of beach slope in this model may be somewhat counter-intuitive given that the presence of significant infragravity band energy is prescribed by the β-dependent ξ_0. However, the inclusion of β_f in the parameterization of the actual magnitudes of S_{IG} has not been supported by our observations. The non-dimensional form of equation 3.12 shows that the efficiency of infragravity energy generation is inversely dependent on deep-water wave steepness, H_0/L_0, where low values are indicative of swell conditions (for a given value of H_0). Infragravity band motions have previously been shown to correlate best with energy from swells rather than that from seas [*Elgar et al.*, 1992].

3.5.3 Evaluation of Swash and Runup Parameterization

Estimated setup, $<\eta>_e$, swash, S_e, and runup peaks, R_{2e}, were calculated from measured offshore wave height, wave period, and foreshore beach slope using the empirical parameterizations for setup, incident swash, and infragravity swash (equations 3.10-3.12) in equation 3.9. Performance of the parameterizations was measured in terms of dimensional differences, Δ, from observations,

$$\Delta <\eta>(t) = <\eta>_e (t) - <\eta>(t), \tag{3.13}$$

$$\Delta S(t) = S_e(t) - S(t), \text{ and} \tag{3.14}$$

$$\Delta R(t) = R_{2e}(t) - R_2(t) \tag{3.15}$$

where $<\eta>(t)$, $S(t)$, and $R_2(t)$ are the observed values at each time, t. The mean difference errors, $\overline{\Delta}$, were calculated for each experiment and for all data as a measure of the bias of the estimator. The rms error of the differences, Δ_{rms}, was used to measure the scatter or noise of the estimate. Mean values for observed setup, swash, and runup ($\overline{<\eta>}$, $\overline{S}$, and $\overline{R}$, respectively) are presented in order to evaluate the significance (or relative magnitudes) of the mean difference errors. Summaries of the error statistics are presented in Table 3.3.

The mean error between setup estimates and observations, averaged over all experiments, $\overline{\Delta<\eta>}$, is -3 cm, while the rms error, $\Delta<\eta>_{rms}$, is 21 cm ($\overline{<\eta>}$ = 49 cm). There is little bias in setup estimates on intermediate and reflective beaches ($\overline{\Delta<\eta>}$ = 2

Table 3.3. Accuracy of setup, swash, and runup parameterizations (cm).

Experiment	$\overline{\Delta<\eta>}$	$\Delta\langle\eta\rangle_{rms}$	$\overline{\Delta S}$	ΔS_{rms}	$\overline{\Delta R}$	ΔR_{rms}
Duck82	3	34	48	58	9	37
Scripps Beach	-5	9	18	19	2	10
Delilah	-6	13	42	57	-32	41
San Onofre	11	16	17	22	-4	17
Gleneden	-2	9	20	27	-17	27
Terschelling*	-6	14	25	31	-1	13
Duck94	-33	40	54	67	-62	69
Agate Beach	-25	28	34	39	-16	27
SandyDuck	11	20	31	37	-2	34
average, all data	-3	21	34	46	-18	38
	$\overline{<\eta>}$=49 cm		$\overline{S}$=149 cm		$\overline{R}$=144 cm	

*The results of the two Terschelling field campaigns are combined in these statistics. Mean observed values of setup, swash, and runup are presented in the last row in order to examine mean error magnitudes relative to observed values.

cm, $\overline{<\eta>}$= 57 cm); however, on dissipative beaches ($\xi_0 < 0.3$), the bulk parameterization underestimates setup elevation by 16 cm ($\overline{<\eta>}$= 27 cm). Accordingly, the largest underestimates of setup occur for large wave events ($H_0 > 1.5$ m, $\overline{\Delta<\eta>}$ = -7 cm) and on the most gentle beach slopes ($\beta_f \leq 0.02$, $\overline{\Delta<\eta>}$ = -17 cm).

The mean difference in swash, $\overline{\Delta S}$, averaged over all data, is 34 cm and the rms difference, ΔS_{rms}, is 46 cm ($\overline{S}$ = 149 cm). The bulk parameterization for runup contains an -18 cm bias ($\overline{R}$ = 144 cm). The rms difference error between runup estimates and observations, $(\Delta R)_{rms}$, is 38 cm. The bias in the runup measurements is two times larger on intermediate and reflective beaches ($\overline{\Delta R}$= -18 cm) than on dissipative sites ($\overline{\Delta R}$= -9 cm); however the observed runup magnitudes are also larger on intermediate and reflective sites ($\overline{R}$ = 148 cm) than dissipative ones ($\overline{R}$ = 84 cm).

3.5.4 Longshore Variability

Runup and incident swash have been shown to be dependent on foreshore beach slope. Accordingly, beaches with significant longshore-variable slopes should exhibit similar longshore variability in swash excursions and runup elevation. However, since S_{IG} showed little or no linear dependence on β_f, spatial variations in the infragravity band swash are expected to be less than those in the incident band. To explore the dependencies on beach slope, the longshore variability of swash and runup was examined using longshore runup arrays from the Delilah (26 lines; total array length, Y, = 250 m), Duck94 (35 lines; Y = 165 m), and SandyDuck (6 lines; Y = 75 m) experiments. Spatial variability observed at each site was characterized by calculating the longshore standard deviation of the total swash excursions, $\sigma S(t)$, as well as that of the incident, $\sigma S_{inc}(t)$, and infragravity, $\sigma S_{IG}(t)$, components. Additionally, spatial squared-correlations, ρ^2_s, were calculated between $S(y)$, $S_{inc}(y)$, $S_{IG}(y)$ and $\beta_f(y)$ in order to determine the amount of longshore variability in swash that may be attributed to a longshore-variable foreshore slope. Table 3.4 presents the details of longshore variability (the standard deviation of S, S_{inc}, and S_{IG}) and the correlation analysis (the percentage of significant correlations and of positive significant correlations) for each of the three experiments considered.

At Delilah and SandyDuck, the total swash excursion was most longshore variable on days when the beach topography was highly three dimensional, either in the form of a regular cusp field, a large mega-cusp embayment, or welded swash bars (σS = 40-50 cm). The values of ρ^2_s (S,β_f) showed a positive correlation between total swash and beach slope, indicating that increases in S corresponded to increases in β_f, consistent with expectations. Correlations were significant at the 95% confidence level 46% (Delilah) and 56% (SandyDuck) of the time (Table 3.4). Correlation values were higher and more often significant for rhythmic, large-scale spatial variations in slope (i.e., megacusps) than for irregular, short-scale slope variations. The time-averaged value of σS_{inc} was higher than σS_{IG}, indicating that most of the observed longshore variability in total swash was contained within the incident band. Additionally, S_{inc} was significantly and positively spatially correlated to β_f for 50% and 59% of the cases at Delilah and SandyDuck,

Table 3.4. Longshore variability of swash (m) and correlations to foreshore beach slope.

Experiment	σS	σS_{inc}	σS_{IG}	$\%\rho^2_s(S, \beta_f)$ significant ($\%\rho_s$ >0)	$\%\rho^2_s(S_{inc}, \beta_f)$ significant ($\%\rho_s$ >0)	$\%\rho^2_s(S_{IG}, \beta_f)$ significant ($\%\rho_s$ >0)
Delilah	0.24	0.23	0.15	45.8 (97.0)	50.0 (100)	13.9 (80.0)
Duck94	0.20	0.24	0.19	31.0 (77.8)	55.2 (100)	38.0 (0)
SandyDuck	0.18	0.18	0.14	55.6 (100)	58.6 (100)	14.8 (100)

The first three columns indicate the spatial standard deviation of swash (m). The last three columns list the percentage of spatial correlations significant at the 95% confidence level. The value in parenthesis indicates the percentage of significant correlations that are positive.

respectively (Table 3.4). Less variability was observed in S_{IG} and correlations with β_f were significant only 15% of the time (Table 3.4), supporting the results that the magnitude of infragravity swash has little or no linear dependence on foreshore beach slope.

During Duck94, when a well-developed cusp field was present, there was less of a relationship between the magnitude of the longshore variability observed in total swash and that observed in beach slope. Spatial correlations between S and β_f were significant only 31% of the time. Correlations between S_{inc} and β_f were significant and positive 55% of the time. When the cusp field was particularly well-developed, longshore variability within the infragravity band increased. Significant correlations between S_{IG} and β_f were more than twice as common during Duck94 than during the other experiments (Table 3.4). Surprisingly, significant values of ρ^2_s (S_{IG}, β_f) were always negative, indicating that S_{inc} and S_{IG} were out of phase within the cusp field. This relationship between S_{IG}, S_{inc}, and beach slope may be related to longshore-variable dynamics due to swash circulation within a cusp field, as opposed to a simple cross-shore flow which has been assumed for the empirical parameterizations presented. An exploration of the longshore variability of setup, swash, and runup and the complex dynamics of incident and infragravity swash, particularly on highly three-dimensional topography, will be presented in detail in a subsequent paper.

The dependence of total swash on β_f will have implications on the practical use of the bulk parameterization of runup on beaches with complex foreshore topography. In order to evaluate how much error can be expected in estimates of R_2 if a longshore-averaged slope, $\overline{\beta_f}$, is used instead of a more accurate measure of slope at each longshore line, $\beta_f(y)$, a relative slope difference was compared to a relative runup error. Relative slope difference, $\delta\beta$, was defined as $(\overline{\beta_f} - \beta_f(y))/\beta_f(y)$. Relative error in runup elevation, δR_2, was defined as $(R_{2avg} - R_{2e}(y))/R_{2e}(y)$, where R_{2avg} is the estimate of runup calculated from a single longshore-averaged beach slope and $R_{2e}(y)$ is the runup calculated using $\beta_f(y)$ measured at each longshore line. The error in a runup estimate calculated from a single longshore-averaged beach slope was found to equal 51% of $\delta\beta$. For example, a 20% difference between $\overline{\beta_f}$ and $\beta_f(y)$ would result in a 10.2% error in estimated runup. Maximum alongshore variability of β_f was observed during the Delilah experiment when megacusps were present (longshore spacing of ~200 m, $\delta\beta$ = -0.25 to 0.75). Here, runup predictions based on a longshore-averaged beach slope may be underestimated by 12% on foreshore locations that are more steeply sloped than $\overline{\beta_f}$ and overestimated by as much as 38% on more gently sloped regions. On a well-developed cusp field, longshore variability in foreshore slope ($\delta\beta$ = -0.3 to 0.5) may result in runup values 15% lower than the true value on steep cusp horns and overestimates of 26% within the more gently sloped cusp embayments. Again, swash circulation within a cusp field may be affecting the observed runup amplitudes, partly explaining why a change in beach slope leads to a 51% change in runup, even though the parameterizations show a linear relationship between the two.

3.6 Discussion

The proper choice of wave height in the parameterization of total swash, S, was explored as a part of this study. The most rigorous comparison between H_s (a locally measured significant wave height), H_0 (deep-water equivalent wave height), and H_b (breaking wave height) could be completed for the Duck experiments because accurate,

daily bathymetry data were available for shoaling the waves and determining an approximate break point. At this site, the dimensional Iribarren-based parameterization for S calculated using H_b ($\rho^2 = 0.46$, $rmse = 57.9$ cm) showed no improvement over the similar swash parameterization calculated using H_0 ($\rho^2 = 0.46$, $rmse = 56.4$ cm). On the dissipative beaches, where daily offshore bathymetry data were not available, an approximation of H_b was made by shoaling H_s over the single offshore profile available for each site. On these beaches, H_b was found to improve the performance of the regression: the correlation was higher, $\rho^2 = 0.80$ ($\rho^2_{sig} = 0.22$) than that for the swash parameterization based on H_0 ($\rho^2 = 0.67$). However, because daily profiles were not measured at these sites and the values of H_b are approximate, the exact relationship between H_b and S cannot be clearly defined here.

While H_b was not shown to offer a significant improvement over H_0 (at Duck), the question of which measure of wave height is most appropriate for practical use in runup parameterizations remains a relevant one. Because of refraction, frictional dissipation across the shelf [*Herbers et al.*, 2000], and white-capping, the wave height measured at a buoy located in deep water may be significantly higher than that which actually reaches the nearshore, so runup predictions using deep-water buoy measurements may be anomalously high. Analysis at Duck, where wave height measurements are available in deep water, 18 m water depth, and 8 m water depth, shows a somewhat stronger relationship between runup and waves measured at 8 m. While H_0 was used in this analysis as an equal measure of wave height between different sites, in practical applications, it may be preferable to use local wave measurement, reverse shoaled to an equivalent deep-water value.

Some researchers have suggested that the slope of the surf zone (β_{sz}) might be more directly related to swash height than β_f; therefore, its use in the empirical parameterization would likely improve runup estimates [*Holman and Sallenger*, 1985; *Nielsen and Hanslow*, 1991]. To test this idea, β_{sz} was substituted in the dimensional, Iribarren-based parameterization for total S. When the entire dataset was used, the correlation of the model ($\rho^2 = 0.03$, $\rho^2_{sig} = 0.01$) decreased significantly from the similar

model calculated using β_f (ρ^2 = 0.68, ρ^2_{sig} = 0.01). The data from Delilah, Duck94, and SandyDuck were examined separately because the detailed, daily bathymetric surveys provided more accurate estimates of β_{sz}. Here, the correlation for the model for *S* using β_{sz} was not significantly different than zero showing that, on these beaches, the foreshore slope has more of an influence on swash processes than the surf-zone slope. When dissipative beaches were isolated from the entire dataset and examined separately, the use of estimated β_{sz} showed similar predictive capabilities (ρ^2 = 0.71, *rmse* = 20.1 cm) as calculations based on β_f (ρ^2 = 0.67, *rmse* = 21.3 cm). However, the correlation of the model for swash on dissipative beaches is highest when slope is completely removed from the parameterization ($S \alpha \left(H_0 L_0\right)^{1/2}$, ρ^2 = 0.78). In order to explore the effects of β_{SZ} on runup more directly, the variations in *S* were studied as the tide rose and fell over a barred profile at Duck. Since β_{sz} is defined between the shoreline and the break point (x_b), a significant change in β_{sz} is observed under certain wave conditions where breaking occurs on the bar at low tide (gentle β_{sz}) and near the shoreline at high tide (steep β_{sz}). Data runs where these conditions were met were isolated from the larger data set. This unique situation allows for a changing surf-zone slope while the input wave conditions remain relatively constant. On most topographies observed, the magnitude of runup and swash did not change dramatically over the change in tide or related changes in x_b. Both R_2 and *S* correlated well with β_f over the entire tidal cycle. (See section for 4.4 for detailed correlations between *S* and β_f.) These results again indicate that β_{sz} offers no significant improvement over β_f for incident-band-dominated sites. (Note: Variability in the magnitude of S_{inc} was observed over a few tidal cycles at Duck94 when beach cusps were present on the foreshore, perhaps related to the complex interactions between incident and infragravity band swash on this rhythmic topography.)

While the goal of this work was to present a parameterization for extreme runup that is useful and accurate on a broad spectrum of beaches, it is important to address the errors that occur during dissipative conditions ($\xi_0 < 0.3$) when R_2 is estimated using the bulk parameterization (equations 3.10-3.12). Under these extreme end-member conditions, increased dissipation likely becomes a significant term in momentum balances and the

parameterization from steeper conditions no longer works. When the dissipative beaches are isolated from the whole data set, the correlation of the parameterization of setup improves ($\rho^2 = 0.67$). Interestingly, when β_f is removed from the parameterization of setup for dissipative conditions, there is no decrease in the correlation of the model. This suggests that the inclusion of β_f in this parameterization is not necessary, supporting earlier work which found that shoreline setup on dissipative beaches was not linearly dependent on beach slope [*Hanslow and Nielsen*, 1993]. The suggested parameterization for setup on dissipative sites, $<\eta>_d$ (Figure 3.8a), is

$$<\eta>_d = 0.016(H_0 L_0)^{1/2} \tag{3.16}$$

($\rho^2 = 0.68$, $\rho^2_{sig} = 0.22$, *rmse* = 11.9 cm). On dissipative beaches, frictional dissipation of large waves over extremely wide, low-sloping surf zones begins to play a larger role in shoreline processes. For a given H_0 (and T_0), the values of $<\eta>$ on a dissipative beach

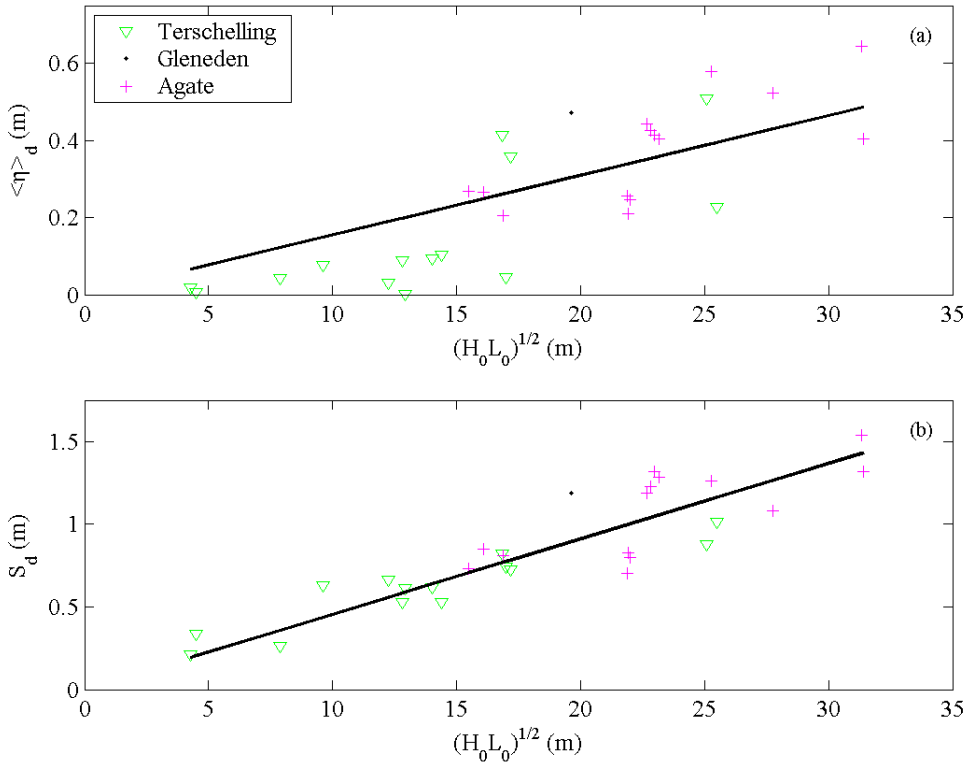

Figure 3.8. Parameterization of (a) setup ($\rho^2 = 0.68$, *rmse* = 11.9 cm) and (b) swash ($\rho^2 = 0.78$, *rmse* = 15.7 cm) during dissipative conditions only ($\xi_0 < 0.3$) using $(H_0 L_0)^{1/2}$. For both models, the correlations are equal or higher than when the bulk parameterizations are used for the dissipative conditions subset.

will be lower than on a reflective or intermediate beach. (This is seen in Figure 3.5a where the values of $<\eta>$ for Terschelling and Agate Beach fall below the below the data cluster and the best-fit line.) Earlier work on setup has shown that $<\eta>$ decreases for lower values of γ [*Bowen et al.*, 1968] and that γ values are lower on dissipative sites [*Bowen et al.*, 1968] and, particularly, on lower sloping beaches [*Sallenger and Holman*, 1985].

The behavior of swash under extremely dissipative conditions is also different than during reflective and intermediate conditions. On low-sloping, high-energy beaches, energy in the incident band is saturated and increases in H_0 contribute only to increases in

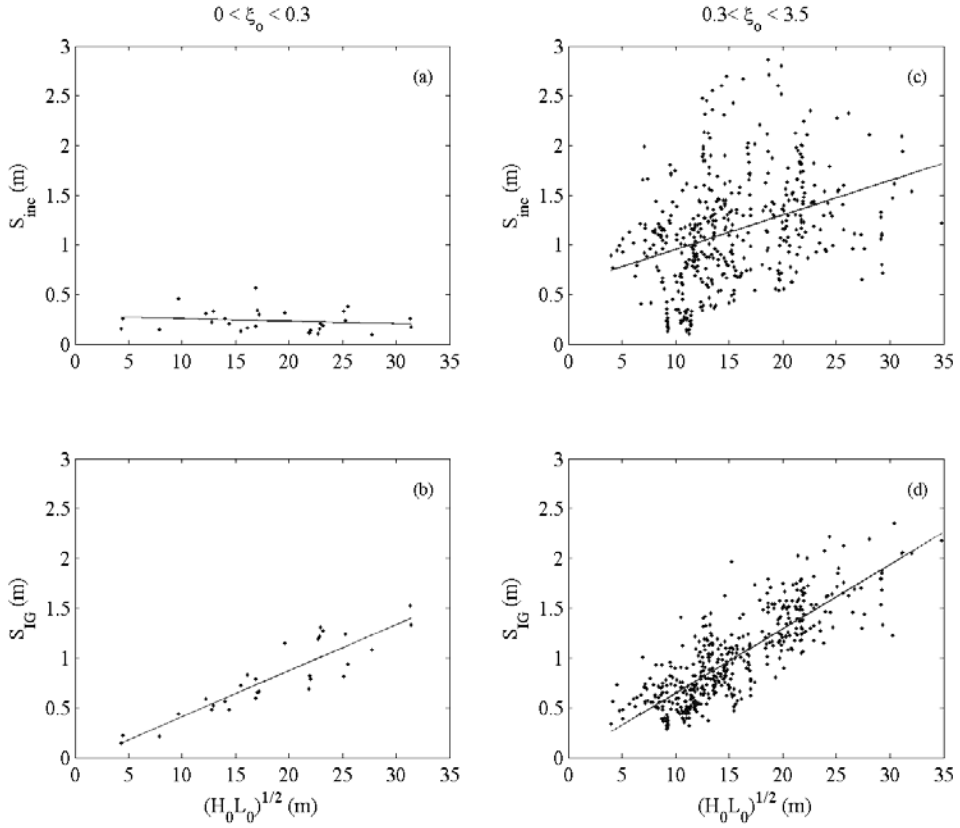

Figure 3.9. Incident and infragravity swash plotted against $(H_0L_0)^{1/2}$ for (a, b) dissipative and (c, d) intermediate/reflective beaches. On dissipative beaches, the incident band (a) is saturated while the magnitude of the infragravity band (b) continues to grow with increasing $(H_0L_0)^{1/2}$. On reflective beaches, both frequency bands respond to increases in $(H_0L_0)^{1/2}$.

the infragravity band [*Guza and Thornton*, 1982; *Holman and Sallenger*, 1985; *Ruessink et al.*, 1998]. This was clearly observed in the swash data when dissipative beaches ($\xi_0 <$ 0.3) were separated from the intermediate and reflective beaches, and S_{inc} and S_{IG} for the two subsets of data were plotted against $(H_0 L_0)^{1/2}$ (Figure 3.9). On intermediate and reflective beaches, swash in both the incident (Figure 3.9c) and infragravity (Figure 3.9d) bands increases as H_0 (and T_0) increase. On the dissipative beaches, the magnitude of the infragravity swash grows with increasing H_0 (Figure 3.9b) while the incident band swash is completely saturated (Figure 3.9a). The saturation of the incident band on dissipative beaches is also revealed by looking at the ratio of $\upsilon = S_{inc}/S_{IG}$ plotted against ξ_0 (Figure 3.10). Cutoff values between dissipative, intermediate, and reflective beaches are defined using an Iribarren equivalent of the Wright & Short [1983] surf-similarity values. Dissipative beaches ($\xi_o < 0.3$) are dominated by infragravity energy ($\upsilon < 1$) for 90% of the data. The energy on intermediate beaches is closely split between incident- and infragravity-dominated conditions (47% incident energy). On the reflective beaches ($\xi_o >$ 1.25), the swash is dominated by incident energy ($\upsilon > 1$) for 90% of the data. This shows that shoreline motions on reflective beaches are dominated by energy in the incident band while shoreline motions on dissipative beaches are dominated by energy in the infragravity band, again supporting what has been observed and explained using data collected from single sites [*Guza and Thornton*, 1982; *Holman and Sallenger*, 1985].

Because total swash on dissipative beaches, S_d, is composed mostly of energy within the infragravity band, it is best parameterized using a form similar to the bulk model describing swash in the infragravity band (equation 3.12). Modeling both the incident and infragravity bands together,

$$S_d = 0.046(H_0 L_0)^{1/2} \tag{3.17}$$

(Figure 3.8b). The correlation for this dissipative-specific parameterization ($\rho^2 = 0.78$, $\rho^2_{sig} = 0.22$) is significantly higher than that for the parameterization of S on dissipative beaches which includes β_f ($\rho^2 = 0.67$). Additionally, the rms error is reduced from 21.3 cm to 15.7 cm when β_f is removed from the expression. Using a small subset of data from infragravity-dominated Agate Beach, Ruggiero et al [2004] found a slope

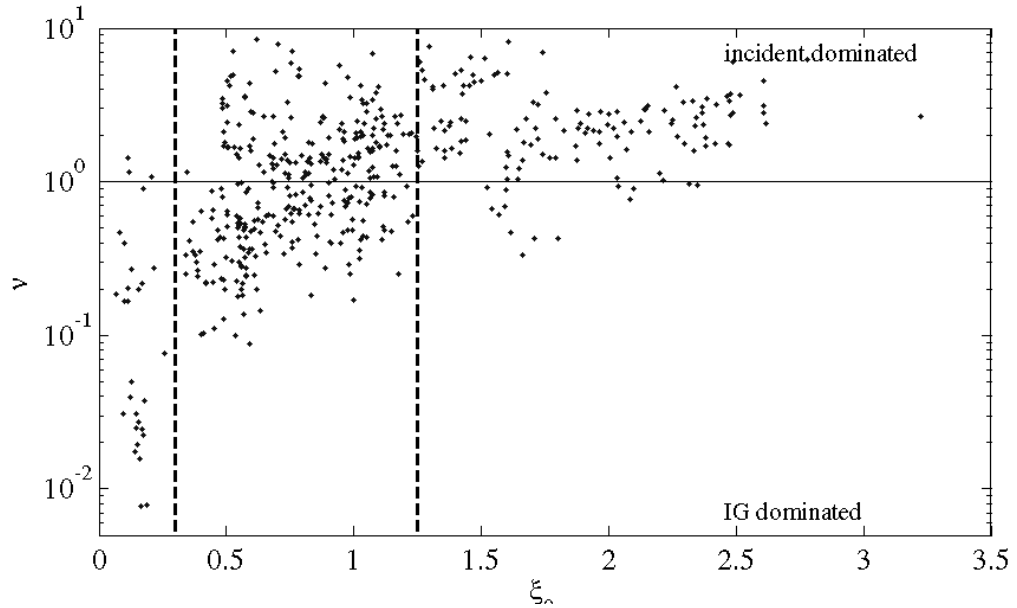

Figure 3.10. Ratio of incident to infragravity swash variance (ν) plotted against the Iribarren number. The vertical dashed lines mark the cutoff values between dissipative (ξ_0 <0.3), intermediate, and reflective beaches (ξ_0 > 1.25). Values above the horizontal line at log(ν) = 1 are incident dominated while those below the line are infragravity dominated.

dependence in spatially-variable swash. However, when all swash data, including the subset used by Ruggiero et al, are examined together, no significant linear slope dependence exists. It has been suggested by other researchers [*Ruessink et al.*, 1998; *Ruggiero et al.*, 2001] that swash on highly dissipative beaches should be scaled using wave height alone; however, the correlation for this model is only 0.37 and the rms error is larger (29.5 cm). The model using $(H_0 L_0)^{1/2}$ has a significantly higher correlation and lower rms error, suggesting that the inclusion of wave period allows for improved predictive capabilities. Based on these dissipative-specific parameterizations and substituting into equation 3.9, runup on sites where $\xi_0 < 0.3$ may be calculated as

$$R_2 = 0.043(H_0 L_0)^{1/2}. \tag{3.18}$$

The improved performance of this model is given in Table 3.5. The setup bias for dissipative sites was reduced from –16 cm to 3 cm. The bias and noise for swash for individual dissipative sites were also significantly reduced. The bias decreased from 29 cm to 13 cm while the ΔS_{rms} decreased from 34 cm to 16 cm. The evaluation of the

estimators across all sites, using the dissipative-specific parameterizations when $\xi_0 < 0.3$, is also presented in Table 3.5.

The final, general expression for runup on all beaches, based on the entire data set and substituting equations 3.10-3.12 into equation 3.9, is

$$R_2 = 1.1\left(0.35\beta_f (H_0 L_0)^{1/2} + \frac{[H_0 L_0 (0.563\beta_f{}^2 + 0.004)]^{1/2}}{2}\right) \qquad (3.19)$$

and may be used over the full range of beach conditions. Given the dissipative-specific formulations, it may seem logical for intermediate- and reflective-specific parameterizations as well. However, when conditions where $\xi_0 > 0.3$ are considered separately, the coefficients of the setup and incident swash parameterization change less than 0.5% and the coefficient of the infragravity parameterization changes ~2.8%. On reflective beaches ($\xi_0 > 1.25$), where swash is dominated by incident energy, the complete expression for runup 2% exceedence elevations (equation 3.19), can be simplified by assuming that the infragravity contribution (the 0.004 term) to total runup is negligible. Here, incident swash and setup have the same parametric dependencies and can be combined,

$$R_2 = 0.73\beta_f (H_0 L_0)^{1/2}. \qquad (3.20)$$

Table 3.5. Accuracy of setup, swash and runup parameterizations for dissipative sites (cm).

Experiment	$\overline{\Delta < \eta >}$	$\Delta\langle\eta\rangle_{rms}$	$\overline{\Delta S}$	ΔS_{rms}	$\overline{\Delta R}$	ΔR_{rms}
Terschelling*	8	14	10	12	3	15
Agate Beach	-1	9	16	17	-9	23
average, $\xi_0 < 0.3$	3	12	13	16	-5	21
average, all sites	-2	21	33	46	-17	38
	$\overline{<\eta>}$ (cm)		$\overline{S}$ (cm)		$\overline{R}$ (cm)	
$\xi_0 < 0.3$	27		85		84	
all sites	49		149		144	

*The results of the two Terschelling field campaigns are combined in these statistics. Mean observed values of setup, swash, and runup are presented in the last two rows in order to examine mean error magnitudes relative to observed values.

While this simplified form is more convenient for practical applications, the rms error under reflective conditions is 47 cm, larger than that for the full expression (equation 3.19, *rmse* = 32 cm). Therefore, our final recommendation is the broad use of the full expression (equation 3.19), with an exception (equation 3.18) for extremely dissipative conditions.

3.7 Conclusions

The elevation of extreme runup peaks, given by the 2% exceedence value, R_2, is dependent on the sum of two dynamically different processes, the time-mean setup, $<\eta>$, and swash, defined in terms of the significant swash height, S, and computed as four times the square root of the swash variance. Extreme runup is defined as the sum of setup and half of the total swash excursion (equations 3.6 and 3.9). Empirical formulations for each of the components have been developed using carefully defined water-level, wave, and topography statistics from 10 field experiments spanning a wide range of environmental conditions. This data set represents a major expansion on the range of conditions for which empirical relationships have been tested.

Dimensional setup is best parameterized ($\rho^2 = 0.48$, *rmse* = 21.3 cm) using foreshore beach slope, estimated over the region of significant swash activity $\left(<\eta> \pm S/2\right)$, and offshore wave height and wavelength (equation 3.10), the dimensionally equivalent form of an Iribarren number dependency. The significant swash excursion can be decomposed into incident ($f_0 > 0.05$ Hz) and infragravity ($f_0 < 0.05$ Hz) frequency bands, $S = \sqrt{(S_{inc})^2 + (S_{IG})^2}$, each of which is be modeled separately. Dimensional incident swash scales with foreshore beach slope, offshore wave height, and offshore wavelength (equation 3.11, $\rho^2 = 0.44$, *rmse* = 46.9 cm). Dimensional infragravity swash also scaled well with $\beta(H_0 L_0)^{1/2}$; however, when foreshore slope was removed from the equation, the correlation of the model improved (equation 3.12, $\rho^2 = 0.65$, *rmse* = 25.7 cm). Additionally, the use of the surf-zone slope, defined as the average slope from the break

point to the mean swash location, in the parameterization offered no significant improvements, even on days when wave breaking was occurring on the sandbar.

The above relationships for setup and swash show large biases under the extreme dissipative conditions of two of the field sites, perhaps reflecting the increasing role of bottom friction on very wide surf zones in the dynamic balances. For Iribarren numbers less than 0.3, setup was best parameterized using only offshore wave conditions (equation 3.16, $\rho^2 = 0.68$, *rmse* = 11.9 cm). Similarly, the total swash, merging both frequency bands, was best parameterized using only offshore wave height and wavelength (equation 3.17, $\rho^2 = 0.78$, *rmse* = 15.7 cm).

Substituting the suggested forms of setup and swash, the final parameterization for the 2% exceedence value of runup peaks on all natural beaches is

$$R_2 = 1.1\left(0.35\beta_f (H_0 L_0)^{1/2} + \frac{[H_0 L_0 (0.563\beta_f{}^2 + 0.004)]^{1/2}}{2} \right).$$

Under extremely dissipative conditions, estimates of R_2 may be improved using the dissipative-specific parameterization

$$R_2 = 0.043(H_0 L_0)^{1/2} \quad \text{for } \xi_0 < 0.3.$$

The performance of the runup parameterizations were tested at each site using data collected along a single transect. The mean difference between the estimated and measured runup was –17 cm, indicating that the parameterization tends to slightly underestimate the elevation of runup peaks. The rms difference between estimated and measured runup was 38 cm.

The longshore variability of runup was examined during the Delilah, Duck94, and SandyDuck experiments where runup data were collected over extensive longshore arrays. On days when foreshore slope was longshore variable, runup, in particular incident band swash, was also spatially variable. Differences between longshore observed runup and runup predictions made using a single longshore-averaged foreshore slope may be as much as 38% when the foreshore topography is highly three-dimensional

(for example, within a megacusp field). Longshore variability in foreshore slope may result in a relative runup error equal to 51% of the fractional variability between the measured and averaged slope.

3.8 Acknowledgments

The authors thank Todd Holland, Peter Ruggiero, and Gerben Ruessink for sharing their swash time series and for providing expert knowledge on the details of their experiments. We also thank John Stanley, Cindy Paden, Joe Haxel, Logan Mitchell, David Sedivy, Nick Parazoo, and Dan Clark for their assistance with runup digitization. Wave data for the different experiments were provided by the U.S. Army Corps of Engineers' Field Research Facility, the NOAA National Buoy Data Center, the Coastal Data Information Program, and Britt Raubenheimer. We thank Bob Guza for his thoughtful review of the manuscript. This research was funded by the U. S. Geological Survey, Coastal and Marine Geology Program as a part of the National Assessment of Coastal Change Hazards.

4.0 A SIMPLE MODEL FOR THE LARGE-SCALE, SPATIALLY-VARIABLE RESPONSE TO HURRICANES

4.1 Abstract

The vulnerability of a beach to extreme coastal change during a hurricane can be estimated by comparing the relative elevations of storm-induced water levels to those of the dune or berm. A simple model that defines four levels of coastal response based on these elevations was used to hindcast the potential impact regime along a 50-km stretch of the North Carolina coast to the landfalls of Hurricane Bonnie on August 27, 1998, and Hurricane Floyd on September 16, 1999. Maximum total water levels at the shoreline were calculated as the sum of modeled storm surge, astronomical tide and wave runup, estimated from offshore wave conditions and the local beach slope using an empirical parameterization. Storm surge and wave runup each accounted for ~48% of the signal (the remaining 4% is attributed to astronomical tides), indicating that wave-driven process are a significant contributor to hurricane-induced water levels. Expected water levels and lidar-derived, pre-storm measures of dune and berm elevation were used to predict the spatially-varying storm-impact regime: swash, collision, or overwash. Predictions were compared to the observed response quantified using a lidar topography survey collected following hurricane landfall. The storm-averaged mean accuracy of the model in predicting the impact regime was 55.4%, a significant improvement over the 33.3% accuracy associated with random chance. Model sensitivity varied between regimes and was highest within the overwash regime where the accuracies were 84.2% and 89.7% for Hurricanes Bonnie and Floyd, respectively.

The model not only allows for prediction of the general coastal response to storms, but also provides a framework for examining the longshore-variable magnitudes of observed coastal change. For Hurricane Bonnie, shoreline and beach-volume changes within locations that experienced overwash or dune erosion were two times greater than locations where wave runup was confined to the foreshore. During Hurricane Floyd, this pattern became more pronounced as magnitudes of change were four times greater within

the overwash regime. Comparisons of pre-storm topography to a calm weather survey collected one year after Hurricane Floyd's landfall show long-term beach volume loss at overwash locations. Here, the volume of sand eroded from the beach was balanced by the volume of overwash deposits, indicating that the majority of the sand removed from the beach was transported landward across the island rather than being transported offshore. In overwash locations, sand was removed from the nearshore system and unavailable for later beach recovery, resulting in a more permanent response than observed within the other regimes. These results support the predictive capabilities of the storm scaling model and illustrate that the impact regimes provide a framework for explaining the longshore-variable coastal response to hurricanes.

4.2 Introduction

Extreme storms and hurricanes play a dominant role in shaping the beaches of the East and Gulf Coasts of the United States. Superimposed upon the general large-scale mean response of the coast to hurricanes is significant spatial variability; within the storm-impact zone, some areas may experience severe dune erosion and overwash while adjacent areas may appear unaffected. Understanding how the coast responds to storms is critical to safe and responsible coastal planning and management. In order to accurately predict the coastal response to large storms, quantification and characterization of the impact of these storms on barrier islands is required. This includes determining the scales of variability in coastal change, the magnitude of change at these scales, and the processes responsible for the observed variability.

Previous studies have suggested a number of possible reasons for a longshore-variable storm response. In some areas, framework geology plays a role in controlling sediment availability thereby limiting a beach's recovery after large wave events [*Cleary et al.*, 1999; *Riggs et al.*, 1995; *Thieler et al.*, 1995]. Some researchers suggest that some variations in erosion rates may be due to non-linear feedback between highly oblique incident waves and the orientation of the shoreline [*Ashton et al.*, 2003]. There is also evidence that erosional hotspots may be associated with the presence or absence of

offshore sand bars. Initial results show a correlation between the presence of an erosional hotspot and the lack of multiple sand bars; however, a causative relationship has not yet been established [*Kannan et al.*, 2003]. On some beaches the longshore variations in erosion during storms have been shown to relate to the presence of rip current channels and embayments that allow storm waves to propagate closer to shore before breaking [*Komar*, 1983; *Komar and Rea*, 1976].

Another possible explanation for the variance observed in a beach's response to storms may be due to the combined effects of longshore-variable morphology of the beach and dune relative to the intensity of the ocean's forcing. These two ideas are merged through a simple model that defines four storm-impact regimes based on the relative relationship between the elevation of a sand dune or beach berm and that of storm-induced water levels, defined as the sum of astronomical tide, storm surge and wave runup [*Sallenger*, 2000]. During storms increased water levels shift runup and the location of wave attack higher on the profile, making berms and dunes more vulnerable to erosion and over-topping. In this storm-impact scaling model, the borders between the impact regimes represent thresholds across which the magnitudes and processes of coastal change are substantially different [*Sallenger*, 2000].

This work examines the large-scale, longshore-variable impact of Hurricane Bonnie and Floyd within the framework of the storm-impact scaling model in order to address the hypothesis that medium- and large-scale spatial patterns, O(0.01 - 1 km), of coastal change may be explained by the combined effects of longshore-variable storm-induced water levels and the existing beach morphology. In locations where storm surge and runup, and associated sediment transport, are confined to the active beach profile (seaward of the dune), sand that is lost from the beach typically returns during more quiescent periods. In contrast, locations where storm-induced water levels overtop the dune or barrier island may undergo larger and more permanent changes to the beach profile if sand is transported across the island and removed from the nearshore system.

The first objective is to quantitatively test the predictive capabilities of Sallenger's storm-impact scaling model for estimating the coastal response to hurricanes. The expected impact regime is calculated from surveys of the pre-storm beach morphology and a hindcast estimate of hurricane-induced water levels. Predictions are then compared to objective classifications of the observed hurricane-impact regime to evaluate the accuracy of the model's predictive capabilities. The second goal is to characterize and quantify the differences in coastal change within each impact regime in order to determine to what extent the processes specific to each regime contribute to the total longshore variability of coastal change. Finally we discuss reasons for prediction errors as well as possible reasons for spatial variability that were not accounted for using Sallenger's model (2000).

4.3 Hurricanes and Study Area

Hurricane Bonnie made landfall on August 27, 1998 at 0330 GMT near Wilmington, NC, as a borderline category two/three storm measured on the Saffir-Simpson scale. The storm exceeded a maximum surface wind speed of 51 m/s (100 knots) for 72 hours prior to landfall [*Avila*, 1998]. The maximum significant wave height (H_s) observed at NOAA CMAN station FPSN7, located on Frying Pan Shoals 55.6 km southeast of Cape Fear, was 8.7 m (corresponding wave period, T_0, = 14.3 s), 15 hours prior to landfall. Wave heights exceeded 6 m for 30 hours prior to the storm's landfall. Just over one year later, on September 16, 1999 at 0630 GMT, Hurricane Floyd made landfall in the same area (Figure 4.1). This strong category-four storm maintained winds speeds between 54 and 69 m/s (105 - 135 knots) for 72 hours before making landfall near Cape Fear, NC as a category two storm [*Pasch et al.*, 1999]. Approximately 1.5 hrs after landfall, NOAA station FPSN7 recorded a maximum significant wave height of 9.21 m (T_0 = 14.3 s). Floyd was a fast moving storm as it neared the coast; therefore, significant wave heights exceeded 6 m for only 17 hrs prior to landfall.

The focus of this research is on the impacts of these two hurricanes along a 50-km stretch of barrier islands in Onslow Bay, North Carolina, from Masonboro Island to

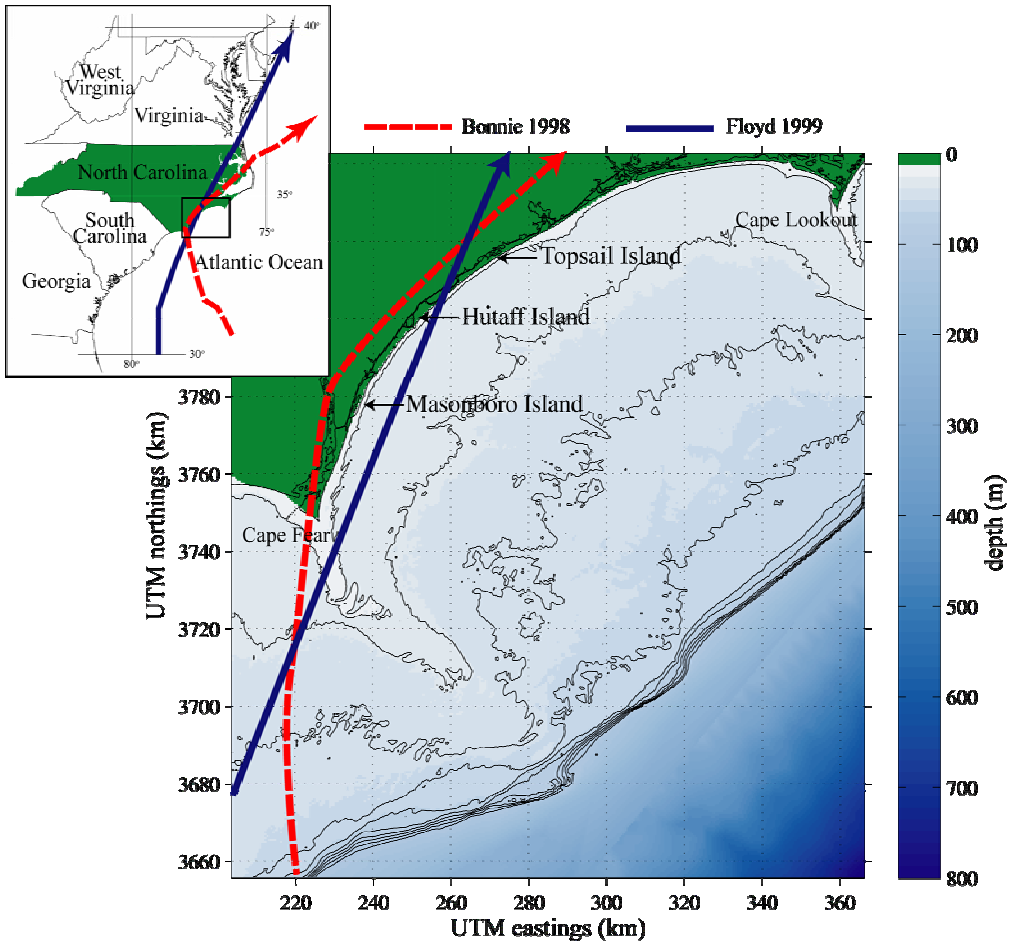

Figure 4.1. Location map of Onslow Bay, NC, with the approximate tracks and landfall locations of Hurricanes Bonnie and Floyd. Depths contours are shown at 10-m intervals out to 100 m, the approximate location of the shelf break.

Topsail Island (Figure 4.1). Onslow Bay, located between Capes Fear and Lookout, is a wave-dominated environment (mean tide range = 1 m) with a broad and shallow continental shelf [*Thieler et al.*, 1995]. The shoreline orientation of these islands changes dramatically in this region, trending approximately 24° (clockwise from north) along Masonboro Island and becoming more NE-SW oriented along Topsail Island (~56°). Major wave events in this area are associated with northeaster storms during the winter months and hurricanes in the summer. A net southerly longshore drift has resulted in accretionary spits located on the southern end of many of the islands [*Thieler et al.*, 1995].

Both developed and undeveloped beaches are present along this stretch of coast. Wrightsville Beach is maintained by regular nourishment projects while other beaches

are supplemented with sand from local dredging projects [*Rogers*, 2000]. Areas that had been impacted by nourishment projects during the study period (Wrightsville Beach, Figure Eight Island, and the northern portion of Masonboro Island) were eliminated from analysis as the measured, hurricane-induced coastal change signal was likely contaminated by the addition of sand at these locations. Inlets, both natural and engineered, play a large role in the morphodynamics of this area [*Cleary et al.*, 2003]. Dramatic coastal change occurring in close proximity to the inlets (~1 km) was not considered in this study because the frequency of beach morphology surveys was not sufficient to differentiate hurricane-induced coastal changes from those due to inlet dynamics. Results are limited to continuous stretches of beach along Masonboro, Hutaff, and Topsail Islands (Figure 4.1). Masonboro Island is a short, undeveloped barrier island bordered by two modified inlets, Carolina Beach and jettied Masonboro Inlets [*Sault et al.*, 1999]. Only the southern 8 km of the island are considered in these analyses because the northern-most end of this island regularly receives an input of sand from the dredging of Masonboro Inlet, most notably in 1998 prior to the passage of Hurricane Bonnie. Hutaff Island is a low-lying, undeveloped, 4-km stretch of beach bounded by Rich and New Topsail Inlets. Prior to the passage of Hurricane Bonnie, Hutaff was composed of two smaller islands, Lea and Hutaff, that were joined after Old Topsail Inlet was closed during the storm [*McGinnis and Cleary*, 2003]. Topsail Island, the northern-most island in the study area, is approximately 35-km in length and is bordered to the south by New Topsail Inlet and to the north by New River Inlet. This thin, dune-backed island contains areas of significant development within the coastal towns of Topsail Beach, Surf City, and North Topsail Beach.

4.4 Methods

To test the validity of the Sallenger [2000] model for predicting storm responses and scaling magnitudes of coastal change, the storm-impact regime was predicted every 20 m along the coast using measurements of pre-storm dune elevation and estimates of hurricane-induced, expected water levels. Estimated water levels were calculated using modeled surge and wave conditions and an empirical parameterization for wave setup

and runup. Dune elevations were extracted from detailed laser-altimetry surveys of beach topography. These surveys were also used to calculate the observed impact on beaches and dunes following each storm and the magnitudes of change within each regime. Details of the storm-impact scaling model, the topographic surveys, coastal change measures, and wave and surge modeling are presented below.

4.4.1 Storm-Impact Scaling Model

The storm-impact scaling model presented by Sallenger [2000] explicitly couples fluid forcing and beach morphology by examining the relationship between the elevation of extreme water levels (R_{low}, R_{high}) and relevant beach morphology (D_{low}, D_{high}). R_{low}, an approximate storm-induced mean water level, is defined as the sum of storm surge, astronomical tide, and wave setup, the super-elevation of the still water level due to the presence of waves (Figure 4.2). This is a slightly different formulation than that of Sallenger [2000], which defined R_{low} using the elevation of the seaward limit of swash. R_{high} represents the highest elevation of the landward margin of swash relative to a fixed vertical datum. This measure includes the combined effects of astronomical tides, storm surge, and the 2% exceedence level for vertical wave runup, including both setup and swash [*Ruggiero et al.*, 2001; *Sallenger*, 2000]. D_{high} is the elevation of a beach's first line of defense against storm waves, either the elevation of the dune crest or, in the absence of a dune, the beach berm (Figure 4.2). D_{low} is the elevation of the toe of the dune.

By considering how R_{high} and R_{low} vary with respect to D_{high} and D_{low}, four impact regimes are defined [*Sallenger*, 2000]. Within the *swash* regime wave runup is confined to the foreshore region ($R_{high} < D_{low}$), and sand that is eroded during storms is generally moved offshore until it is returned to the beach during more quiescent periods. The *collision* regime occurs when the maximum water level exceeds the base of the dune, $D_{high} > R_{high} > D_{low}$. Here, runup collides with the dune causing erosion that may be more long-lasting than foreshore erosion as dunes are typically rebuilt through slower aeolian processes. As R_{high} increases, *overwash* will occur when $R_{high} > D_{high}$. Within this regime,

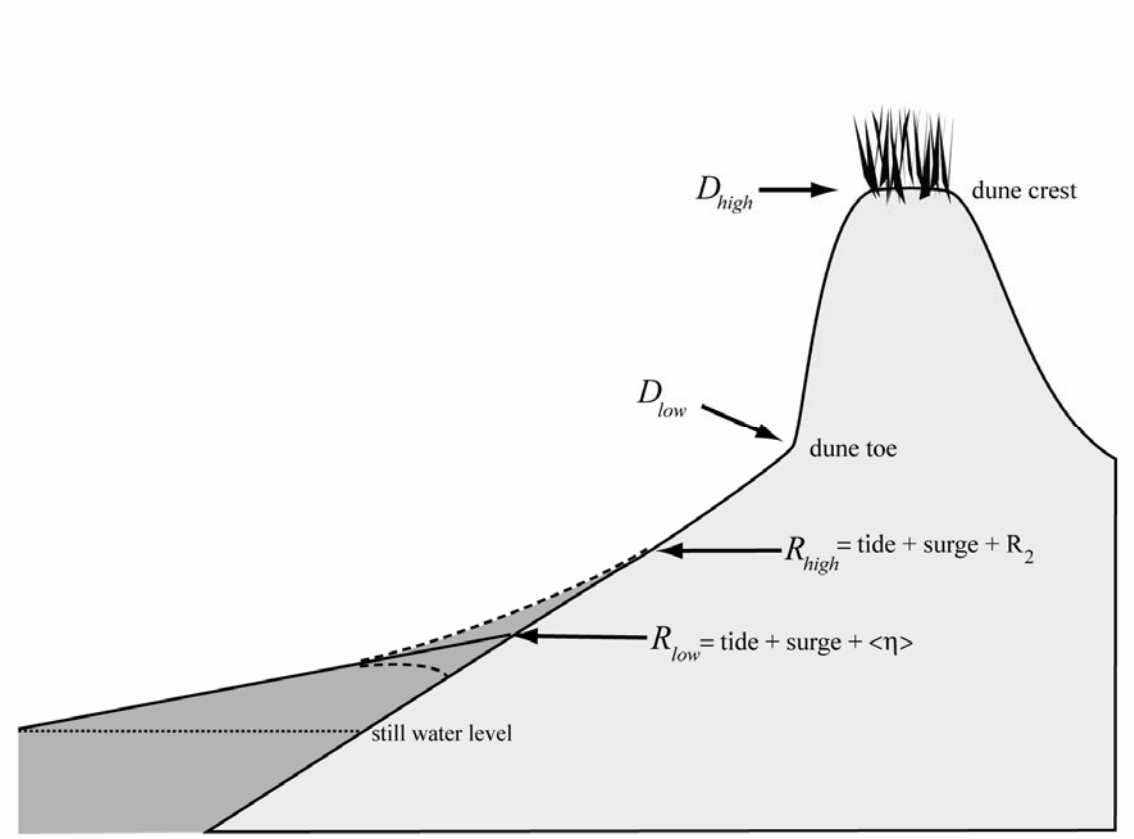

Figure 4.2. Definition sketch showing R_{high}, R_{low}, D_{high} and D_{low}. The dashed lines represent the swash excursion about wave setup (solid line). (Modified from Sallenger, 2000)

sand is transported landward and not readily returned to the seaward side of the island. The final and most extreme regime, *inundation*, occurs when $R_{low} > D_{high}$, and the beach and dunes are completely and continually subaqueous. Measurements (or estimates) of R_{high}, R_{low}, D_{high}, and D_{low} are allowed to vary in the longshore direction creating spatial variability of the impact regime and, presumably, of the observed response due to different processes at work within each regime.

4.4.2 Coastal Morphology

4.4.2.1. Lidar Topographic Surveys

Surveys of beach and dune topography were collected using NASA's Airborne Topographic Mapper (ATM), a scanning laser altimeter (lidar) that is used for mapping

coastal change and assessing storm impacts on subaerial beaches [*Brock et al.*, 1999; *Krabill et al.*, 2000]. The ATM beach surveys provide a dense data set of subaerial beach topography with both large spatial coverage and high spatial resolution. For each survey over 100 km of coast were sampled with one laser shot collected every ~2 m^2. The root-mean-square (rms) vertical error of the ATM has been estimated as 15 cm [*Sallenger et al.*, 2003]. The lidar data allow objective estimates of coastal change, such as shoreline and beach volume change, that are spatially extensive, synoptic, and of sufficient accuracy to resolve a wide range of beach variability.

A baseline topography survey was conducted on September 20, 1997, defining the pre-storm beach state for both hurricanes. This survey was collected after a long period of fair weather and is assumed to define the characteristic, calm-weather profile shape for these beaches based on typical summer wave conditions as well as sediment type and availability. Hurricane-induced coastal change is quantified by comparing the calm-weather 1997 lidar topographic survey to data collected after each hurricane came ashore. The impact of Hurricane Bonnie (hereinafter referred to only as Bonnie) was documented by a lidar survey on September 5, 1998, nine days following landfall. Portions of the coast are expected to have recovered somewhat in those nine days; however, a large wave event (H_s ~ 5 m) that occurred one day before the lidar survey likely prevented significant post-storm accretion from having significantly altered the record of hurricane-induced change. A third lidar survey on September 18, 1999 was used to calculate coastal change resulting from Hurricane Floyd (hereinafter referred to only as Floyd) that came ashore two days earlier. A final survey collected on August 3, 2000, prior to the onset of fall and winter storm waves, was used to determine the amount of post-storm recovery and the three-year cumulative impacts of two hurricanes.

4.4.2.2. Defining Coastal Morphology and Change

A number of measures of beach morphology and coastal change were extracted from digital elevation models (DEMs) of gridded lidar data and cross-shore profiles through the original (x, y, z) data. The position of the dune crest was coarsely digitized on 1-m gridded DEMs, every 2 m along the coast [*Elko et al.*, 2002]. In areas where no dune was

present, the berm crest was digitized as the highest point on the beach. The precise cross-shore location and elevation (relative to NAVD88) of the dune or berm crest (x_{dc}, $z_{dc;}$ see Figure 4.3) were then automatically identified as the highest elevation within a 6-m wide swath centered on the digitized line. Where a dune was present, the horizontal position and elevation of its toe (x_{dt}, $z_{dt;}$ see Figure 4.3) were calculated as the location of maximum slope change within a region around a coarsely digitized line. The vertical rms accuracy of this technique, based on a repeatability analysis of multiple digitizers, is 37 cm [*Elko et al.*, 2002]. These selections of dune and berm positions were visually verified to insure that a consistent or similar feature was selected at all sites and that structures and vegetation were not mistakenly selected as dunes.

Additional measures of beach morphology were quantified from cross-shore profiles of lidar data evenly spaced in the longshore direction (dy = 20 m). The horizontal position of the mean high water (MHW, z_{sl} = 0.36 m, NAVD88) shoreline, $x_{sl}(y)$, was calculated along each lidar profile from a linear regression fit to data located in a window around z_{sl} [*Stockdon et al.*, 2002]. Based on the accuracy of the lidar system, we expect to obtain a horizontal shoreline accuracy of ±1.5 m on beaches with a typical foreshore slope of 0.1. Comparisons between lidar-derived and ground-measured shorelines in North Carolina revealed a rms difference of 2.9 m [*Stockdon et al.*, 2002]. The width of the beach, $X_b(y)$, was defined as the horizontal distance between the shoreline and the base of the dune or, in the absence of a dune, the crest of the berm, ($x_{sl} - x_{dt}$). The mean slope of this region, $\beta_m(y)$, was defined as ($z_{sl} - z_{dt}$)/ X_b. Figure 4.3 illustrates the above-defined quantities, as well as D_{high} and D_{low}, on example lidar profiles from Topsail Island. The cross-shore profiles form the basis for all subsequent analyses including measures of coastal change and the determination of impact regime.

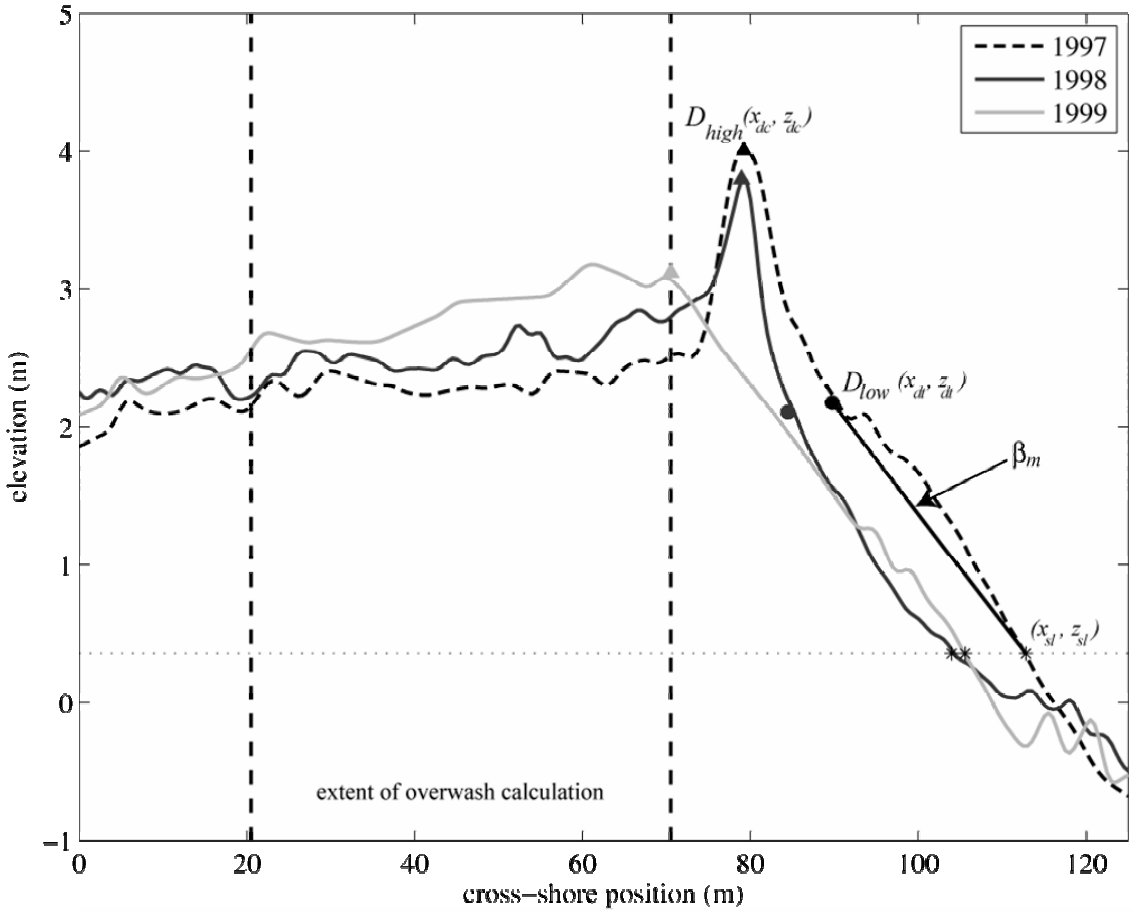

Figure 4.3. Example lidar profiles for September 20, 1997, September 5, 1998, and September 18, 1999 from Topsail Island, NC defining measures of coastal morphology and change. The location of the MHW (z = 0.36 m) shoreline (x_{sl}, z_{sl}) is indicated with an asterisk. The location of the dune crest (x_{dc}, z_{dc}), dune toe (x_{dt}, z_{dt}), and the mean beach slope (β_b) for the 1997 profile are also shown. Vertical dashed lines indicate the horizontal extent over which inland volume change, δV_i, is calculated between the 1999 and 1997 surveys.

Shoreline change, $\delta x_{sl}(y)$, was calculated as

$$\delta x_{sl}(y) = x_{sl2}(y) - x_{sl1}(y) \tag{4.1}$$

where the post-storm shoreline position is given by $x_{sl2}(y)$, and the 1997 calm-weather shoreline position, $x_{sl1}(y)$, is taken as the reference from which change is calculated. While the horizontal change of the MHW contour over a one year period also includes the beach's response to seasonal changes in wave climate, the magnitude of the storm-induced signal is expected to exceed that related to inter-annual variability. Beach volume change, $\delta V_b(y)$, is used to document more extreme changes that are likely to be

attributed to the hurricanes. Beach volume change at each profile was defined between $x_{sl1}(y)$ and the 1997 horizontal position of the dune or berm, $x_{dc1}(y)$, as

$$\delta V_b(y) = \int_{x_{dc1}(y)}^{x_{sl1}(y)} (z_2 - z_1) dx \tag{4.2}$$

where dx, the cross-shore spacing between interpolated lidar survey data, is 0.5 m. (Note, all volume change quantities are m^3 per m in the longshore.)

4.4.3 Hurricane-induced Water Levels

Estimates of hurricane-induced water levels, R_{low} and R_{high}, are needed for prediction of impact regimes and for examining the role of combined longshore-variable fluid forcing and morphology on coastal change. Measures of R_{low} and R_{high} require knowledge of the tide, storm surge, and wave runup (and setup) associated with each hurricane landfall. Storm surge levels and astronomical tides were calculated using the FLOW module of Delft 3D [*Delft*, 2003]. The elevation of wave runup and setup were calculated from modeled offshore wave conditions [*Booij et al.*, 1999] using empirical parameterizations [*Stockdon et al.*, 2006].

4.4.3.1. Storm Surge and Tide Modeling

Measured tides during Bonnie and Floyd were not available because no open coast tidal gauges were operational during either storm. Therefore, storm surge and astronomical tides were modeled using Delft3D-FLOW, a hydrodynamic model that calculates the unsteady flow from tidal and meteorological forcing [*Delft*, 2003]. The model allows for space- and time-varying wind and atmospheric pressure fields, necessary for correctly modeling the variability of hurricane-induced water levels.

Nearshore and inner shelf bathymetry data for Onslow Bay were obtained from the National Geographic Data Center's (NGDC) Geophysical Data System (GEODAS) for hydrographic surveys (horizontal resolution = ~ 90 m). Bathymetry seaward of the shelf

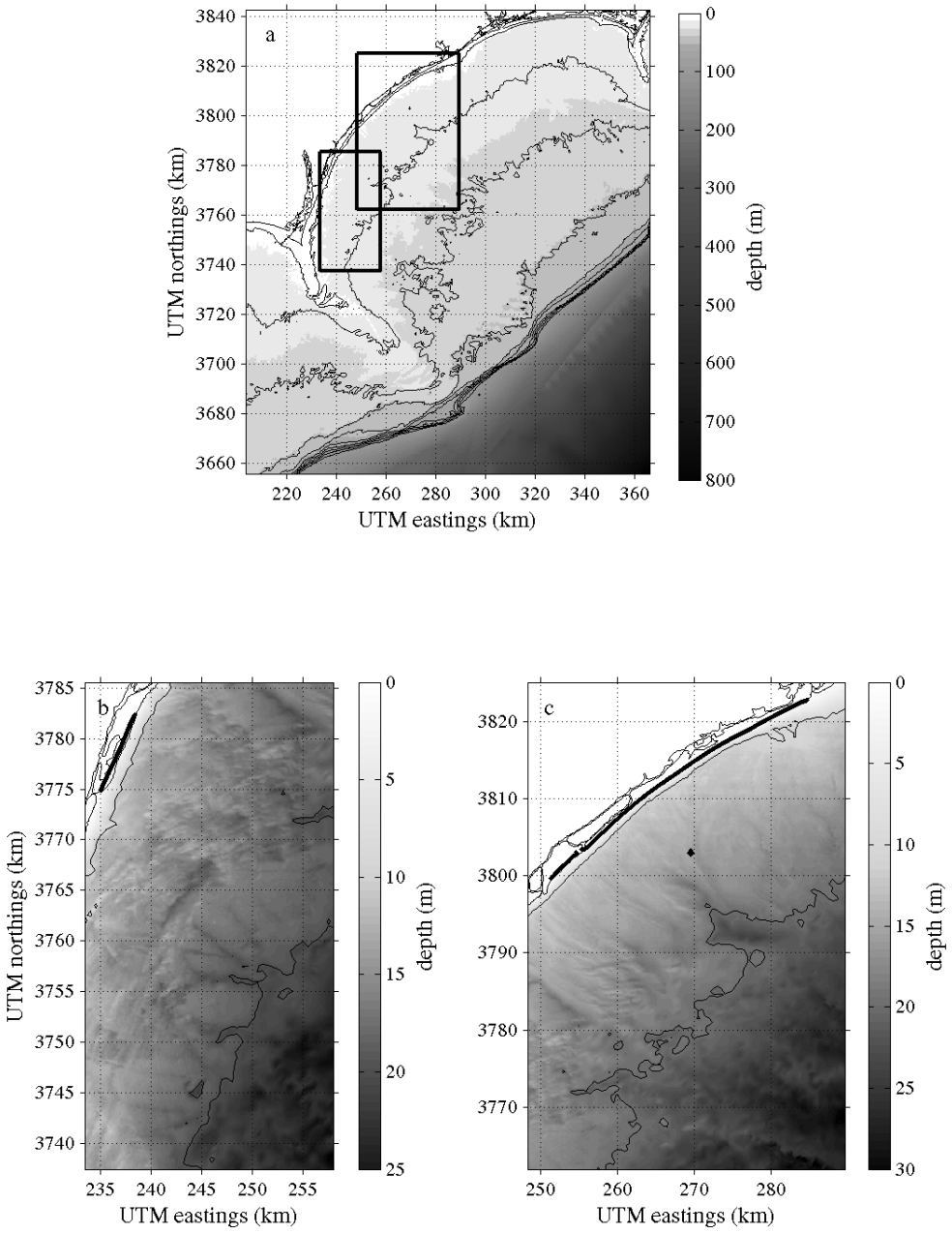

Figure 4.4. The input bathymetry grids for wave and surge modeling for the (a) whole domain and for the 500-m resolution nested grids containing (b) Masonboro Island and (c) Hutaff and Topsail Islands. Depth contours are given at 10-m intervals out to a depth of 100 m, the approximate location of the shelf break. The maximum contour shown in panels (b) and (c) is h = 20 m.

was extracted from the NGDC's 2-minute gridded global relief dataset (eTopo2). The merged data set was gridded at 500-m resolution in a 162-km by 186.5-km domain, which included both Capes Fear and Lookout (Figure 4.4a).

Ten tidal constituents, derived from the TPX06.2 global inverse tide model [*Egbert and Erofeeva*, 2002], were specified along the open boundaries of the model domain. The accuracy of Delft3D-modeled tide in this region was validated by comparing the modeled tides for the month of January 2005 to tides measured at a NBDC gauge in Wilmington Beach, NC, approximately 10 km south of Masonboro Island. After the model stabilized, the rms difference between the modeled and measured values was -1.3 cm indicating that the astronomical tides were correctly represented.

Wind grids from the NCEP North American Regional Reanalysis (NARR) program were used as input when the hurricanes were located outside of the model domain. When the storm track was within the study area, the input wind fields for Bonnie and Floyd were defined using data from NOAA's Hurricane Research Division (HRD). These gridded data consist of observations of maximum sustained wind speed and direction collected every three hours from a variety of sources (e.g. ships, buoys, reconnaissance aircraft, etc.), post-processed to conform to a standard 1-min averaging period measured 10-m above the surface [NOAA, 2005]. The blended NARR and HRD data set was gridded on a 177-km by 204-km domain with a 6-km resolution that encompassed the bathymetry grid. The radial distribution of surface pressure associated with each hurricane was then calculated from the merged HRD/NARR gridded wind field using the formulation given by Holland [1980].

The computational time step for the model was 15 minutes, and model results were output every 30 minutes. Water levels for Bonnie were modeled from August 24, 1998, 0000 GMT through landfall, ending on August 27, 1998, 2100 GMT. Water levels for Floyd were modeled from September 14, 1999, 0000 GMT through September 17, 1999, 0800 GMT. Modeled water-level elevation time series, $\eta(t,y)$, representing both the

astronomical tide and storm surge, were extracted along the shoreline at each lidar profile longshore location. The maximum, open-coast storm surge level during Bonnie was 1.7 m along Topsail and Hutaff Islands, approximately 10.5 hours before landfall. (It is not uncommon for water levels to peak before or after landfall of a storm's geographic eye, which may differ from landfall of the center of wind circulation and the location of maximum surge-producing wind stress.) Maximum surge levels decreased gradually along the coast to 1.5 m approaching Masonboro Island. Storm surge for Floyd first peaked along Masonboro Island (η = 2.1 m) on September 16, 1999, 0530 GMT, one hour prior to landfall. As the storm continued to move onshore, surge levels continued to rise along Hutaff (η = 2.2 m) and Topsail Island (η = 2.1 m), peaking during landfall.

The model results could not be confirmed with measured water levels because no open coast gauges were operational during the storms. The National Hurricane Center's (NHC) final reports on Bonnie and Floyd provide only limited observations of storm tides (astronomical tides plus storm surge). For Masonboro Island the reported storm tide was ~1 m above the Delft3D-modeled values [*Avila*, 1998; *Pasch et al.*, 1999]. However, values could not be confirmed as open-coast since details of the location of the measurement were not provided in the reports and data sources were not given. Observed water levels on Wrightsville Beach, located within the study area between Masonboro and Hutaff Islands, during Bonnie were reported to be 2.1 – 2.2 m [*Avila*, 1998], similar to the modeled values for this area (η = 2.0 m).

4.4.3.2. Wave Modeling

The nearshore wave field for each hurricane was modeled using Simulating WAves Nearshore (SWAN) [*Booij et al.*, 1999], a third-generation wave model used to estimate the wave conditions in nearshore coastal waters. The model solves the spectral action balance equation in which the rate of change and the propagation of wave action are balanced by source terms including wind generation, dissipation (bottom friction and white-capping), and nonlinear wave-wave interactions [*Booij et al.*, 1999]. The bathymetry grid used for storm surge modeling was used to define the SWAN model domain (Figure 4.4a). Two nested grids with 100-m resolution were included to better

characterize the spatial variability of wave height within the specific study area (Figure 4.4b and 4.4c). The HRD wind field data, originally gridded at 5.58-km resolution for Bonnie and 2.79 km for Floyd, were spatially interpolated to the 500-m resolution bathymetry grid and used as input in the SWAN model. The maximum gridded HRD wind speed for both storms was approximately 45 m/s, slightly under-representing observed maxima. Both storms entered the model domain from the southwest resulting in east-southeast winds blowing almost directly onshore. Initial offshore wave conditions were not specified as model input because observations of sufficient resolution for modeling the spatial variability of hurricane wave conditions were not available. Comparisons between non-stationary model runs using only HRD wind input and runs using both HRD winds and modeled, gridded wave heights (WaveWatch III) as input show a mean difference of less than 15 cm at the 10-m isobath during the peak of storm, indicating that the strong winds are the dominant forcing. Observations of wave conditions at buoys located outside of Onslow Bay show that no significant wave energy not forced by the hurricanes was entering the model domain at the time of these storms, indicating that local wave conditions could be sufficiently modeled using only wind input.

A number of sensitivity tests evaluating the performance of the SWAN model in hurricane conditions confirmed that the default values provided the most accurate results, as defined by comparison to observations at NOAA station FPSN-7. The model was run in a non-stationary mode for both hurricanes over the time period for which HRD wind data were available. The computation time step was 10 minutes and results were output every 30 minutes. For Bonnie, the model was run for nine hours (August 26, 1998, 1030 – 1930 GMT), ending approximately eight hours before the official landfall of the eye. The wave field for Floyd was modeled for 20.5 hours starting on September 15, 1999, 1030 GMT and continuing through landfall the next day at 0630 GMT. Local wave height, defined by that observed at the 10-m isobath, was extracted from each 30-minute output interval, t, of the model run. These data were then interpolated to the longshore locations of lidar profiles to provide $H_s(t,y)$ for estimating wave runup and setup.

The accuracy of the model results were tested by comparing computed H_s to that measured at NOAA station FPSN7 located on Frying Pan Shoals (water depth = 19.5 m). The gauge at FPSN7 did not operate throughout the duration of either storm and no observations were made at landfall; however, a 5- and 16-hour time series of observed H_s during Bonnie and Floyd, respectively, were available for comparison with a subset of the modeled H_s time series. SWAN-modeled H_s on Frying Pan Shoals during Bonnie compares reasonably well to observed values. The time-averaged (5-hr) mean difference, ΔH_s, was = 1.18 m (positive differences indicate that observations were larger than modeled values) and the rms difference was 1.29 m. At the time of maximum observed H_s, 13 hours prior to landfall, ΔH_s = 0.92 m (12.0% error). Modeled H_s for Floyd was consistently less than the observed values; over the 16-hr comparison, ΔH_s = 2.52 m and the rms difference was 2.7 m. However, errors were smaller during the 6 hours immediately prior to storm landfall when the HRD wind grids were available and within the model domain, and the hurricane wind field was more accurately represented. During this time period, ΔH_s = 1.18 m and the rms difference was 1.19 m. At the time of maximum observed H_s, 3.5 hrs prior to landfall, ΔH_s = 1.61 m (19.5% error). Because FPSN7 is located on the dynamic shoals offshore of Cape Fear, differences between observed and modeled wave height may be due to inaccuracies in the input bathymetry and the resulting errors in modeling wave shoaling, breaking, and refraction. However, the sensitivities of the model nearshore ($h \leq 10$ m) are expected to be low. Precise calibration of the SWAN model during hurricane conditions is beyond the scope of this work.

4.4.3.3. Estimation of Wave Runup and Setup

Wave runup is the sum of setup, the time-averaged water-level elevation at the shoreline due to waves (excluding tides and surge), and swash, the time-varying, vertical fluctuations about the temporal mean. The elevation of runup maxima has been shown to be dependent on deep-water wave height (H_0), wave period (T_0) and the foreshore beach slope (β_f). The elevation of the 2% exceedence level for runup, R_2, can be calculated using the empirical parameterization

$$R_2 = 1.1\left(0.35\beta_f (H_0 L_0)^{1/2} + \frac{[H_0 L_0 (0.563\beta_f{}^2 + 0.004)]^{1/2}}{2}\right), \quad (4.3)$$

which includes both wave-induced setup and swash, where L_0 is the deep-water wavelength, defined as $gT_0^2/2\pi$ [*Stockdon et al.*, 2006]. The full expression for runup is used because conditions for both hurricanes were intermediate to reflective (Iribarren Number, $\xi_0 = \beta / (H_0/L_0)^{1/2} < 0.3$).

Foreshore beach slope used in equations 4.3 is defined over the area of significant swash activity [*Stockdon et al.*, 2006]. However, for application of these equations to hurricane-induced runup where large waves will likely move the swash zone higher on the profile, the mean beach slope, $\beta_m(y)$, between the dune (or berm) and the MHW shoreline, was defined as the relevant slope measure (Figure 4.3). Additionally, the mean beach slope was thought to provide a more stable measure of profile slope that was less sensitive to daily changes in wave energy. Because topography surveys were not collected immediately prior to the hurricanes and pre-storm β_f could not be measured, the mean beach slope is likely more representative of slopes typical for this site. It is also expected that any berm located within the swash zone will likely erode with the arrival of the storm waves, quickly reducing the foreshore slope to that of the mean profile.

H_0 specific to equation 4.3 is defined as a local measure of significant wave height, H_s, that has been reverse shoaled to deep water [*Stockdon et al.*, 2006]. SWAN-modeled $H_s(t,y)$ represents the local (h = 10m), spatially-variable wave height within the study area that has dissipated across the shelf and refracted over local bathymetry. To obtain $H_0(t,y)$ for use in the runup parameterization, $H_s(t,y)$ was reverse shoaled to deep water using linear theory. $R_2(t,y)$ was then estimated every 20 m along the each island using $H_0(t,y)$ and lidar-derived, pre-storm $\beta_m(y)$. Based on equation 4.3, variability in $H_0(y)$ and $\beta_m(y)$ result in a corresponding spatial pattern in runup.

4.5 Results

4.5.1 Estimated Storm-Impact Regime

For estimation of the likely hurricane-impact regime, D_{high} and D_{low} were defined as the 1997 elevations of the dune (or berm) crest, z_{dc}, and toe, z_{dt}. Using 1997 data as the pre-storm morphology for Floyd assumes complete recovery after Bonnie and no significant change to dunes. The validity of this assumption is addressed within the Discussion section. Both quantities were extracted at each lidar profile location to collocate morphology measurement with water-level estimates (Figure 4.5). The mean value, μ, of $D_{high}(y)$ across all profiles was 3.56 m with significant spatial variability (standard deviation, σ, = 1.48 m). On the uninhabited, low-lying barriers (longshore locations y = 0-10 km and 30-35 km, Figure 4.5), 91.4% of the profiles were berm-backed and μD_{high} was over 2 m less than that on dune-backed Topsail Island (y = 35-70 km) where μD_{high} = 4.46 m and $\mu D_{low}(y)$ = 2.14 m. Spatially-averaged, pre-storm beach slope and dune elevations for each island and over the whole study area are presented in Table 4.1.

$R_{high}(t,y)$ was calculated as $R_2(t,y) + \eta(t,y)$, the sum of parameterized runup and modeled water level (tide plus surge). The variability of R_{high} , as well as its components $R_2(t,y)$ and $\eta(t,y)$, are illustrated in timestacks which show temporal variations at each profile location associated with hurricane approach (Figure 4.6). During Bonnie, the maximum values of R_{high} on Masonboro Island preceded those along Topsail Island by approximately 30 minutes (1630 and 1700 GMT, respectively). The same temporal variability was observed during Floyd where R_{high} and η peaked first along Masonboro Island on September 16, 1999 between 0530 and 0600 GMT and then approximately 30 minutes later along Topsail Island. While the peak values over the study area as a whole occurred over a period of 1-2 hours, the maximum value of R_{high} for an individual island generally occurred at a single time step. For the remainder of the analyses, only the maximum value of $R_{high}(t, y)$ at each location, $R_{high}(y)$, was considered.

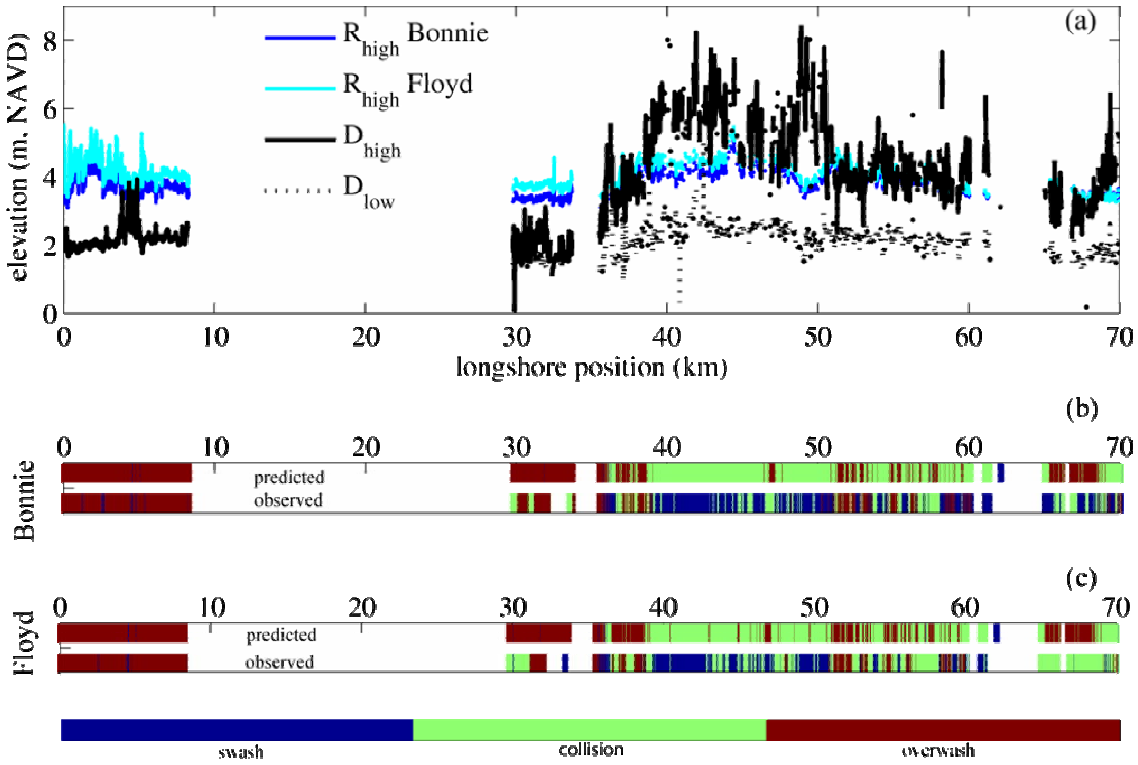

Figure 4.5. (a) Elevations of D_{high} (black), D_{low} (dashed) and R_{high} for Masonboro (y = 0 – 10 km), Hutaff (y = 30 - 35 km) and Topsail Islands (y = 35 - 70 km). D_{low} was not defined on Masonboro and over most of Hutaff Islands because dunes were not present. The 20-km gap in the record corresponds to Wrightsville Beach and Figure Eight Island, which were not considered in this study. The predicted regime (top row) for Bonnie (b) and Floyd (c) was calculated as: swash (light gray) = $R_{high} < D_{low}$; collision (dark gray) $R_{high} > D_{low}$; overwash (black) $R_{high} > D_{high}$. The observed regime (bottom row in panels (b) and (c)) was determined from calculations of dune erosion and overwash volumes.

Over the whole region the mean magnitude of R_{high} was 22 cm greater during Floyd, despite somewhat smaller wave heights and runup. Storm surge accompanying Floyd was 38 cm higher than that for Bonnie (see Table 4.2). During both storms the spatial variability of R_{high} ($\sigma R_{high} \approx 41$ cm) was approximately four times larger than that of H_s and surge (σH, $\sigma\eta$ = O(10cm), Table 4.2). The relative change in H_s across the study area was 2.5%, significantly less than the relative change in slope (36%); therefore, most of the longshore variability of $R_{high}(y)$, particularly along a single island, was due to variations in β_m and subsequent spatial patterns in R_2. The empirical parameterization for runup shows that for beaches with a mean slope of 0.055, a 36% increase (decrease) in

Table 4.1. Spatial mean (and standard deviation) of pre-storm beach morphology.

	D_{high} (m)	D_{low} (m)	β_m
Masonboro[+]	2.17 (0.29)	n/a	0.062(0.02)
Hutaff[+]	1.94 (0.43)	1.53(0.24)	0.027(0.007)
Topsail	4.46(1.16)	2.14(0.41)	0.056(0.02)
whole area	3.56(1.48)	2.11 (0.42)	0.055(0.02)

[+]Undeveloped barrier island

beach slope will lead to a 20% (-18%) relative change in R_2. Similar spatial patterns of $R_{high}(y)$ for Bonnie and Floyd result from the use of the 1997 beach slope as input in the runup parameterization for both storms.

While storm surge is commonly viewed as the main contributor to increased water levels during a hurricane, wave runup was also found to be a significant component of the maximum total water level attained in each storm. During Bonnie, R_2 made up 48.3% of the total R_{high} signal. 44.3% of the signal was attributed to surge, leaving 7.4% to astronomical tides. The percent contribution of R_2 to total water levels was similar during Floyd (47.1%); however, during this category-4 storm, storm surge accounted for 51.4% of the R_{high} signal. The relative contributions of runup, surge, and tide observed over the whole study area were also present on Masonboro and Topsail Islands. On Hutaff Island, storm surge made up the dominant part of R_{high} signal for both Bonnie and Floyd (49.3% and 59.0%, respectively). Runup elevations were not as high here because of the gentle mean beach slope found along the length of the island. The similar relative contributions of both R_2 and storm surge to the total, hurricane-induced water level emphasize the importance of including wave-driven processes (setup and swash) in coastal vulnerability assessment in that they may double the water-level beyond that due to storm surge alone.

Using the above quantities for dune morphology and storm-induced water levels, the occurrence of three impact regimes were predicted for Bonnie and Floyd (Figures 4.5b and 4.5c); swash ($R_{high} < D_{low}$), collision ($D_{high} > R_{high} > D_{low}$), and overwash ($R_{high} > D_{high}$). The inundation regime was not distinguished from overwash in this study because

Table 4.2. Spatial mean (and standard deviation) of hurricane-induced water level, wave height, surge, and tide at the time of maximum Rhigh.

	R_{high} (m)	H_s (m)	surge (m)	tide (m)
Hurricane Bonnie				
Masonboro	3.84(0.39)	3.79(0.04)	1.50(0.01)	0.36
Hutaff	3.37(0.11)	3.83(0.04)	1.66(0.04)	0.33
Topsail	3.81(0.36)	3.74(0.11)	1.70(0.03)	0.25
whole area	3.78(0.37)	3.76(0.10)	1.66(0.08)	-
Hurricane Floyd				
Masonboro	4.18(0.40)	3.69(0.04)	2.03(0.05)	0.10
Hutaff	3.74(0.11)	3.73(0.03)	2.21(0.01)	0.11
Topsail	3.99(0.46)	3.64(0.14)	2.02(0.14)	0.04
whole area	4.00(0.44)	3.66(0.12)	2.04(0.13)	-

difficulties using the lidar profiles to determine whether the island was completely submerged make accuracy testing not possible within this regime. The spatial variability of the estimated storm response was due to both D_{high} and R_2 while temporal variability occurred as H_s and η increased as each storm moved ashore (Figure 4.6). The impact regime predicted to occur at each cross-shore location was specified at the time of maximum R_{high} (shown by solid vertical line in each panel in Figure 4.6). Overwash was the most often predicted response for both Bonnie and Floyd, estimated to occur at 56.2% and 61.7% of the profiles, respectively. Collision was predicted for 43.0% of the profiles during Bonnie and 37.6% during Floyd. The minimum impact, swash, was expected for less than 1% of the profiles. For both storms, Masonboro and Hutaff Islands were predicted to overwash at 99% of the longshore locations. Because dunes were not present on these islands, the prediction and occurrence of the collision regime was not possible. Spatial variability of D_{high} (σD_{high} = 1.16 m) along Topsail Island resulted in a mix of predicted responses. During Bonnie, 69.5% of the profiles on Topsail Island were predicted to fall within the collision regime and 29.9% were expected to overwash. A similar spatial pattern was observed during Floyd with the majority of Topsail predicted to experience collision (60.9%); however, more of the island (38.5% of the profiles) was expected to overwash due to higher elevations of R_{high} associated with Floyd.

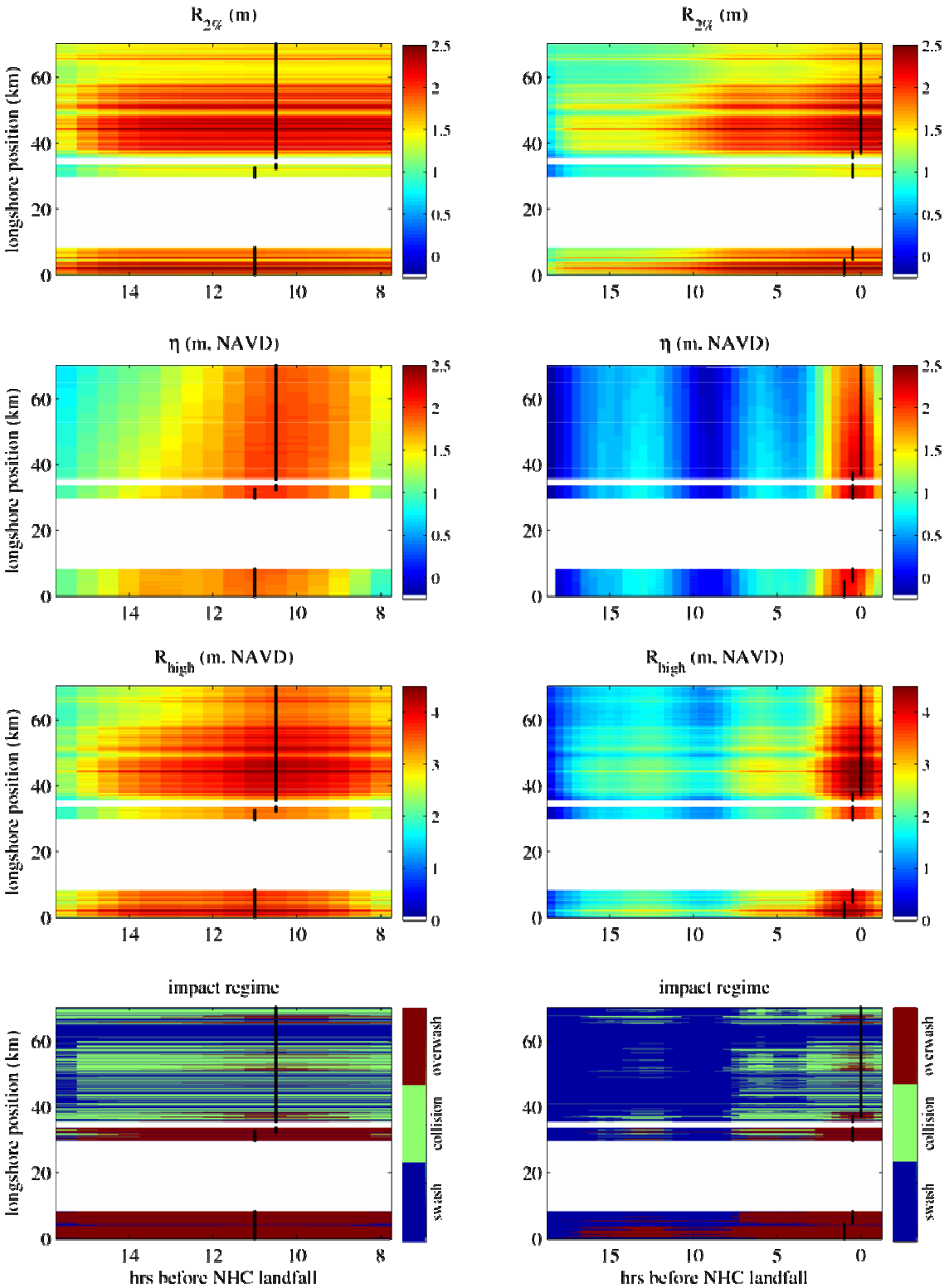

Figure 4.6. Timestacks of R_2, η, R_{high}, and the predicted impact regime for Hurricanes Bonnie (left column) and Floyd (right column). The time of maximum R_{high} is shown in each panel by the vertical black line. The white area in each panel corresponds to beaches not considered in this study.

4.5.2 Observed Storm-Impact Regime

Objective determinations of impact regime were made by comparing the 1997 calm-weather and post-storm cross-shore topography profiles. The profiles were spatially averaged in the longshore direction using a sliding 40 m window (the average of three cross-shore profiles), reducing noise in the data and allowing patterns of coastal change to be more easily identified. The swash regime was designated as the minimum level of impact at each profile location. The occurrence of higher-impact levels was determined based on volume change calculations made on the averaged profiles.

Dune volume change, δV_d, was calculated between the pre-storm horizontal positions of D_{high} and D_{low} as

$$\delta V_d = \int_{x_{dc1}}^{x_{dt1}} (z_2 - z_1) dx \,. \tag{4.4}$$

When δV_d exceeded a critical value of -2.5 m^3, the observed impact regime was defined as collision. Volume change inland of the dune or berm,

$$\delta V_i = \int_{x_{dc2}-50m}^{x_{dc2}} (z_2 - z_1) dx \,, \tag{4.5}$$

was calculated over a limited 50-m region landward of the post-storm D_{high} (Figure 4.3) in order to minimize the inclusion of buildings and structures. When δV_i exceeded a threshold of 7.5 m^3 the observed impact was classified as overwash. Threshold values for collision and overwash were set as low as possible to detect coastal change yet high enough to avoid spurious classification resulting from noise associated with data resolution, structures and/or vegetation.

The objective classification of impact regime was examined through comparison to subjective designations made by viewing pre- and post-Bonnie profiles. On Masonboro and Hutaff Islands where overwash was predicted to be the dominant response to the storms, the objective and subjective designations agreed for 92.6% of the profile locations. On Topsail Island, where a mix of regimes was expected, the subjective and objective determinations agreed on 66.8% of the profiles. Some of the discrepancies

were due to the presence of houses masking the overwash signal in the objective determination. Areas where houses were a significant problem and produced differences in the observed regime over a continuous area were manually edited (3.8 % of the profiles).

The impact of both hurricanes along this stretch of coast was severe: 44.6% of the alongshore locations experienced overwash. Impacts during Floyd were more severe, with 17% of the profiles experiencing a higher impact regime than they had as a result of Bonnie. During Floyd, 34% of the area experienced dune erosion compared to 19% during Bonnie. It is possible that during the storms some locations along the coast were in the collision or overwash regime but were not classified as such because significant coastal change was not measured, either because it was below detectable levels or because no change occurred. This may lead to discrepancies between the predicted and observed regimes that are not necessarily related to inaccuracies of the storm scaling model.

4.5.3 Accuracy of Storm-Impact Scaling Model

The observed impact regime was compared to the predicted regime to evaluate the accuracy of the storm-impact scaling model in predicting the mode of coastal change during a hurricane. The overall accuracy of the storm-impact scaling model for correctly predicting one of three observed impact regimes was 51.6% for Bonnie (N= 1424) and 59.1% for Floyd (N = 1307), which show significant improvements over the accuracy associated with random chance (33.3%). Prediction errors were generally the result of an overestimate of the impact regime (or, perhaps, an under-detection of the storm-induced coastal change): the predicted regime was more severe than observed along 40.7% and 36.2% of the longshore locations for Bonnie and Floyd, respectively. The accuracy of predictions within a single regime varies markedly and was evaluated using a presence/absence (or binary decision) model in which the presence of each regime is predicted. The performance of these types of models can be summarized in a confusion matrix that presents the number of observations and predictions of both the presence and

absence of a particular regime [*Fielding and Bell*, 1997]. In the presence/absence model the total number of correct predictions, N_c, can be viewed with respect to either the number of observations of a particular regime, N_o, or the number of predictions of that particular regime, N_p. The sensitivity, *s*, of the model is the probability that a particular regime was classified correctly and is calculated as N_c/N_o. Positive predictive power, *P*, is a measure of the predictive capabilities of the model. *P*, calculated as N_c/N_p, defines the probability that a particular regime will occur if predicted by the storm scaling model. Regime-specific accuracy statistics, as well as N_p, N_o, and prevalence (N_o/N, a measure of the occurrence of each regime over the whole domain), are presented in Table 4.3 for each hurricane.

For both storms, *P* for the swash regime was relatively high (P_B = 63.6% and P_F = 44.4%, the subscripts *B* and *F* refer to Hurricanes Bonnie and Floyd, respectively) indicating that swash would occur where predicted an average of 54% of the time. However, these high values of *P* may be somewhat misleading in this case since the swash regime was predicted to occur over only 8% of the profiles. Sensitivity within the swash regime was much lower (s_B = 1.5% and s_F = 1.4%) indicating that the model did a poor job of classifying the observed locations of swash. The low sensitivity values for swash are overwhelmingly due to the prediction of dune erosion (collision regime) in

Table 4.3. Regime-specific accuracy of hurricane-impact regime predictions using Sallenger's model (2000), where *P* is the predictive power of the model, N_p is the number predicted, *s* is the model sensitivity, and N_o is the number observed.

	swash	collision	overwash
Hurricane Bonnie			
$P(N_p)$	0.636 (11)	0.234 (655)	0.759 (758)
s (N_o)	0.015 (468)	0.560 (273)	0.842 (683)
prevalence	0.329	0.192	0.480
Hurricane Floyd			
$P(N_p)$	0.444 (9)	0.451 (543)	0.693 (755)
s (N_o)	0.014 (283)	0.556 (441)	0.897 (583)
prevalence	0.217	0.337	0.446

locations where swash was observed. This type of error is also revealed in the mediocre P values for the collision regime (P_B = 23.4% and P_F = 45.1%). Sensitivity for collision model was somewhat higher for both storms, s = 56%, indicating that the model correctly classified the collision regime over half of the domain. The storm scaling model's best performance as a predictor of storm response was within the overwash regime where s and P were both high. Locations that overwashed during the hurricanes were correctly predicted to do so for 84.2% and 89.7% of longshore locations for Bonnie and Floyd, respectively (P_B = 75.9% and P_F = 69.3%). Errors within this regime were due to the overprediction of overwash at locations where dune erosion was observed.

4.5.4 Coastal Response within Each Regime

The hurricane-induced coastal response, as measured by shoreline change, δx_{sl}, and beach volume change, δV_b, calculated between the 1997 and post-storm surveys, was observed to be highly longshore-variable. The mean shoreline change, $\mu\delta x_{sl}$, in response to Bonnie was -9.15 m (negative values indicate erosion); however the standard deviation was of the same order of magnitude, $\sigma\delta x_{sl}$= 8.52 m. Similarly after Floyd, the variability of shoreline change was almost equal to the mean value ($\mu\delta x_{sl}$ = -12.30 m, $\sigma\delta x_{sl}$= 12.13 m). Considerable longshore variability was also observed in beach volume change ($\mu\delta V_b \pm\sigma\delta V_b$): -22.31±14.86 m^3/m resulting from Bonnie and -28.91±19.46 m^3/m from Floyd. (Note: The magnitudes of coastal change during Floyd may be somewhat elevated if the beach did not fully recover after Bonnie to its 1997-state. In particular, δV_b, calculated between the shoreline and the crest of the dune, may contain part of the Bonnie signal of change as beach recovery on the upper part of the profile is slower than that in the foreshore region. However, δV_b, calculated between the 1999 post-Floyd and 1998 post-Bonnie surveys ($\mu\delta V_b \pm\sigma\delta V_b$ = 14.45±20.40 m^3/m) likely underestimates the beach response to Floyd because it assumes no recovery after the storm (Table 4.4).)

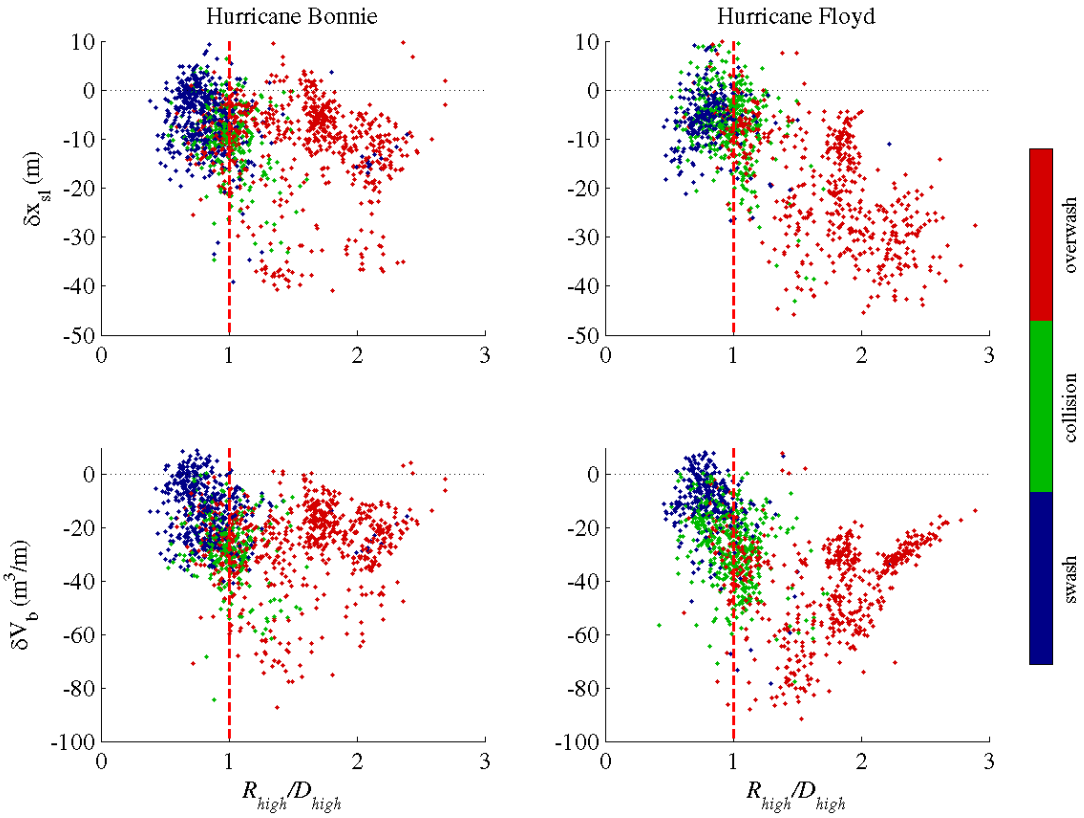

Figure 4.7. Shoreline and beach volume change for Hurricanes Bonnie (left column) and Floyd (right column) shown as a function of R_{high}/D_{high}, the predictive ratio for the overwash regime. The color of each data point represents the observed impact regime. Magnitudes of coastal change, particularly erosion of the beach face, increase with severity of the impact regime.

Part of the longshore variability in the observed hurricane response can be attributed to differences in the nature and magnitude of coastal change within each observed regime. In the swash regime (based on the objective, post-storm classification), where runup is confined to the beach seaward of the dune, magnitudes of δx_{sl} and δV_b were smaller than within the other regimes (Figure 4.7). The means and standard deviations for shoreline and volume change during both storms were on the order of 10 m and 10 m^3/m, respectively. (Regime-specific measures of δx_{sl} and δV_b for each storm are presented in Table 4.4.) While the foreshore slope flattened in these areas in response to storm waves, the mean beach slope was observed to steepen slightly, particularly after Floyd, as a direct result of shoreline retreat.

Within the collision regime, the magnitude and variability of shoreline change were similar to that observed in the swash regime, O(10 m); however, beach-volume change was twice as high (Figure 4.7): $\mu\delta V_b$ = -27.8 m^3/m for Bonnie and $\mu\delta V_b$ = -26.3 m^3/m for Floyd. While the magnitude of mean δx_{sl} was similar to that observed in the swash regime, $\mu\delta\beta_m$ was insignificant due to an accompanying retreat of the base of the dune (-5.2 m and -6.7 m following Bonnie and Floyd, respectively). In these areas, the loss of beach sand was accompanied by the loss of an additional 8.25 m^3/m of mean dune erosion (average for both storms).

Within the overwash regime, the magnitude of coastal change was observed to be cumulative with successive storm impacts. After Bonnie, mean shoreline and volume change were similar to those observed in the collision regime (δx_{sl} = -10.9 ± 9.5 m, δV_b = -26.0 ± 15.0 m^3/m). After Floyd made landfall one year later, the shoreline change in overwash locations doubled and volume change increased by 50% (Figure 4.7, Table 4.4). The observed response of the mean beach slope was also different than that observed within other regimes. Here the beach tended to flatten during the storms due to the rapid retreat of the berm crest (-22.68 m after Bonnie, -40.51 m after Floyd) relative to a slower shoreline retreat ($\mu\delta x_{sl}$ = -10.9 m after Bonnie and $\mu\delta x_{sl}$ = -19.4 m after Floyd). Mean slope change following Floyd ($\mu\delta\beta_m$ = -0.028) was greater than that following Bonnie ($\mu\delta\beta_m$ = -0.017). Comparison between the 1997 and 2000 surveys showed little permanent change in mean beach slopes over the three-year period indicating that slopes steepened again after Floyd. (Note: Coastal change during Floyd that was calculated using the 1998 post-Bonnie survey as the pre-storm conditions shows the same relationship to observed impact regime even though the magnitudes of change are smaller than that calculated using the 1997 data.)

While the profile shape in overwash locations returned to the pre-storm slope, the horizontal position of the berm did not recover. Cumulative volume change, as calculated between the two calm weather lidar surveys from 1997 and 2000, showed no

Table 4.4. Mean (and standard deviation) post-storm and cumulative shoreline, beach volume, and slope change within each hurricane-impact regime.

	all regimes	swash	collision	overwash
post-Bonnie (1997 - 1998)				
δx_{sl} (m)	-9.11 (8.47)	-6.1 (6.6)	-9.8 (7.1)	-10.9 (9.5)
δV_b (m^3/m)	-22.26 (14.80)	-13.6 (11.1)	-27.8 (13.5)	-26.0 (15.0)
$\delta \beta_m$	-0.005 (0.024)	0.007 (0.015)	0.003 (0.015)	-0.017 (0.027)
post-Floyd (1997 - 1999)				
δx_{sl} (m)	-12.08 (11.92)	-5.5 (6.7)	-6.4 (8.1)	-19.4 (12.1)
δV_b (m^3/m)	-28.87 (19.58)	-10.3 (14.1)	-26.3 (13.9)	-39.8 (18.0)
$\delta \beta_m$	-0.007 (0.031)	0.026 (0.020)	0.000 (0.019)	-0.028 (0.027)
post-Floyd (1998 post-Bonnie - 1999)[+]				
δx_{sl} (m)	-3.69 (10.58)	-1.8 (8.3)	2.6 (7.6)	-10.2 (10.9)
δV_b (m^3/m)	-14.45 (20.40)	-5.4 (16.7)	-6.6 (9.4)	-29.4 (21.2)
$\delta \beta_m$	0.002 (0.023)	-0.010 (0.026)	0.004 (0.021)	0.011 (0.018)
cumulative (1997 - 2000)				
δx_{sl} (m)	-15.41 (14.01)	-9.6 (6.4)	-7.9 (6.8)	-23.9 (16.4)
δV_b (m^3/m)	-25.17 (22.27)	-13.3 (13.1)	-15.1 (14.4)	-38.6 (23.4)
$\delta \beta_m$	0.008 (0.025)	0.026 (0.025)	0.013 (0.018)	-0.005 (0.023)

[+]Regime designations were also calculated between the 1998 and 1999 surveys. Magnitudes of coastal change are likely underestimated because of the comparison to a post-storm profile.

recovery (δV_b = -38.6 ± 23.4 m^3/m) and the shoreline continued to erode (δx_{sl} = -23.9 ± 10.0 m) in response to typical winter storms during the year following Floyd. The permanence of the response in these locations is likely due to the transport of sand across the island in addition to, or instead of, typical offshore transport. The cross-island transport of sand in the overwash regime was identified by comparing the volume loss from the beach to the overwash volume calculated in an area 50-m landward of the berm (δV_i). After Bonnie, $\mu\delta V_b$ = -26.0 m^3/m and $\mu\delta V_i$ = 23.9 m^3/m, resulting in a net volume change, $\mu\delta V_{net}$, of -2.1 m^3/m. A net change near zero indicates a conservation of mass as the island moves inland. This process continued after Floyd where the mean volume loss from the beach was -39.8 m^3/m; yet, $\mu\delta V_i$ = 33.0 m^3/m leaving a net volume change along these profiles of -6.8 m^3/m. To more adequately capture the full horizontal extent of overwash deposits during Floyd, the landward limit of inland volume change was

increased to 100-m resulting in a net volume change of almost zero ($\mu\delta V_{net}$ = -0.53 m^3/m). Again, this shows that in the overwash locations sand was transported to the sound side of the island and, consequently, lost from the nearshore system, making it unavailable to calm weather waves which typically bring sand back to the beach after a storm. This is in contrast to the swash and collision regimes where no overwash was observed and the net volume change across the profile was approximately equal to the volume of sand eroded from the beach face. In these locations, sand was transported offshore where it potentially was available to be transported back to the beach between storms, as evidenced by the similarity of shoreline and volume change magnitudes for the two storms.

Further evidence of the cumulative nature of net landward migration of the overwash sites was found on Masonboro Island, where overwash was the dominant response to both storms. Here, lidar surveys covered the entire width of the island allowing for the calculation of the center of mass at each longshore location. The horizontal location of the center of mass was observed to retreat 15.9 m landward after Bonnie and an additional 6.1 m following Floyd. One year after Floyd, no significant seaward recovery of the center of mass was observed, resulting in a 21.8 m landward retreat of the island. This retreat was also observed in the horizontal movement of the berm (D_{high}) despite pronounced changes in the overall profile shape. After each storm's landfall, the mean beach slope flattened and D_{high} retreated landward. Then, in the year following Floyd the profile began to recover as the berm moved slightly seaward and began to regain its steeper, pre-storm shape (Table 4.4). Beach slope change calculated between the two calm-weather surveys was near zero ($\mu\delta\beta_m$ = -0.005) indicating near recovery of the 1997 slope. Despite this readjustment of profile shape, the 2000 horizontal position of the berm still remained 20.6 m landward of its 1997 pre-storm position. The landward migration of barrier islands via overwash deposits has been documented extensively [*Doughty et al.*, 2004; *Hosier and Cleary*, 1977; *Leatherman*, 1979; *Leatherman*, 1981]. The landward migration of overwashed Masonboro Island supports the observation that coastal change in overwash locations is larger in magnitude and more permanent than changes within the other two impact regimes, because of sand loss across the island.

The observed differences in magnitude of coastal change within each regime help to explain the overall longshore variability of this region's response to hurricanes. To further demonstrate this, Topsail Island, where a mix of regimes was observed, was isolated from overwash-dominated Masonboro Island to test whether the bulk patterns of coastal change observed over the study area as a whole also exist on a smaller scale. On Topsail Island, after Bonnie, the magnitudes of the shoreline and beach volume change within the collision and overwash regimes ($\mu\delta x_{sl}$ = -9.2 m, $\mu\delta V_b$ = -26.8 m^3/m) were approximately twice that observed within the swash regime. After Floyd, shoreline change was similar within all three regimes ($\mu\delta x_{sl}$ = -5.9 m); however, beach volume change was significantly higher in the overwash regime ($\mu\delta V_b$ = -30.5 m^3/m) than in the swash regime ($\mu\delta V_b$ = -8.8 m^3/m). This shows that smaller-scale variations in the magnitude of beach volume change may also be attributed to differences in regime on islands where a mix of storm-impact regimes occurs.

While observed differences in the magnitude of shoreline and volume change within each regime helps to explain the overall spatial variability of the storm response, differences in regime along a single island do not appear to directly contribute to a longer-term three-year pattern of change observed between 1997 and 2000. Spatial averages of three-year shoreline and volume change on Topsail Island were similar for all regimes. In the swash regime, mean volume change over three years was -12.1 m^3/m, suggesting that these areas have not recovered from the -8.8 m^3/m loss after Floyd. In overwash locations, mean cumulative volume change of -16.5 m^3/m indicates that the beach volume is starting to recover from the -30.5 m^3/m volume loss measured following Floyd. This pattern of continued erosion in places of minimal storm-induced change and accretion in locations of maximum storm-induced change tends to reduce longshore-variability of shoreline position. Here, longshore processes are likely redistributing the sand as the beach recovers from the storm. This is further evidenced by examining the variance of the actual shoreline position using wavenumber spectra. The variance of shoreline position at scales less than 1 km (those scales associated with significant spatial variability of the observed impact regime) increased by 33% after the passage of Bonnie

and 58% after the passage of Floyd, before returning to its pre-storm (1997) level in August 2000.

Masonboro and Hutaff Islands, which were dominated by overwash, showed continued shoreline retreat and beach erosion after the passage of two hurricanes. Shoreline and beach volume change over the three-year period ($\mu\delta x_{sl}$ = -30.1 m , $\mu\delta V_b$ = -47.0 m^3/m) was slightly larger than that measured after Floyd ($\mu\delta x_{sl}$ = -24.1 m , $\mu\delta V_b$ = -43.3 m^3/m) as the islands migrate landward. Over the whole study area, islands characterized by different response regimes showed more permanent large-scale, longshore variability resulting from the hurricanes.

4.6 Discussion

Accuracy assessment of Sallenger's storm-impact scaling model shows that it may be used to reasonably predict the coastal response to hurricanes and to explain part of the spatial variability observed in the magnitudes of shoreline and beach-volume change. However, before practical application of this model for forecasting the likely coastal impact of an approaching hurricane, it is important to address potential reasons for: (1) discrepancies between the predicted and observed storm-impact regime; and (2) the portion of the longshore-variability response not explained by the scaling model.

Discrepancies between the expected and observed regime are due to errors in the prediction and/or errors in the objective classification of the storm-induced regime. Errors in the post-storm classification may occur if calculated volumes of dune erosion or overwash deposition are below threshold values or obscured by noise in the lidar topographic data. Additionally for Floyd, objective classifications were made by comparing the post-storm survey to the 1997 survey, which may have resulted in anomalous classifications of the collision or overwash regime if the coastal change signal from Bonnie remained one year later and was included in the Floyd calculation. While objective regime designation for Floyd made using comparisons of the 1998 (post-Bonnie) and 1999 surveys produced minor differences in observed regime, the accuracy

statistics are similar to those for designations based on the 1997 pre-storm data. The overall accuracy was 51.3%, with improved accuracy (model sensitivity) of 89.8% within the overwash regime (collision, s = 66.9%; swash, s = 0.8%; See Table 4.3 for regime-specific accuracy based on comparisons to the 1997 survey.)

Differences between the expected and observed regimes may also be due to errors in the predictions associated with measurements of beach morphology, estimates of storm-induced water levels, or interactions between the two. First, measurements of D_{high} and D_{low} for both hurricanes Bonnie and Floyd were based on a single calm-weather survey from 1997. The validity of using this survey to represent the pre-storm beach conditions for Floyd may be questionable due to the passage of Bonnie one year prior, particularly in areas of significant dune erosion or overwash. However, the spatially-averaged elevation change of D_{high} and D_{low} showed only 8-cm and 10-cm decreases, respectively, after Bonnie. Additionally, given the sensitivity of runup to beach slope, the use of the 1997 survey for measuring the pre-Floyd slope for input into the runup parameterization may also have produced errors if there were lasting changes to slope following Bonnie. However, within the swash regime there were minimal changes to mean beach slope following Bonnie. At overwash locations the mean beach slope was observed to recover one year following Floyd, as the profile began to readjust to its pre-storm shape despite an overall inland migration of the island (Table 4.4). Therefore, the 1997 topography survey proved to be appropriate for determining both the relevant mean beach slope and dune elevations for both hurricanes.

Errors in the prediction may also be caused by incorrect measures of the storm-induced, extreme water levels, R_{high}. Accurate predictions of impact regime depend on how well the magnitudes and full spatial-variability of R_{high} can be resolved for each storm. First errors in R_{high} may arise from modeled waves and storm surge, which are required for using the storm-scaling model in a predictive mode. The size of the model grid spacing and inaccuracies of model input, including wind fields and offshore bathymetry, limit the ability to resolve the full spatial variability of R_{high}. Incorporating

observations into the estimates of the total, hurricane-induced water level may provide predictions that are more representative of the actual storm conditions.

Additionally, errors in the predicted regime may be due to the use of the extreme-value runup statistic, R_2, to represent the wave-driven processes and to define the threshold between regimes. This statistic represents the elevation exceeded by wave runup 2% of the time (for 10-second wave, this would equate to seven waves per hour), which may be too infrequent to cause measurable dune erosion or overwash. Consequently, the use of this statistic may result in the overprediction of the impact regime. Further research is needed to determine precisely which statistic of runup (i.e. mean, significant, etc.) serves as the best proxy for measurable dune erosion and/or landward sediment transport.

A final reason for potential errors in the prediction of storm-impact regime is that a time-dependent process (profile evolution during a storm) is examined using a non-time-dependent model (R_{high}/D_{high}). Timestacks of storm-induced water levels and the predicted impact regime show that most areas of the coast entered the collision regime hours before the storms' landfalls (Figure 4.6). Dune erosion in the early stages of the storm, and subsequent dune collapse, may lower dune elevation in some locations making them more prone to overwash. This type of error was less likely in this study because vertical dune changes after Bonnie were small (O(cm), see above). Alternatively, changes in the mean beach slope (flattening or steepening) throughout the course of the storm (Table 4.4) will have a corresponding effect on R_2, decreasing or increasing the modeled elevation, respectively (equation 3), thereby changing this area's vulnerability to dune erosion or overwash. The scaling model presented here provides a bulk estimate of the potential coastal response to hurricanes, identifying areas that may be more vulnerable to large magnitudes of shoreline and volume change. To fully capture the evolution of the profile throughout the duration of the storm, detailed modeling of the profile's time-dependent response to increasing waves and surge is required [*Fauver*, 2005].

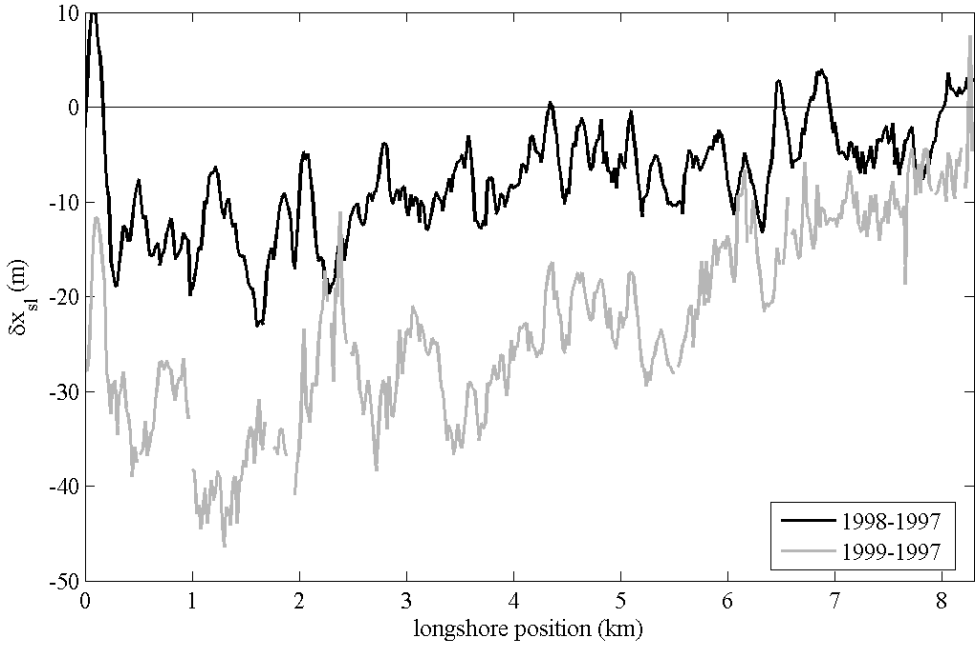

Figure 4.8. Shoreline change along Masonboro Island, NC. The mean change was -7.8 m after Hurricane Bonnie (black line) and -23.3 m after Hurricane Floyd (gray line).

In addition to understanding the nature of prediction errors, it is also important to address the observed spatial patterns in hurricane-induced shoreline and beach-volume change that were not explained within the framework of the storm-impact scaling model. For example, the overwash regime was shown to have greater magnitudes of change than the other regimes; however, significant shoreline-change variability was present within this single impact regime. On Masonboro Island, where the entire length of the island overwashed, the standard deviation of δx_{sl} was 5.7 m after Bonnie and 10.0 m after Floyd (Figure 4.8). Based on the observation that the magnitude of shoreline change was larger within the overwash regime, it was hypothesized that the amount of change within this regime might then scale with the height of R_{high} above the berm crest (R_{high} - D_{high}). The correlation, ρ, between δx_{sl} and (R_{high} - D_{high}) was 0.41 for Bonnie and 0.38 for Floyd (95% significance level, ρ_{sig}, = 0.12). Since the elevation of D_{high} did not change significantly along the length of the island (D_{high} = 2.17 ± 0.29 m, see Figure 4.5), the relationship can be simplified to a correlation between δx_{sl} and R_{high}. Because wave height was also relatively constant along this island, the variability in the predicted R_{high}

signal was dominated by spatial patterns in mean beach slope (Table 4.4). Therefore, the correlation was ultimately reduced to show a relationship between δx_{sl} and β_m (Bonnie, ρ = 0.32; Floyd, ρ = 0.38). The positive correlation indicates that more shoreline change was observed in locations where beach slopes were steeper and the corresponding runup elevation was higher.

Much of the spatial variability of shoreline change can be tied to the large-scale trend in beach slope along the island ($\mu\beta_m$ = 0.062, $\sigma\beta_m$ = 0.02). At the southern end of Masonboro Island, beach slopes were steeper, predicted runup was higher, and more coastal change was observed. Variance partitioning of the slope and shoreline change signals into 100-m bins revealed that the majority of the variance was contained in the alongshore trend: 20.7% of the total β_m variance and 18.3% and 41.7% of the total δx_{sl} variance, for Bonnie and Floyd respectively. Wavenumber analysis of δx_{sl} revealed a minor peak at L = 755m; however significant correlations with β_m, beach width, or R_{high} were not identified to help explain observed periodicity at this scale. A peak at L = 755 m was present in the spectra for the 1997, 1998, and 1999 shoreline positions indicating that part of the variance of the shoreline change signal was related to the pre-existing shape of the shoreline position.

Unexplained variance within the overwash regime may also be related to time evolution of the profile and transition to the inundation regime. During Bonnie, R_{high} was greater than the elevation of D_{high} along Masonboro Island for seven hours, from four hours before the maximum predicted water levels until the end of the model run. During Floyd, the modeled elevation of R_{high} was higher than the berm for least 15 hours prior to landfall. At the time of maximum R_{high} during Bonnie and Floyd, water levels were predicted to be 1.7 m and 2.0 m above the elevation of the berm. It is likely that at some point during these storms, portions of the Masonboro Island were completely submerged. Within the inundation regime, processes of sediment transport are different than transport due to swash processes. Under these extreme conditions, cross-island flows (both wind-driven and due to pressure gradients related to storm surge) dominate the fluid processes, and parameters defining swash processes are no longer expected to scale with resulting

coastal change. In order to quantify the amount of coastal change associated with the inundation regime, it is first necessary to determine objective criteria for identifying this regime using post-storm topography surveys. Then, change specific to locations where the island is completely subaqueous may be isolated from that within the overwash regime.

Finally, because the storm-impact scaling model assumes that cross-shore processes are dominant, unexplained spatial patterns in shoreline and beach-volume change may be the result of longshore fluid processes. The relative importance of longshore processes during Hurricanes Bonnie and Floyd was considered by calculating longshore sediment transport due to oblique wave approach using the energy flux model [*Komar*, 1998]. Immersed weight transport was calculated for all time steps of the modeled wave climates and then integrated over the duration of the storm to determine the bulk transport for each hurricane. Gradients in transport were converted to horizontal change in shoreline position using the sediment continuity equation, $dx/dt = -(dQ/dy)/d$, where d is the depth of the active profile [*Rosati et al.*, 2003]. The correlation between observed shoreline change and that due to gradients in longshore transport was not significant for either hurricane, indicating that longshore transport gradients, as predicted with this simple modeling approach, were not a major contributor to the observed hurricane-induced coastal change during Bonnie and Floyd.

4.7 Conclusion

The longshore-variable coastal response to Hurricanes Bonnie and Floyd was examined within the framework of a storm-impact scaling model, which defines four levels of coastal response based on the relative elevations of storm-induced water levels and those of the dune or berm. Because fluid observations were not available along the coast, the hurricane wave field and storm surge at the shoreline were modeled using observed wind grids for each storm. R_{high}, the hurricane-induced total water level, was defined along the coast using longshore-variable tide, surge, and empirically-defined wave runup. Storm surge and runup each accounted for ~48% (averaged over both

storms) of the R_{high} signal, indicating that, in these storms, wave-driven processes may be equally as important as surge to the maximum, total water level attained during hurricanes. The elevation of the dune or berm was measured from lidar topographic surveys. The impact regime for both hurricanes was hindcast every 20 m along a 50-km stretch of coast. The coastal response to each storm was objectively defined along the coast as swash, collision, or overwash based on quantitative measures of coastal change.

Comparisons of the estimated and observed storm response indicate that Sallenger's model is a reasonable predictor of hurricane-impact regime, based on an accuracy of 55.4%, which is a significant improvement over the accuracy associated with random chance (33.3%). The accuracy, as defined by model sensitivity, varied widely between regimes. In the overwash regime, the combined accuracy for both storms was 87.0%. The mean accuracy for the collision and swash regimes, averaged over both Bonnie and Floyd, was 55.8% and 1.5%, respectively. Errors in the predictions were overwhelmingly due to overestimates of storm response. Discrepancies between the expected and observed regime may be due to misclassification of the observed regime, an inaccurate representation of the water levels defining the threshold between regimes (due to either errors in the modeling of hurricane waves and surge or in the statistical representation of the runup elevation relevant to dune erosion and overwash), or the time-evolution of the beach profile during the storm.

The magnitude of shoreline and beach-volume change varied between impact regimes leading to a spatially-variable storm response on stretches of coast where a mix of regimes was observed. The magnitudes of shoreline and volume change in the overwash regime were twice as large as that measured in the swash regime for Hurricane Bonnie. The differences were even more pronounced after Hurricane Floyd when the magnitudes of change were four times greater within the overwash regime. Not only was the magnitude of beach-volume change larger within the overwash regime, the change was also observed to be more permanent. Beach volume change calculated between the pre-storm survey and one collected a year after Floyd made landfall showed no recovery. In this regime, mean beach volume change was -39.8 m^3/m; however, overwash deposit

volumes were nearly the same. This resulted in a net volume change near zero indicating that sand was transported across the island and deposited inland, making it unavailable to calm weather waves that typically bring sand back to the beach. The inland transport of sand also tended to flatten the mean beach slope within the overwash regime, while beaches in the swash regime were observed to steepen. Additional longshore-variability of coastal change within the overwash regime was shown to be related to large-scale variability in beach slope along a single island. Areas with steeper slopes had correspondingly higher runup elevations and experienced more shoreline change during the hurricanes. Gradients in longshore transport, integrated over the duration of each storm, did not appear to contribute significantly to the observed patterns of hurricane-induced shoreline change.

4.8 Acknowledgments

Lidar data were collected as a part of cooperative research program between the USGS and NASA. David Thompson (USGS) provided assistance with surge modeling. The authors also wish to acknowledge contributions by Spencer Rogers (North Carolina Sea Grant), Bill Dennis (USACE Wilmington), Kristy Guy (USGS), Karen Morgan (USGS), Jeff List (USGS), Nicole Elko, and Ava Thompson. Funding was provided by the USGS Coastal and Marine Geology Program as a part of the National Assessment of Coastal Change Hazards.

5.0 CONCLUSIONS

The large-scale impacts of hurricanes on barrier islands have been observed to be highly longshore variable. Observations of shoreline and beach volume change resulting from these storms show that the standard deviation of change may be of the same order of magnitude as the mean response. This has serious implications for future attempts at predicting the vulnerability of a stretch of coast to an approaching storm. One area may experience significant dune erosion or overwash, while an adjacent area may be virtually unaffected. An accurate prediction of the large-scale response of barrier islands to hurricanes requires an understanding of both the magnitudes of change and the processes driving the observed patterns.

The longshore-variable signal of coastal change may be examined using a storm-impact scaling model that compares the elevations of dune morphology and hurricane-induced water levels to define four impact regimes. When water levels are confined to the active beach face (*swash* regime), sand eroded from the beach is transported offshore and generally returns to the beach during more quiescent periods. If water levels reach or exceed the base of the dune (*collision* regime), storm waves may begin to erode the dune face. In the *overwash* regime, runup levels exceed the elevation of the dune crest, often resulting in the landward transport of sediment. When total water levels continuously exceed the elevation of the dune, the system has reached the *inundation* regime and cross-island flows dominate the fluid forcings. Within each of these regimes, the processes and magnitudes of sediment transport are unique.

In order to begin to characterize the nature and magnitude of hurricane-induced coastal change, techniques were developed to extract accurate and synoptic measures of coastal morphology from high-resolution laser altimetry topographic surveys. An objective method for extracting contour-based, horizontal shoreline position and change, as well as the associated 95% confidence interval, was shown to have an accuracy of 1.5 m (rms difference error) as compared to ground-based surveys. Measures of morphology

such as beach slope, dune height, and beach volume were also extracted from the lidar topography to allow for detailed quantification of the large-scale coastal response. Additionally, lidar-derived measures of pre-storm beach morphology were used as input for the storm-impact scaling model to make predictions of the hurricane-impact regimes.

The maximum total water level at the shoreline expected during a hurricane was modeled as the sum of astronomical tide, storm surge, and wave runup. Since a complete hydrodynamic model of wave runup is impractical in this case because of the expected lack of data on the input wave spectra and boundary conditions, an empirical parameterization was used to approximate the 2% exceedence value for wave runup. The elevation of runup was parameterized as the sum of two dynamically different processes, setup and swash, using water-level data collected at 10 field experiments representing a wide range of beach and wave conditions. Dimensional setup and incident-band ($f_0 > 0.05$ Hz) swash were best parameterized using the offshore wave height, wave period, and foreshore beach slope, estimated over the region of significant swash activity. The magnitude of infragravity-band ($f_0 < 0.05$ Hz) swash scaled similarly; however, the model improved significantly when slope was removed from the parameterization.

Special relationships for swash and setup exist under highly dissipative conditions where bottom friction likely plays a larger role in the dissipation across very wide surf and swash zones. For Iribarren numbers less than 0.3, setup and total swash (modeling both frequency bands together) are each parameterized using only offshore wave height and period. The inclusion of foreshore or surf zone slope does not offer any improvement to the empirical formulation for dissipative conditions. Using the suggested formulations for setup, incident swash, and infragravity swash, the final empirical formulation for the 2% exceedence level of runup on natural beaches is

$$R_2 = 1.1\left(0.35\beta_f (H_0 L_0)^{1/2} + \frac{[H_0 L_0 (0.563\beta_f{}^2 + 0.004)]^{1/2}}{2}\right).$$

At sites where the Iribarren number is less than 0.3, estimates of runup may be improved by using the dissipative-specific equation

$$R_2 = 0.043(H_0 L_0)^{1/2}.$$

Comparisons of runup estimates made using these composite parameterizations to 491 observations of runup revealed a mean difference of -17 cm, indicating a slight underestimate of runup, and an rms difference of 38 cm. On intermediate and reflective beaches with highly three-dimensional topography, the dependence of setup and incident swash on foreshore beach slope will force corresponding longshore-variability in runup.

The storm-impact scaling model was used to examine the long-shore variable coastal response to Hurricanes Bonnie (1998) and Floyd (1999), which made landfall near Cape Fear, North Carolina. Because high-resolution observations of the fluid forcing were not available during each storm, the hurricane-induced total water level was hindcast along the coast using modeled surge and wave conditions. Storm surge and wave runup each accounted for ~48% of the total signal (astronomical tides contributed the remaining 4%), indicating that wave-driven process are a significant contributor to hurricane-induced water levels. Spatially-varying water levels were compared to measurements of dune morphology, D_{high} and D_{low}, extracted every 20 along 50-km of coast to predict three storm-impact regimes: swash, collision, and overwash. (The occurrence of the inundation regime was not predicted because of difficulties in using the lidar surveys to determine locations where the islands were submerged during the storm.) Comparisons to the observed regime, quantified using measures of hurricane-induced dune erosion and overwash volumes, reveal an overall accuracy of 55.4%, an improvement over the 33.3% accuracy associated with random chance. Model sensitivity, the ratio of the number of correct predictions of a regime to the number of occurrences of that regime, varied widely and was highest within the overwash regime (86.9%). Accuracy within the collision and swash regimes was 55.8% and 1.5%, respectively. Low accuracy in the swash regime is because very few instances of swash were predicted (9*)* relative to the number observed (473, averaged between both storms). Errors in prediction were commonly overestimates of the storm response, possibly due to regime responses that were below measurable thresholds (under-measurement), inappropriateness of the 2% exceedence level as the runup elevation to trigger significant response, and inappropriateness of mean beach slope as a proxy for the time-varying slope for regime predictions.

The magnitudes of shoreline and beach volume change were observed to vary within each storm-impact regime, leading to a spatially variable storm response over the 50-km stretch of coast. Magnitudes of hurricane-induced beach volume change were more than twice as large in the overwash regime as they were in the swash regime. The amount of recovery after the hurricanes also differed between the impact regimes. Cumulative shoreline and beach volume change calculated over a three-year period showed that coastal change within the hurricane overwash regimes was almost three times that observed in the swash regimes. Islands dominated by overwash experienced a net landward retreat of over 20 m, as measured one year after the storms, and were shown to experience a more permanent loss of sand from the beach. Here, the volume of sand eroded from the beach face was balanced by the volume of overwash deposits, indicating that sand was transported across the island, deposited inland, and removed from the nearshore system making it unavailable to calm-weather waves that tend to bring sand back to the beach. Additional longshore-variability of measured shoreline change within the overwash regime was related to a large-scale trend in beach slope. Areas with steeper slopes, and correspondingly higher runup, experienced more erosion during each hurricane.

BIBLIOGRAPHY

Anders, F.J., and M.R. Byrnes, Accuracy of shoreline change rates as determined from maps and aerial photographs, *Shore and Beach*, 17-26, 1991.

Ashton, A., J.H. List, A.B. Murray, and A.S. Farris, Links between erosional hotspots and alongshore sediment transport, in *International Conference on Coastal Sediments 2003*, World Scientific Publishing Corp. and East Meets West Productions, Clearwater Beach, FL, 2003.

Avila, L.A., Preliminary Report: Hurricane Bonnie, pp. http://www.nhc.noaa.gov/1998bonnie.html, National Hurricane Center, 1998.

Baldock, T.E., and P. Holmes, Simulation and prediction of swash oscillations on a steep beach, *Coastal Engineering*, *36* (3), 219-242, 1999.

Battjes, J.A., Surf similarity, in *Proceedings of the 14th Conference of Coastal Engineering*, pp. 466-480, ASCE, 1974.

Birkemeier, W.A., and C. Mason, The CRAB: A unique nearshore surveying vehicle, *Journal of Survey Engineering*, *110*, 1-7, 1984.

Booij, N., R.C. Ris, and L.H. Holthuijsen, A third generation model for coastal regions, 1. Model description and validation, *Journal of Geophysical Research*, *104* (C4), 7649-7666, 1999.

Bowen, A.J., D.L. Inman, and V.P. Simmons, Wave 'set-down' and 'set-up', *Journal of Geophysical Research*, *73* (8), 2569-2577, 1968.

Brock, J., A. Sallenger, W. Krabill, R. Swift, S. Manizade, A. Meredith, M. Jansen, and D. Eslinger, Aircraft laser altimetry for coastal processes studies, in *Coastal Sediments 99'*, pp. 2414-2428, Am. Soc. Civ. Eng., Long Island, NY, 1999.

Cleary, W.J., C.W. Jackson, J.T. Jarrett, M. Sault, and J.M. Welsh, Inlet-induced shoreline change: Bogue and New River Inlets, NC, in *International Conference on Coastal Sediments 2003*, World Scientific Publishing Corp. and East Meets West Productions, Clearwater Beach, FL, 2003.

Cleary, W.J., C.D. Johnsen, M.K. Johnston, and M. Sault, Storm impacts and shoreline recovery in SE NC: Role of the geologic framework, in *Coastal Sediments '99*, pp. 1798-1813, Am. Soc. Civ. Eng., Long Island, NY, 1999.

Crowell, M., S.P. Leatherman, and M.K. Buckley, Historical shoreline change: Error analysis and mapping accuracy, *Journal of Coastal Research*, *7* (3), 839-852, 1991.

Delft, Delft3D-FLOW: Simulation of multi-dimensional hydrodynamic flows and transport phenomena, including sediments, WL | Delft Hydraulics, Delft, The Netherlands, 2003.

Dolan, R., B.P. Hayden, P. May, and S. May, The reliability of shoreline change measurements from aerial photographs, *Shore and Beach*, *48*, 22-29, 1980.

Doughty, S.D., W.J. Cleary, and B.A. McGinnis, The recent evolution of storm-influenced retrograding barriers in southeastern North Carolina, USA, *Journal of Coastal Research*, *SI 39*, 2004.

Egbert, G.D., and S.Y. Erofeeva, Efficient inverse modeling of barotropic ocean tides, *J. Atmos. Oceanic Technol.*, *19* (2), 183-204, 2002.

Elgar, S., T.H.C. Herbers, M. Okihiro, J. Oltman-Shay, and R.T. Guza, Observations of infragravity waves, *Journal of Geophysical Research*, *97* (C10), 15573-15577, 1992.

Elko, N., A. Sallenger, K. Guy, H. Stockdon, and K. Morgan, Barrier island elevations relevant to potential storm impacts: 1. Techniques, U.S. Geological Survey, 2002.

Fauver, L.A., Toward predicting barrier island vulnerability: Simple models for dune erosion, University of South Florida, St. Petersburg, FL, 2005.

Fielding, A.H., and J.F. Bell, A review of methods for the assessment of prediction errors in conservation presense/absence models, *Environmental Conservation*, *24* (1), 38-49, 1997.

Goldenberg, S.B., The recent increase in Atlantic hurricane activity: causes and implications, *Science*, *293*, 474-479, 2001.

Guza, R.T., and E.B. Thornton, Local and shoaled comparisons of sea surface elevations, pressures and velocities, *Journal of Geophysical Research*, *85* (C3), 1524-1530, 1980.

Guza, R.T., and E.B. Thornton, Wave set-up on a natural beach, *Journal of Geophysical Research*, *86* (C5), 4133-4137, 1981.

Guza, R.T., and E.B. Thornton, Swash oscillations on a natural beach, *Journal of Geophysical Research*, *87* (C1), 483-491, 1982.

Hanslow, D., and P. Nielsen, Shoreline set-up on natural beaches, *Journal of Coastal Research*, *SI* (15), 1-10, 1993.

Hapke, C., and B. Richmond, Monitoring beach morphology changes using small-format aerial photography and digital softcopy photogrammetry., *Environmental Geosciences*, *7(1)*, 32-37, 2000.

Herbers, T.H.C., E.J. Hendrickson, and W.C. O'Reily, Propagation of swell across a wide continental shelf, *Journal of Geophysical Research*, *105* (C8), 19729-19737, 2000.

Holland, G.J., An analytic model of the wind and pressure profiles in hurricanes, *Mon. Wea. Rev.*, *108*, 1212-1218, 1980.

Holland, K.T., and R.A. Holman, The statistical distribution of swash maxima on natural beaches, *Journal of Geophysical Research*, *98* (C6), 10,271-10,278, 1993.

Holland, K.T., and R.A. Holman, Field observations of beach cusps and swash motions, *Marine Geology*, *134*, 77-93, 1996.

Holland, K.T., R.A. Holman, T.C. Lippmann, J. Stanley, and N. Plant, Practical use of video imagery in nearshore oceanographic field studies, *IEEE Journal of Oceanic Engineering*, *22* (1), 81-92, 1997.

Holland, K.T., B. Raubenheimer, R.T. Guza, and R.A. Holman, Runup kinematics on a natural beach, *Journal of Geophysical Research*, *100* (C3), 4985-4993, 1995.

Holman, R.A., Extreme value statistics for wave run-up on a natural beach, *Coastal Engineering*, *9*, 527-544, 1986.

Holman, R.A., and A.J. Bowen, Longshore structure of infragravity wave motions, *Journal of Geophysical Research*, *89* (C4), 6446-6452, 1984.

Holman, R.A., and R.T. Guza, Measuring run-up on a natural beach, *Coastal Engineering*, *8*, 129-140, 1984.

Holman, R.A., and A.H. Sallenger, Jr., Setup and swash on a natural beach, *Journal of Geophysical Research*, *90* (C1), 945-953, 1985.

Hosier, P.E., and W.J. Cleary, Cyclic geomorphic patterns of washover on a barrier island in southeastern North Carolina, *Environmental Geology*, *2*, 23-31, 1977.

Howd, P.A., J. Oltman-Shay, and R.A. Holman, Wave variance partitioning in the trough of a barred beach, *Journal of Geophysical Research*, *96* (C7), 12781-12795, 1991.

Hunt, I.A., Design of seawalls and breakwaters, *Journal of Waterways and Harbours Division, ASCE*, *85* (WW3), 123-152, 1959.

Iribarren, C.R., and C. Nogales, Protection des ports, in *XVIIth International Naval Congress*, pp. 31-80, Lisbon, 1949.

Kannan, S., T. Lippmann, and J.H. List, The relationship of nearshore sandbar configuration to shoreline change, in *International Conference on Coastal Sediments 2003*, pp. CD-ROM, World Scientific Publishing Corp. and East Meets West Productions, Clearwater Beach, FL, 2003.

Komar, P.D., The erosion of Siletz Spit, Oregon, in *CRC Handbook of Coastal Processes and Erosion*, pp. 65-76, CRC Press, Boca Raton, Florida, 1983.

Komar, P.D., *Beach Processes and Sedimentation*, 429 pp., Prentice-Hall, Inc., 1998.

Komar, P.D., and C.C. Rea, Erosion of Siletz Spit, Oregon, *Shore and Beach*, *44*, 9-15, 1976.

Krabill, W., C. Wright, R. Swift, E. Frederick, S. Manizade, J. Yungel, C. Martin, J. Sonntag, M. Duffy, W. Hulslander, and J. Brock, Airborne laser mapping of Assateague National Seashore Beach, *Photogrammetric Engineering & Remote Sensing*, *66* (1), 65-71, 2000.

Krabill, W.B., C.F. Martin, R.H. Thomas, W. Abdalati, J.G. Sonntag, R.N. Swift, E.B. Frederick, S.S. Manizade, and J.G. Yungel, Aircraft laser altimetry measurement of elevation changes of the Greenland ice sheet: technique and accuracy assessment, *Journal of Geodynamics*, *34* (3-4), 357-376, 2002.

Krabill, W.B., R.H. Thomas, C.F. Martin, R. Swift, and E.B. Frederick, Accuracy of airborne laser altimetry over the Greenland ice sheet, *Int. Journal of Remote Sensing*, *16*, 1211-1222, 1995.

Leatherman, S.P., Migration of Assateague Island, Maryland, by inlet and overwash processes, *Geology*, *7*, 104-107, 1979.

Leatherman, S.P., *Overwash Processes*, 376 pp., Hutchinson Ross, Pennsylvania, 1981.

List, J., and A. Farris, Large-scale shoreline response to storms and fair weather, in *Coastal Sediments '99*, pp. 1324-1338, ASCE, Long Island, NY, 1999.

List, J.H., A.S. Farris, B. Irwin., K.M. Konicki, M.E. Hansen., and T.E. Reiss, A vehicle - based method for quantifying shoreline position on tidal coasts as the horizontal position of the mean high water contour: methods and error assesments, U.S. Geological Survey, 2000.

Longuet-Higgins, M.S., and R.W. Stewart, A note on wave set-up, *Journal of Marine Research*, *21*, 4, 1963.

Longuet-Higgins, M.S., and R.W. Stewart, Radiation stresses in water waves; a physical discussion, with applications, *Deep-Sea Research*, *11*, 529-562, 1964.

McGinnis, B.A., and W.J. Cleary, Late Holocene stratigraphy and evolution of a retrograding barrier: Hutaff Island, North Carolina, in *International Conference on Coastal Sediments 2003*, World Scientific Publishing Corp. and East Meets West Productions, Clearwater Beach, FL, 2003.

Miche, R., Le pouvoir réfléchissant des ouvrages maritimes exposés à l'action de la houle, *Ann. Ponts Chaussees*, *121*, 285-319, 1951.

Morton, R.A., Accurate shoreline mapping: Past, present, and future., *Coastal Sediments '91 (Seattle, Washington, ASCE)*, pp. 997-1010, 1991.

Morton, R.A., M.P. Leach, J.G. Paine, and M.A. Cardoza, Monitoring beach changes using GPS surveying techniques., *Journal of Coastal Research*, *9(3)*, 702-720, 1993.

National Climate Data Center, Climate Monitoring - Tropical Cyclones: Hurricanes, Typhoons and Cyclones, pp. http://www.ncdc.noaa.gov/oa/climate/research/hurricanes.html, NOAA, 2006.

Nielsen, P., and D.J. Hanslow, Wave runup distributions on natural beaches, *Journal of Coastal Research*, *7* (4), 1139-1152, 1991.

NOAA, Hurricane Research Division, Background on the HRD Surface Wind Analysis System, pp. http://www.aoml.noaa.gov/hrd/Storm_pages/surf_background.html, 2005.

Overton, M.F., and J.S. Fisher, Shoreline analysis using digital photogrammetry., *25th International Conference on Coastal Engineering (Orlando, Florida, ASCE)*, 3750-3761, 1996.

Pasch, R.J., T.B. Kimberlain, and S.R. Stewart, Preliminary Report: Hurricane Floyd, pp. http://www.nhc.noaa.gov/1999floyd.html, National Hurricane Center, 1999.

Plant, N.G., R.A. Holman, and W.A. Birkemeier, Kinematics of alongshore propagating sand waves at Duck, *Trans. American Geophysics Union*, *77* (46), 388, 1996.

Raubenheimer, B., and R.T. Guza, Observations and predictions of run-up, *Journal of Geophysical Research*, *101* (C10), 25575-25587, 1996.

Raubenheimer, B., R.T. Guza, and S. Elgar, Field observations of wave-driven setdown and setup, *Journal of Geophysical Research*, *106* (C3), 4629-4638, 2001.

Raubenheimer, B., R.T. Guza, S. Elgar, and N. Kobayashi, Swash on a gently sloping beach, *Journal of Geophysical Research*, *100* (C5), 8751-8760, 1995.

Revell, D., P. Komar, and A. Sallenger, An application of LIDAR to analyses of El Nino erosion in the Netarts littoral cell, Oregon, *Journal of Coastal Research*, *18* (4), 792–801, 2002.

Riggs, S.R., W.J. Cleary, and S.W. Snyder, Influence of inherited geologic framework on barrier shoreface morphology and dynamics, *Marine Geology*, *126*, 213-234, 1995.

Rogers, S.M., Beach nourishment for hurricane protection: North Carolina project performance in hurricanes Dennis and Floyd, in *National Beach Preservation*

Conference, American Shore and Beach Preservation Association, Maui, HI, 2000.

Rosati, J., T. Walton, and K. Bodge, Longshore Sediment Transport, in *Coastal Engineering Manual, Part III, Coastal Sediment Processes*, edited by D. King, pp. 119, U.S. Army Corps of Engineers, Washington, DC, 2003.

Ruessink, B.G., M.G. Kleinhaus, and P.G.L. van den Beukel, Observations of swash under highly dissipative conditions, *Journal of Geophysical Research*, *103* (C2), 3111-3118, 1998.

Ruggiero, P., J. Cote, G. Kaminsky, and G. Gelfenbaum, Scales of variability along the Columbia River littoral cell, in *Coastal Sediments*, pp. 1692-1707, ASCE, 1999.

Ruggiero, P., R.A. Holman, and R.A. Beach, Wave run-up on a high-energy dissipative beach, *Journal Geophysical Research*, *109* (C6), 2004.

Ruggiero, P., P.D. Komar, W.G. McDougal, J.J. Marra, and R.A. Beach, Wave runup, extreme water levels and the erosion of properties backing beaches, *Journal of Coastal Research*, *17* (2), 407-419, 2001.

Ruggiero, P., and B. Voigt, Beach Monitoring in the Columbia River littoral cell, 1997-2000, Coastal Monitoring & Analysis Program, Washington Department of Ecology, 2000.

Sallenger, A.H., Storm impact scale for barrier islands, *Journal of Coastal Research*, *16* (3), 890-895, 2000.

Sallenger, A.H., P. Howd, J. Brock, W.B. Krabill, R.N. Swift, S. Manizade, and M. Duffy, Scaling winter storm impacts to Assateague Island, MD, VA, in *Coastal Sediments 99'*, pp. 1814-1825, Am. Soc. Civ. Eng., Long Island, NY, 1999a.

Sallenger, A.H., Jr., and R.A. Holman, Wave-energy saturation on a natural beach of variable slope, *Journal of Geophysical Research*, *90* (C6), 11939-11945, 1985.

Sallenger, A.H., W. Krabill, J. Brock, R. Swift, M. Jansen, S. Manizade, B. Richmond, M. Hampton, and D. Eslinger, Airborne laser study quantifies El Nino-induced coastal change, *EOS, Trans. Am. Geophysical Union*, *80* (8), 89, 92-93, 1999b.

Sallenger, A.H., W. Krabill, R. Swift, J. Brock, J. List, M. Hansen, R.A. Holman, S. Manizade, J. Sontag, A. Meredith, K. Morgan, and H. Stockdon, Evaluation of airborne scanning lidar for coastal change applications, *Journal of Coastal Research*, *19*, 125-133, 2003.

Sault, M., W.J. Cleary, and C.D. Johnsen, Hurricane impacts and shoreline recovery along Masonboro Island, NC, in *Coastal Sediments '99*, pp. 597-611, Am. Soc. Civ. Eng., Long Island, NY, 1999.

Schlax, M.G., and D.B. Chelton, Frequency domain diagnostics for linear smoothers, *Journal of the American Statistical Association*, *87* (420), 1070-1081, 1992.

Seymour, R.J., M.H. Sessions, and D. Castel, Automated remote recording and analysis of coastal data, *Journal of Waterway, Port, Coastal, and Ocean Engineering*, *111* (2), 388-400, 1985.

Stafford, D.B., An aerial photographic technique for beach erosion surveys in North Carolina., *U.S. Army Corps of Engineers, Coastal Engineering Research Center, Technical Memorandum*, *36*, 1971.

Stockdon, H.F., R.A. Holman, P.A. Howd, and A.H. Sallenger, Empirical parameterization of setup, swash, and runup, *Coastal Engineering*, *53* (7), 573-588, 2006.

Stockdon, H.F., A.H. Sallenger, P.A. Howd, and R.A. Holman, Longshore variability of the coastal response to Hurricanes Bonnie and Floyd, in *International Conference on Coastal Sediments 2003*, pp. CD-ROM, World Scientific Publishing Corp. and East Meets West Productions, Clearwater Beach, FL, 2003.

Stockdon, H.F., A.H. Sallenger, J.H. List, and R.A. Holman, Estimation of shoreline position and change from airborne scanning lidar data, *Journal of Coastal Research*, *18* (3), 502-513, 2002.

Thieler, R.E., A.L. Brill, W.J. Cleary, C.H. Hobbs, and R.A. Gammisch, Geology of Wrightsville Beach, North Carolina shoreface: Implications for the concept of shoreface profile of equilibrium, *Marine Geology*, *126*, 271-287, 1995.

Thornton, E.B., R.A. Dalrymple, T. Drake, E. Gallagher, R.T. Guza, A. Hay, R.A. Holman, J. Kaihatu, T.C. Lippmann, and T. Ozkan-Haller, State of nearshore processes research: II, Naval Postgraduate School, Monterey, CA, 2000.

Thornton, E.B., and R.T. Guza, Energy saturation and phase speeds measured on a natural beach, *Journal of Geophysical Research*, *87* (C12), 9499-9508, 1982.

Thornton, E.B., and R.T. Guza, Transformation of wave height distribution, *Journal of Geophysical Research*, *88* (C10), 5925-5938, 1983.

Webster, P.J., G.J. Holland, J.A. Curry, and H.-R. Chang, Changes in tropical cyclone number, duration, and intensity in a warming environment, *Science*, *309*, 1844-1846, 2005.

Wright, L.D., and A.D. Short, Morphodynamics of beaches and surf zones in Australia, in *CRC Handbook of Coastal Processes and Erosion*, edited by P.D. Komar, pp. 35-64, CRC Press, Boca Raton, 1983.